Stony Brook University

The chromatin remodeler Chd5 orchestrates repackaging of the sperm genome

A Dissertation Presented

by

Wangzhi Li

to

The Graduate School

in Partial Fulfillment of the

Requirements

for the Degree of

Doctor of Philosophy

in

Molecular and Cellular Biology Program

Stony Brook University

December 2013

Stony Brook University

The Graduate School

Wangzhi Li

We, the dissertation committee for the above candidate for the

Doctor of Philosophy degree, hereby recommend

acceptance of this dissertation.

Dr. Alea A. Mills – Dissertation Advisor
Professor, Cold Spring Harbor Laboratory

Dr. Nicholas Tonks – Chairperson of Defense
Professor, Cold Spring Harbor Laboratory

Dr. Arne Stenlund
Associate Professor, Cold Spring Harbor Laboratory

Dr. Raffaella Sordella
Associate Professor, Cold Spring Harbor Laboratory

Dr. Howard C. Crawford
Associate Professor of Cancer Biology, Mayo Clinic

This dissertation is accepted by the Graduate School

Charles Taber
Dean of the Graduate School

Abstract of the Dissertation

The chromatin remodeler Chd5 orchestrates repackaging of the sperm genome

by

Wangzhi Li

Doctor of Philosophy

in

Molecular and Cellular Biology Program

Stony Brook University

2013

One of the most remarkable chromatin remodeling processes occurs during the post-meiotic phase of sperm development, namely spermiogenesis. In mammals, this process results in the majority of the somatic histones being replaced with sperm-specific basic proteins called protamines, which repackage the genome into the distinctive and highly compact chromatin structure characteristic of mature sperm. This poorly understood process is not only crucial for male fertility, but also offers a unique experimental system to elucidate mechanisms of chromatin remodeling. Here I identified a critical role of Chromodomain helicase DNA binding protein 5 (Chd5) in the histone-to-protamine chromatin remodeling process. I found that Chd5 deficiency led to defective compaction of sperm chromatin and infertility in mice, mirroring the observation that low CHD5 levels correlated with male infertility in humans. I revealed that Chd5 was critical for orchestrating a cascade of molecular events required for efficient histone removal and replacement. I also discovered that Chd5 deficiency led to disruption of the homeostasis of sperm-specific basic proteins that replace histones, including transition protein 1

(Tnp1), transition protein 2 (Tnp2), protamine 1 (Prm1) and protamine 2 (Prm2), aberrant expression of which compromises fertility. These findings defined Chd5 as a multi-faceted modulator of the histone-to-protamine remodeling process, and also depicted the cascade of molecular events underlying the histone removal process during spermiogenesis, providing a guiding model for further elucidation of this elusive process of extensive chromatin remodeling.

Table of Contents

List of Figures

List of Tables

List of Illustrations

List of Abbreviations

BRK	Brahma and Kismet domain
BSA	bovine serum albumin
ChIP	chromatin immunoprecipitation
CS	condensed spermatids
DAPI	4',6-Diamidino-2-Phenylindole, Dihydrochloride
DFI	DNA Fragmentation Index
DSB	double-strand break
DTT	dithiothreitol
ECS	elongating and condensing spermatids
EDTA	ethylenediaminetetraacetic acid
H3K4me3	trimethylated Lys4 of histone H3
H3K27me3	trimethylated Lys27 of histone H3
H3K9me3	trimethylated Lys9 of histone H3
HAT	histione acetyltransferase
HDR	homologous recombination DNA repair
MAR	matrix Attachment Region
NDA	dipotassium 2-Naphthol-6,8-disulfonate
NHEJ	nonhomologous end joining
PBS	phosphate-buffered saline
PHD	Plant Homeo Domain
PMSF	phenylmethylsulfonyl fluoride

PS	pachytene spermatocytes
qRT-PCR	quantitative reverse transcription polymerase chain reaction
RES	round and early elongating spermatids
RNP	ribonucleoprotein particles
RS	round spermatids
SANT	Switching-defective protein 3, Adaptor 2, Nuclear receptor co-repressor, Transcription factor IIIB domain
SCSA	Sperm Chromatin Structure Assay
SDS-PAGE	SDS-polyacrylamide gel electrophoresis
TBS	Tris-buffered saline
TEM	transmission electron microscopy
TUNEL	terminal deoxynucleotidyl transferase dUTP nick end labeling

Acknowledgments

I would like to thank many people whose guidance, collaboration, help and friendship have supported and inspired me through my PhD years. Foremost, I am very grateful to my advisor, Alea Mills, for her guidance, support, encouragement, trust and care. Only with Alea's tremendous trust, support and guidance, I was able to initiate this work on spermatogenesis and made the achievements presented in this thesis, as the lab and almost the whole CSHL campus has little experience in the field to borrow from. I still recalled the time when we flied together to the hot Huston from cold New York, and spent days and nights learning the laborious elutriation technique at MD Anderson Cancer Center. The lovely and scary "spider, ants and thunder" stories she shared along the trip were equally vivid. Outside research, Alea has given me many great advices about career and life in general, and I learned a lot from her about writing and presenting. Also grateful for the delicious soups and dishes she has made for me from time to time.

I am also grateful to my thesis committee, Nick Tonks, Arne Stenlund, Raffaella Sordella and Howard Crawford. Their invaluable feedback, input and advice were crucial for me in proceeding and improving my research. Their encouragement and support were also important for me to march through the roadblocks along the project.

Also many thanks to Mills lab members and alumni. Bill Keyes, Shirley Guo, Shilpi Paul and Emma Vernersson-Lindahl provided a lot of help and support when they were at the lab. Guy Horev provided great feedbacks on research and help with statistics. Yon Chang organized the lab neatly. Assaf Vestin and Dong-Woo Hwang have been great PhDmates in the lab, and special thanks to Ellen Son for helping with genotyping and proofreading of this manuscript.

Many appreciations also go to the great support on CSHL campus. Sang-Yong Kim was very helpful with generation of mouse models and characterization of fertility phenotypes. Stephen Hearn provided great help with microscopy. Lisa Bianco and Gula Nourjanova were very helpful with mouse husbandry and pathology. I'd also like to thank Marv Meistrich and Ming Zhao at MDACC for teaching me elutriation and providing help with my research, and Stephen Kistler at University of South Carolina-Columbia for providing tips on biochemical assays for transition proteins and protamines, and offering antibodies.

Also thanks to my classmates An-Yun Chang, Bin Xue, Deepika Vasudevan, Fauzia Chaudhary, Hyejin Cho, Marcin Stawowzck and Nihan Kara, whose friendships and sharing of fun with PhD and life were integral to my PhD years.

Lastly, I'd like to specially thank my parents, my sister and my brother. Their love, encouragement and understanding have been a constant and essential support.

Publications

Chd5 orchestrates chromatin remodeling during sperm development
Wangzhi Li, Sang-Yong Kim, Jie Wu, Ming Zhao, Michael Zhang, Marvin Meistrich, Alea Mills *Nature Communications* 2013 (in revision)

Chromatin remodeling in cancer, development and neuropsychiatric diseases
Wangzhi Li, Alea Mills *Epigenomics* (invited review)

ΔNp63α is an oncogene that induces Lsh expression and promotes stem-like proliferation
William M. Keyes, Matteo Pecoraro, Victoria Aranda, Emma Vernersson-Lindahl, **Wangzhi Li,** Hannes Vogel, Xuecui Guo, Elvin L. Garcia, Grigori Enikolopov, Senthil K. Muthuswamy, and Alea A. Mills *Cell Stem Cell* 8(2):164-76, Feb. 2011

This paper showed that ΔNp63α is an oncogene that enables bypass of Ras-induced senescence which promotes stem-like proliferation to drive tumorigenesis *in vivo*. Furthermore, the chromatin-remodeling protein *Lsh* was identified as a new target of ΔNp63α that is an essential mediator of ΔNp63α-mediated senescence bypass. My main contribution in this study was that I identified *Lsh* as a novel direct target of ΔNp63α from a large number of potential ΔNp63α targets reveal by microarray experiments through ChIP analyses. *Lsh* was then functionally shown to be essential for ΔNp63α-mediated senescence bypass.

TAp63 induces senescence and suppresses tumorigenesis *in vivo*
Xuecui Guo, William M. Keyes, Cristian Papazoglu, Johannes Zuber, **Wangzhi Li**, Scott W. Lowe, Hannes Vogel, Alea A. Mills *Nature Cell Biology* 11(12): 1451 – 1457, December 2009

This paper demonstrated that TAp63 is a tumor suppressor that induces senescence and overrides Ras-driven transformation of p53-deficient cells. Expression of TAp63 prevents tumor initiation and inhibits progression of established tumors *in vivo*. The TAp63-mediated senescence is independent of p53 or $p19^{Arf}$ and $p16^{Ink4a}$, but requires $p21^{Waf/Cip1}$ and Rb. My main contribution in this study was that I performed Western blot to show the independence of $p16^{Ink4a}$ and $p19^{Arf}$, and dependence of $p21^{Waf/Cip1}$ for TAp63-meidated senescence.

Chapter 1

Introduction

1.1 Chromatin Remodeling

In somatic nuclei of eukaryotic cells, DNA wraps around histone octamers to form nucleosomes, which act as the fundamental unit to form higher-order folds and loops and eventually chromatin [1-3]. Such packaging both compacts the DNA and allows control of DNA accessibility through chromatin remodeling, a process that alters chromatin structure without changing the primary DNA sequence [1, 3]. During all DNA-templated cellular processes, chromatin structures undergo dynamic remodeling to allow optimal states for efficient transcriptional regulation, DNA replication, recombination and repair, as well as chromosome condensation and segregation. Such dynamic regulation of chromatin is enabled through the interplay of elaborate mechanisms including remodeling by ATP-dependent chromatin remodelers, covalent histone modifications, exchange of histone variants, DNA methylation and non-coding RNA functions [4]. In particular, chromatin remodelers play critical roles in regulating chromatin structure and DNA accessibility through mobilizing and restructuring nucleosomes using energy derived from ATP hydrolysis. These ATP-dependent chromatin remodelers are highly conserved across organisms from yeast to human, and contain an ATPase domain similar to the SNF2 (sucrose non-fermenting 2) family of DNA translocases [5]. Based on the presence of other distinct domain structures, SNF2 chromatin remodelers consist of four well-characterized families: the SWI/SNF (switching defective/sucrose non-fermenting) family, the ISWI (imitation SWI) family, the INO80 (inositol requiring 80) family, and the CHD (chromodomain helicase DNA binding) family[5]. Chromatin remodelers have been shown to

play important roles in regulation of gene transcription, DNA replication, recombination and repair as well as chromatin assembly and segregation, and have been implicated in a number of biological processes and human diseases including cancer and developmental disorders [5-7].

1.2 Extensive chromatin remodeling during sperm development

Although chromatin remodeling takes place across many cellular and biological processes, one of the most remarkable chromatin remodeling processes occurs during spermatogenesis, a complex developmental process during which diploid spermatogonial stem cells differentiate through multiple stages and ultimately give rise to haploid spermatozoa. During spermatogenesis, a dramatic reorganization of the genome takes place to repackage the somatic genome into the distinctive chromatin structure in mature sperm that condenses the sperm DNA tightly making it resistant to mechanical stresses [8, 9], thus offering sperm protection from physical and chemical damages as they traverse a potentially harsh and barrier-laden female reproductive tract to penetrate the oocyte [10]. In mammals, spermatogenesis results in the majority of the somatic histones, such as core nucleosome histones H2A, H2B, H3, H4 and linker histone H1, being replaced by sperm-specific basic proteins called protamines, which package the genome from the nucleosome-based structure into a toroid structure and enable the tight DNA packaging of mature sperm [10-13]. Such dramatic chromatin restructuring is achieved through extensive chromatin remodeling during spermatogenesis. Thus, spermatogenesis provides an excellent *in vivo* process to illustrate chromatin remodeling and to understand its underlying mechanism. However, this process remains poorly understood, partially due to the intrinsic complexity of the process itself and the lack of *in vitro* experimental system to study it.

1.2.1 Spermatogenesis

Spermatogenesis takes place along the seminiferous epithelium in testis. The two main cell types within the tubules involved in spermatogenesis are the germ cells, which develop into sperm, and the somatic cells known as Sertoli cells, which nurture the germ cells throughout their development. Spermatogenesis is divided into three main phases: mitosis, meiosis and spermiogenesis (Illustration 1). Spermatogonial stem cells first multiply by repeated mitosis and

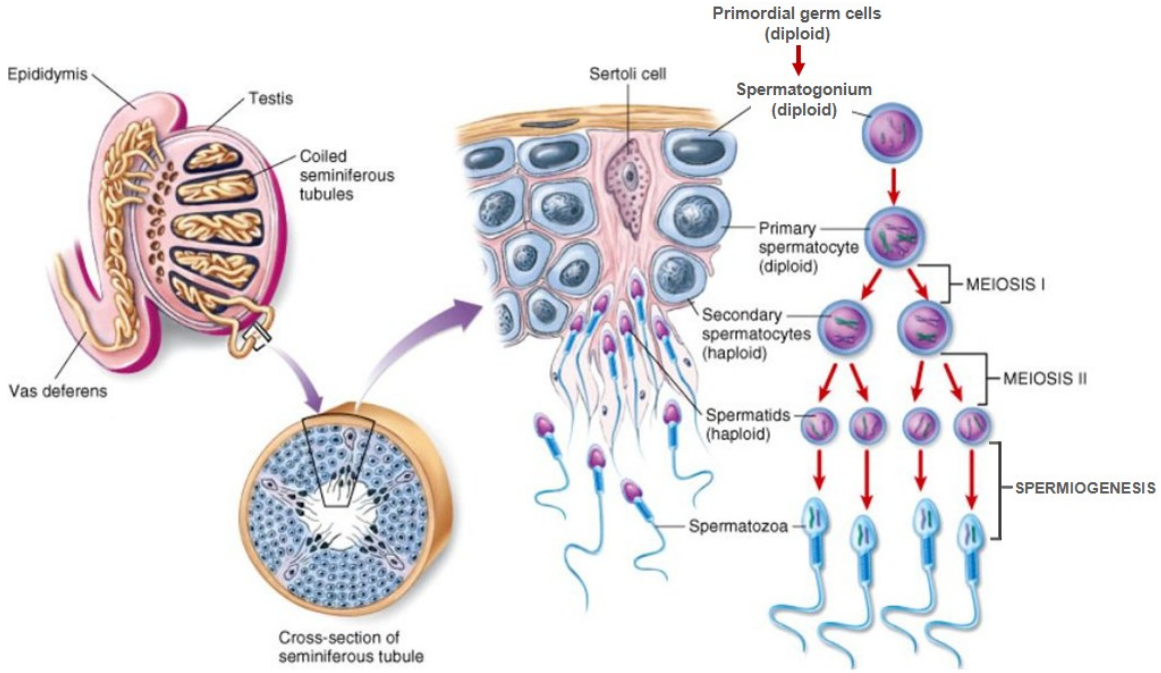

Illustration 1. Overview of spermatogenesis

Spermatogenesis occurs in seminiferous tubules in testis. Through three main sequential phases, namely mitosis, meiosis and spermiogenesis, one diploid spermatogonium stem cell generates four haploid spermatozoa. Adapted from www.nicerweb.com

then differentiate into primary spermatocytes. Diploid primary spermatocytes undergo meiosis and become haploid round spermatids. Round spermatids then elongate and condense with profound molecular changes to eventually mature into highly specialized sperm cells. The differentiation of round spermatids into sperm cells is called spermiogenesis. It consists of the

final phase of spermatogenesis and comprises a number of characteristic changes including:

- Nuclear condensation: elongation and condensation of the round nuclei into a hook-shaped sperm head.
- Acrosome formation: forming a cap (acrosome) covering the cranial part of the head. Acrosome is derived from the Golgi apparatus and contains hydrolytic enzymes to allow fusion of sperm and egg for fertilization.
- Flagellum formation: generation of the sperm cell tail for motility.
- Cytoplasma reduction: shedding most excess cytoplasm as residual body.

Spermatogenesis lasts over 34 days in mouse and progresses through precisely timed and highly organized cycles along the seminiferous tubules [14, 15]. To facilitate the study of this lengthy and complex process, spermatogenesis is subdivided into separate stages according to distinct compositions of cellular components (spermatogonia, spermatocytes and spermatids) which can be analyzed on tubular cross sections [15]. Although spermatogenesis is artificially divided into multiple stages, it is a continuous process, leading to transitional areas between two stages. In mouse, twelve stages (stage I-XII) are defined originally according to the changes during formation of the spermatid acrosome, which can be visualized by Periodic acid-Schiff (PAS) or lectin staining (Illustration 2) [16]. Meanwhile, the maturation process of spermatids is further divided into 16 steps (step 1-16) according to changes of both acrosome formation and nuclear morphology of the spermatids [14-17]. A binary decision scheme for staging mouse seminiferous tubules has been developed by Meistrich and Hess *et al.* [18] (Illustration 2). Detailed characteristics for determining each stage of individual seminiferous tubules, as reviewed by Ahmed *et al.* [17], are described below and in Illustration 2:

Stage I: One type of spermatocytes (pachytene spermatocytes) and two types of spermatids (step 1 and step 13 spermatids) are present. Step 1 spermatids have the initial appearance of a proacrosomal vesicle but no PAS-positive acrosomic granules.

Stage II: One type of spermatocytes (pachytene spermatocytes) and two types of spermatids (step 2 and step 14 spermatids) are present. Two to three small PAS-positive acrosomic granules are present in the proacrosomic vesicle of step 2 spermatids. Pachytene spermatocytes are near the basal membrane and have sex body formed. The
A spermatogonia divide into intermediate (In) spermatogonia, which have ovoid nuclei and a prominent rim of heterochromatin along the inner nuclear membrane.

Stage III: One type of spermatocytes (pachytene spermatocytes) and two types of spermatids (step 3 and step 15 spermatids) are present. The PAS-positive acrosomic granules seen in step 2 spermatids merge into one round granule in stage III.

Stage IV: One type of spermatocytes (pachytene spermatocytes) and two types of spermatids (step 4 and step 15 spermatids) are present. The round acrosomal granule present in stage III flattens and moves to touch the nuclear membrane of the spermatids. Mid-pachytene spermatocytes have obvious sex bodies and start to move more towards the lumen of the tubules. Large intermediate (In) spermatogonia start division into B spermatogonia. B spermatogonia show more heterochromatin than the In spermatogonia.

Stage V: One type of spermatocytes (pachytene spermatocytes) and two types of spermatids (step 5 and step 15 spermatids) are present. The acrosomal granule of the round spermatids forms a flat rim in the middle with its two flanking perimeter remaining straight. Elongated spermatids are still embedded deep in the seminiferous epithelium.

Stage VI: Two types of spermatocytes (pachytene and preleptotene spermatocytes) and two types of spermatids (step 6 and step 15 spermatids) are present. The acrosomal rim spreads and bends to cover less than one-third of the spermatid nuclear surface. As the rim bends, a cap is formed. Elongated spermatids move towards the tubule lumen but are not yet released. The B spermatogonia divide into preleptotene spermatocytes.

Stage VII: Two types of spermatocytes (pachytene and preleptotene spermatocytes) and two types of spermatids (step 7 and step 16 spermatids) are present. The acrosomal cap covers over one third of spermatid nuclear surface. The majority of the round spermatids have not yet orientated themselves to have their acrosomal caps point to the basal membrane.

Stage VIII: Three types of spermatocytes (pachytene, preleptotene and leptotene spermatocytes) and two types of spermatids (step 8 and step 16 spermatids) are present. Most of the round spermatids are now orientated to point with their acrosomal cap towards the tubule basal membrane. Elongated spermatids are being released into the lumen as spermatozoa. The preleptotene spermatocytes develop into leptotene spermatocytes which are characterized by the appearance of thin threads of chromatin.

Stage IX: Two types of spermatocytes (pachytene and leptotene spermatocytes) and one type of spermatids (step 9 spermatids) are present. Round spermatids start to elongate and are no longer round. The nucleus becomes more flattened.

Stage X: Four types of spermatocytes (pachytene, diplotene, leptotene and zygotene spermatocytes) and one type of spermatids (step 10 spermatids) are present. The spermatids are further elongated and bilaterally flattened. However, the spermatid nuclei do not yet start to

compact. The chromatin threads in the spermatocytes become thicker and heavily stained as the spermatocytes go from leptotene to zygotene phase.

Stage XI: Two types of spermatocytes (zygotene and diplotene spermatocytes) and one type of spermatids (step 11 spermatids) are present. Elongation becomes more extreme. The nuclei of elongated spermatids begin to compact and become more darkly stained

Stage XII: Stage XII is characterized by the presence of spermatocytes in meiotic division (meiotic figure) and/or secondary spermatocytes.

1.2.2 Chromatin remodeling and histone removal during spermiognenesis

One of the most remarkable chromatin remodeling processes occurs during post-meiotic spermatid maturation, namely spermiogenesis (Illustration 3). Following meiosis, early round spermatids inherit a nucleosome-based haploid genome. During mammalian spermiogenesis, nucleosomes are globally destabilized and evicted, canonical histones are removed and replaced by histone variants including many testis-specific histone variants, and testis-specific small basic proteins called transition proteins, which are subsequently replaced by protamines [10-13]. The molecular events that enable and orchestrate such nucleosome disposition and histone removal remain poorly understood. However, two nucleosome-destabilizing mechanisms have been described: incorporation of testis-specific histone variants and a transient increase of global hyperacetylation of core histones, particularly histone H4 [19-25]. Incorporation of histone variants was shown to make nucleosomes less stable *in vitro* [26, 27]. Therefore, histone variants are believed to facilitate chromatin decondensation and histone removal *in vivo* during spermiogenesis. Another hallmark for the massive histone removal is an acute elevation of histone H4 during early elongating steps of spermiogenesis [21-23], which was shown to be

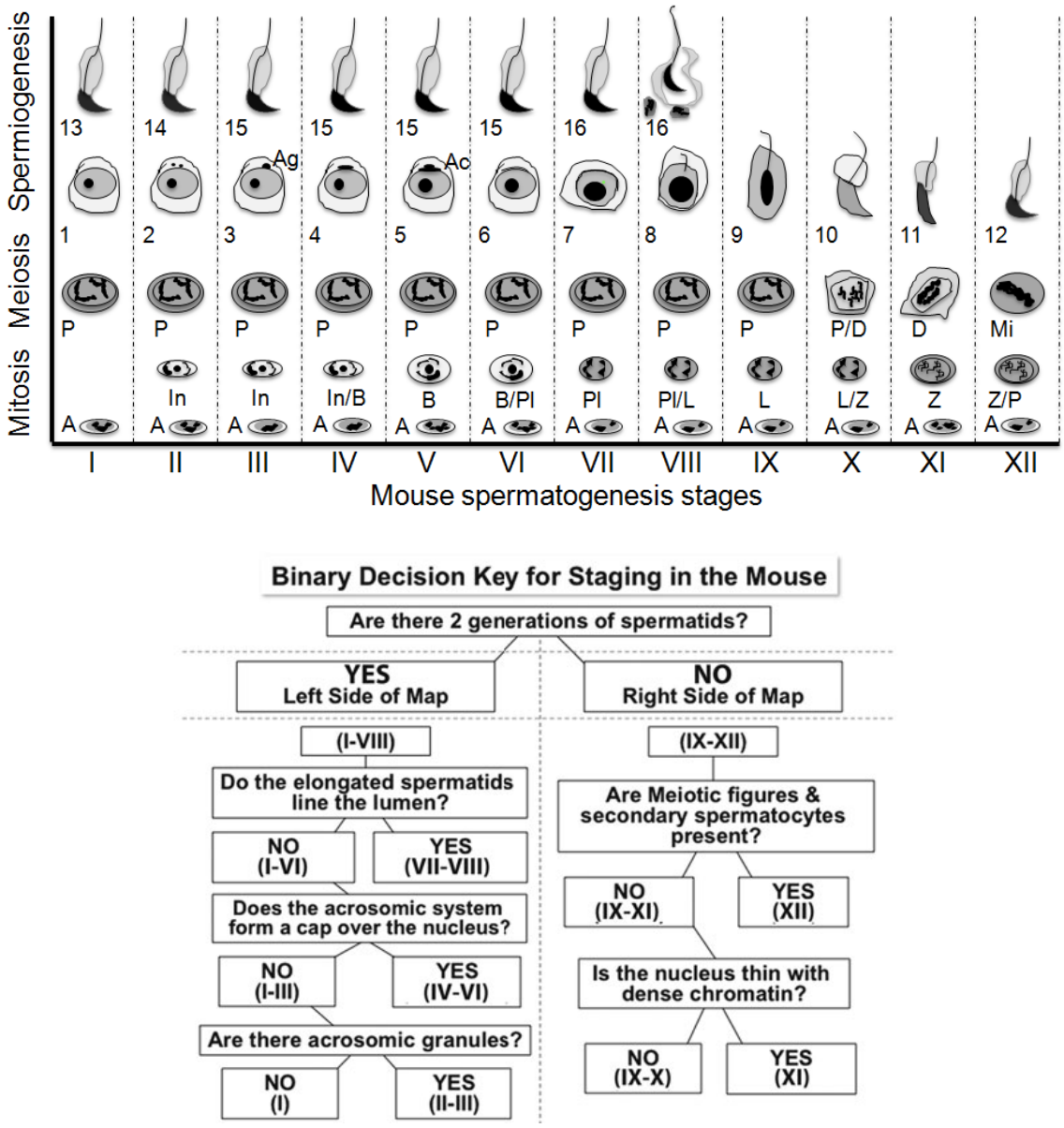

Illustration 2. Staging of spermatogenesis

Top: spermatogenesis is divided into twelve stages (stage I-XII) and each stage includes distinct cellular composition. Spermiogenesis, the maturation process of haploid spermatids, is further divided into 16 steps (step 1-16). Roman numerals (I-XII) indicate the spermatogenic stages. Arabic numbers (1-16) designate spermiogenic steps of the speramtids. A, In, B: spermatogonia; Pl, preleptotene spermatocytes; L, leptotene spermatocytes; Z, zygotene spermatocytes; P, pachytene spermatocytes; D, diakinesis; Mi, meiotic figure; Ag, acrosomic granule; Ac, acrosomic cap. Bottom: A binary decision tree was developed by Dr. Marvin Meistrich and Dr. Rex Hess to guide staging of seminiferous tubules on testis sections stained with periodic acid Schiff (PAS)-hematoxylin [18]. Adapted from Meistrich, M.L. and R.A. Hess, *Assessment of spermatogenesis through staging of seminiferous tubules.* Methods Mol Biol, 2013. 927: p. 299-307.

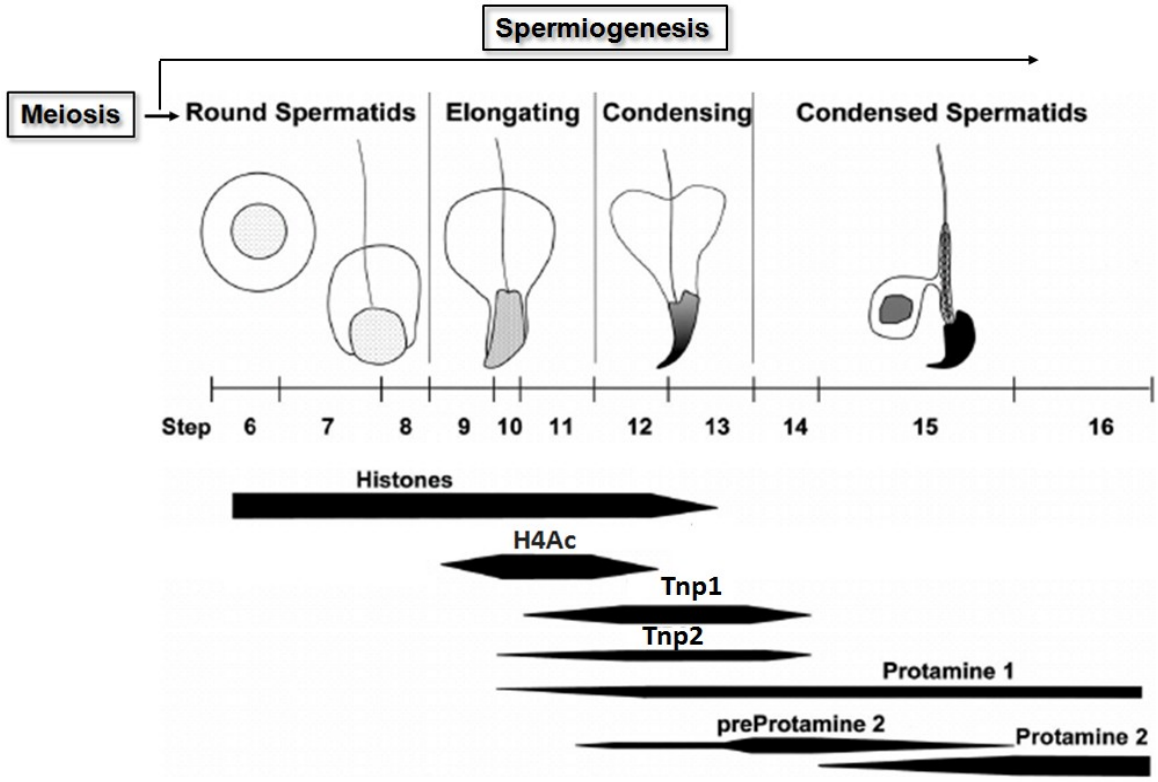

Illustration 3. Overview of histone-to-protamine replacement during spermiogenesis

H4Ac, histone H4 pan-acetylation; preProtamine 2, precursor of Protamine 2. The width of the bar reflects the relative levels of the protein and the length of the bar indicates the specific spermiogenic steps during which the protein is present. Modified from Meistrich, M.L., *et al.*, *Roles of transition nuclear proteins in spermiogenesis.* Chromosoma, 2003 [28].

essential for normal proceeding of the histone-to-protamine replacement in *Drosophila* [24]. H4 acetylation could then be recognized by bromodomain-containing readers which could trigger loosening of the nucleosome and decondensation of chromatin. BRDT (bromodomain, testis-specific) is a testis-specific member of the bromodomain BRD proteins that are capable of reading and binding acetylated histone tails, and shown to remodel chromatin *in vitro* [29]. Structural studies revealed that one of BRDT's two bromodomains recognizes acetylated lysine 5 and 8 on histone 4 [30] and deletion of its first bromodomain in the mouse leads to abnormal spermiogenesis from step 9 elongating spermatid onward and consequently, sterility [31],

suggesting that BRDT-mediated binding to acetylated histones is required for normal progression of spermiogenesis. However, how BRDT mediates nucleosome destabilization and histone removal remains elusive. Likely, BRDT recruits ATP-dependent chromatin remodelers to remodel and loosen the acetylated nucleosome. In general, chromatin remodelers are thought to be required for the nucleosome eviction and histone removal that occur during spermiogenesis, but chromatin remodelers functioning during spermiogenesis have not been identified. The chromatin remodeler Smarca4 (SWI/SNF related, matrix associated, actin dependent regulator of chromatin, subfamily a, member 4), also known as Brg1, was shown to be essential for meiosis in male mice. Deficiency of Brg1 leads to meiotic arrest at prophase of meiosis I with global alterations to histone modifications and chromatin structure [32], revealing an essential role of chromatin remodelers during meiosis. However, chromatin remodelers functioning during post-meiotic spermiogenesis remain to be identified.

Another major question is how the acute and transient acquisition of histone hyperacetylation is modulated during spermiogenesis. Histone acetyltransferases Cdyl and Kat6b (also known as Myst4) [33-35] and deacetylases (HDAC1 and HDAC2) [33, 36] have been implicated in histone hyperacetylation during spermiogenesis. Recently, the E3 ubiquitin ligase RNF8 that mediates H2A and H2B ubiquitination in elongating spermatids, has been shown to be essential for H4 hyperacetylation and for nucleosome removal [37]. However, the mechanism regulating H4 hyperacetylation during spermiogenesis remains poorly understood. During my thesis research, I revealed that the chromatin remodeler Chd5 (Chromodomain Helicase DNA binding protein 5), a member of the CHD chromatin remodeling protein family, is critical for H4 hyperacetylation and efficient nucleosome eviction during spermiogenesis. I identified Chd5 as the first chromatin remodeler implicated in spermiogenesis, and revealed that Chd5 played

multifaceted roles in orchestrating the histone-to-protamine remodeling process during spermiogenesis.

1.2.3 Transition proteins and protamines

In male gametes of mammals, histones are first replaced by transition proteins (Tnp1 and Tnp2), which are subsequently replaced by protamines (Prm1 and Prm2). Tnp1 and Tnp2 are small basic proteins that play important roles in histone displacement, sperm nuclear morphology, chromatin condensation and maintenance of DNA integrity [28]. Depletion of either Tnp1 or Tnp2 protein leads to subfertility in males with modest impairment in sperm counts, motility, morphology and nuclear condensation [28, 38]. However, combined deficiency of Tnp1 and Tnp2 results in male sterility [39]. These results suggest partially overlapping functions of Tnp1 and Tnp2. Protamines are cysteine and arginine-rich basic proteins of approximately 50 residues. The high positive charge of protamines can completely neutralize the negative charges of DNA, allowing protamines to bind the major groove of the DNA tightly [40, 41]. This enables protamines to package DNA without adding much volume of themselves [40, 41]. In contrast, in nucleosome-based DNA packaging, histone octamers occupy larger volume than the DNA they package [40, 41]. Balhorn proposed that the uncharged protamine-DNA strands could be packaged side by side in a linear array [41]. Hud *et al.* demonstrated that protamines fold the DNA into tightly packaged toroids each containing roughly 50 kb of DNA [13, 42]. The abundance of cysteine in protamine also enables extensive disulfide bond formation between neighboring protamines to stabilize the chromatin structure [43]. Together, these features allow protamines to package the DNA in sperm at least six fold more compacted than the DNA of mitotic chromosomes in somatic cells [9, 44, 45]. Such higher compaction of sperm DNA is

necessary, as sperm nuclei are much smaller than somatic nuclei and do not have the volume required for nucleosome-based DNA packaging [9, 46]. The highly compacted chromatin enabled by protamine in sperm also provides additional advantages: 1) it generates a compact and hydrodynamic nucleus that facilitates fast movement of sperm in the aqueous female reproductive tract; 2) it protects the paternal DNA from mechanical and chemical damage through making it inaccessible to nucleases and mutagens; 3) it removes transcription factors and other proteins from the sperm DNA to allow its reprogramming by the oocyte in the developing zygote [47]. Meanwhile, a small portion of histones and nucleosomes are retained in chromatin of sperm. In human sperm, such retention of nucleosomes is significantly enriched at loci of developmental importance, including imprinted gene clusters, microRNA clusters, *HOX* gene clusters, and the promoters of genes encoding crucial developmental transcription and signalling factors [48].

Protamines are well conserved among human, mouse, rat and other mammals, and there is evidence suggesting that protamines evolved from linker histone H1 [45, 49]. Whereas all mammals have Prm1 in sperm nuclei, only a few mammals, such as human and mouse, contain Prm2. Prm1 is translated as the mature form, but Prm2 is generated via proteolytic processing of a larger precursor. In mice, both protamines are essential for normal sperm function, as haploinsufficiency in either Prm1 or Prm2 leads to infertility in chimeric mice, preventing transmission of both the mutant and wild-type alleles [50]. Haploinsufficiency of Prm2 correlates with reduced chromatin compaction and increased DNA damage in sperm [51], indicating that Prm2 is essential for maintaining the integrity of sperm chromatin. Furthermore, a precise Prm1: Prm2 ratio, which is approximately 0.8-1.0 in human sperm, seems critical for normal fertility, as

either an increase or decrease in the ratio of Prm1: Prm2 ratio is associated with compromised sperm number, motility, morphology and fertility [47, 52-54].

The chromatin condensation in elongating spermatids results in cessation of transcription at a time when many proteins need to be synthesized and assembled for the condensation of the spermatid nuclei, the development of the acrosome, and the formation of the flagellum [55]. Thus, many genes such as those encoding transition proteins and protamines are transcribed within round spermatids with their transcripts being stored in translationally repressed ribonucleoprotein particles (RNPs) until they are later translated into protein within elongating and elongated spermatids [55-60]. This temporal uncoupling of transcription and translation is essential for normal nucleoprotein exchange and differentiation of round spermatids into mature sperm [55-60]. For example, premature translation of Prm1 mRNA in a transgenic mouse model causes precocious condensation of spermatid nuclear DNA, abnormal head morphogenesis and incomplete processing of Prm2 protein, leading to arrest of spermatid differentiation and male sterility [61].

In mouse and human, *Prm1*, *Prm2* and *Tnp2* map in tandem in chromosome 16, whereas *Tnp1* is located on a separate chromosome [62]. Transcriptional regulation includes priming the genes for transcription via association with nuclear matrix attachment regions (MARs), and binding of *trans*-regulatory factors to the promoter region [63, 64]. The 5′ and 3′ regions surrounding *Prm1/Prm2/Tnp2* genes contain MARs, which are *cis*-regulatory units guiding attachment of the DNA to the nuclear matrix in an organized manner of loop domains that prime genes for transcription [63]. In addition, *trans*-regulatory factors, such as TBP (TATA-box protein), Crem (cAMP response element modulator), Y-box proteins and Kdm3a (lysine (K)-specific demethylase 3A) also regulate protamine transcription [65-70]. Disruption of these

transcriptional regulators of transition proteins and protamines can result in male infertility. For example, deficiency of Kdm3a, also known as Jhdm2a, compromises *Tnp1* and *Prm1* transcription and causes post-meiotic chromatin condensation defects, leading to infertility in mice [70]. Targeted disruption of the *Crem* gene blocks the differentiation program in the first step of spermiogenesis, defining Crem as a key regulator of gene expression during spermiogenesis [71]. The mechanism for translational regulation is poorly understood. However, Y-box proteins Ybx2 (Y box binding protein 2, also known as Contrin in human and Msy2 in mouse) and Tsn (Translin) as well as the kinesin Kif17b (kinesin family member 17) have been shown to be essential for transport of the RNP to the cytoplasm and for delayed translation [72-75]. Msy2 knockout male mice are sterile [76], whereas mice lacking Tsn are able to sire offspring but have reduced sperm production [77]. Also, Prbp (protamine 1 RNA-binding protein), known as TRBP (TAR RNA-binding protein) in humans, can regulate *Prm1* mRNA translation, as it contains two RNA-binding domain that binds to the 3′-UTR of *Prm1* [78]. Depletion of Prbp in mice leads to severe oligozoospermia and infertility as protamine transcripts fail to be translated, which causes delayed replacement of transition proteins and subsequent failure of spermiogenesis [79]. Protamines also undergo post-translational modifications, including phosphorylation and dephosphorylation, disulfide bond formation and proteolytic processing of protamine 2 precursor into mature protamine 2 [80-82]. Decades of research have demonstrated the critical roles of transition proteins and protamines in spermiogenesis and male fertility, and have identified a number of factors required for the transcription, processing and modification of transition proteins and protamines. However, the factors responsible for limiting the transcription of transition protein and protamine genes remain elusive. In addition, little is known about the mechanisms whereby the degradation of transition proteins and protamines are

regulated. During my thesis study, I identified Chd5 as a negative mediator for both transition proteins (Tnp1 and Tnp2) and protamines (Prm1 and Prm2). I revealed that deficiency of Chd5 led to increased *Prm1* transcription and elevated protein levels of all protamines and transition proteins.

1.3 CHD chromatin remodeler family and CHD5

CHD5 is a member of the CHD chromatin remodeler family. The CHD family compasses nine members (CHD1-9) that are highly conserved across species [83, 84]. CHD proteins are characterized by the SNF2-like helicase-ATPase domain located in the central region and signature tandem chromodomains (chromatin organization modifier) located in the N-terminal region of the proteins [83-86]. The SNF2-like ATPase domain defines the ATP-dependent chromatin remodeling function of CHD proteins [84, 87-91]. The chromodomain is an evolutionarily conserved motif that mediates chromatin interactions by binding directly to DNA, RNA or methylated histone H3 [92-98]. The nine CHD proteins are divided into three subfamilies based on presence of additional distinct domains in addition to the common domains [83, 84] (Illustration 4). Subfamily I members (CHD1 and CHD2) are characterized by the presence of a defined DNA-binding domain with a preference for binding AT-rich DNA motifs [86]; subfamily II members (CHD3, 4, 5) lack the standard DNA-binding domain but harbor dual N-terminal PHD (Plant Homeo Domain) zinc fingers upstream of the tandem chromodomains. PHD fingers bind either histone H3 tail trimethylated at Lys4 (H3K4me3) or unmodified histone H3 tail [99-104]. Subfamily III (CHD6, 7, 8, 9) is defined by additional functional motifs in the C-terminal region, including paired BRK (Brahma and Kismet) domains, a SANT-like (switching-defective protein 3, adaptor 2, nuclear receptor co-repressor, transcription factor IIIB)

domain, CR (cysteine-rich) domains, and less-defined DNA binding domain. SANT domains interact primarily with unmodified histone tails and couple histone binding to chromatin remodeling [105], whereas functions of the BRK and CR domain are poorly understood. The diverse functions of domains suggest that CHD proteins could have multifaceted functions as ATP-dependent chromatin remodelers, histone marker readers and DNA-binding factors, whereas the distinct domains that define different CHD subfamilies could equip the individual CHD proteins with unique functions.

CHD proteins are implicated in a variety of processes, such as transcription, chromatin assembly, nucleosome remodeling, DNA damage repair, RNA processing, ribosomal RNA (rRNA) biogenesis, cell proliferation, differentiation and development [83, 84, 106-115]. Increasing evidence also links lesions in CHD proteins to a range of human diseases including cancer, developmental disorders and neuropsychiatric diseases [83, 84, 112, 116-129]. Notably, a number of CHD proteins have been implicated in developmental disorders. For example, mutations in *CHD7* gene are a major cause of CHARGE syndrome, a developmental disease characterized by a constellation of birth defects including ocular coloboma, congenital heart defects, choanal atresia, retardation of growth and development, genital hypoplasia, and ear anomalies associated with deafness [119, 130-134]. In mice, Chd4 is required from T-cell development and establishment of the epidermis [122, 123]. In *Drosophila,* Chd1 mutants result in abnormal wing development, male infertility and female subfertility [135].

CHD5 (Chromodomain Helicase DNA binding protein 5) is a recent member of the CHD family. It was first identified in 2003 and contains two PHD domains, two chromodomains, one ATPase/Helicase domain and a less defined DNA-binding domain [136]. CHD5 shares over 80% of amino acid sequence with the subfamily II members CHD3 and CHD4, both of which are

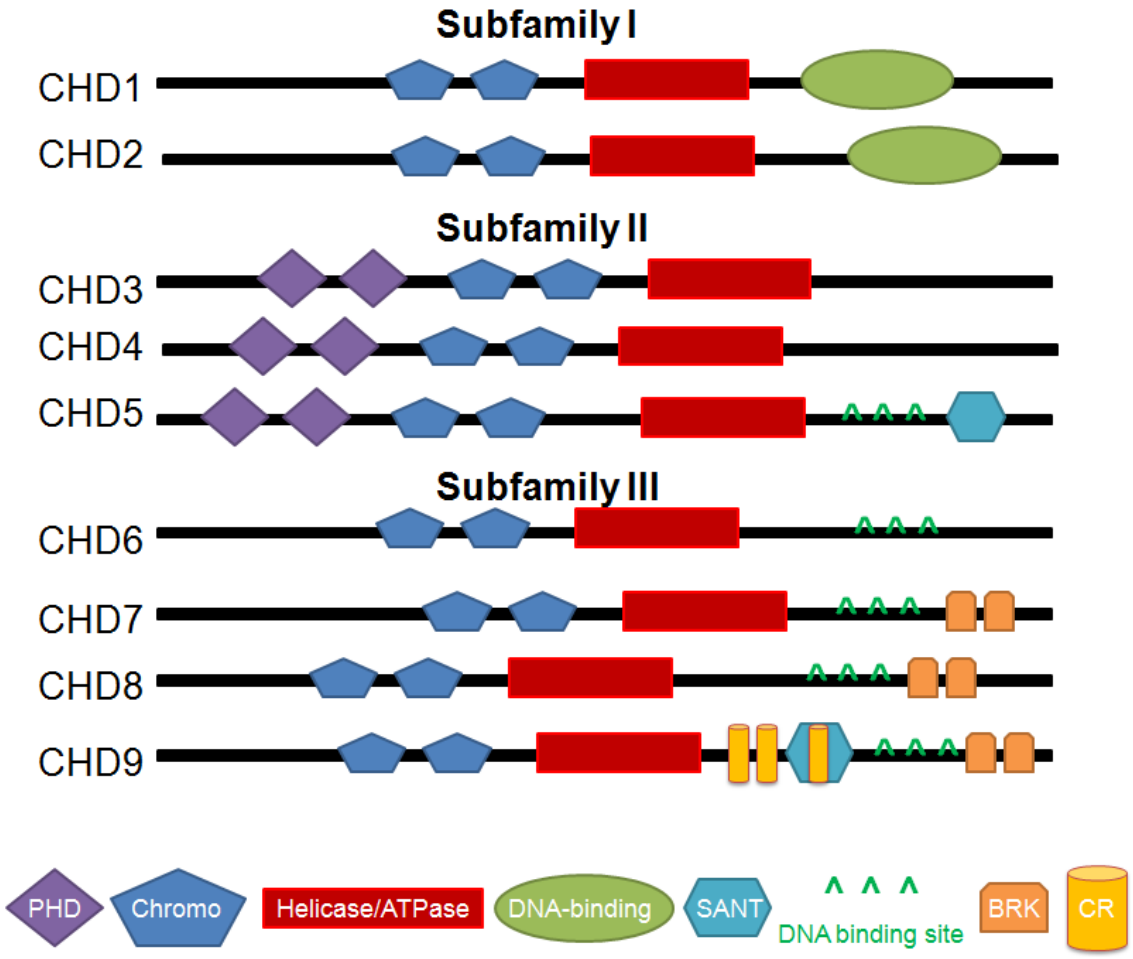

Illustration 4. Overview of CHD protein family

components of the Mi-2/NuRD (nucleosome remodelling and histone deacetylase) complex that has important roles in many processes such as transcription, chromatin assembly, cell cycle progression and genomic stability [137]. In 2007, our lab identified CHD5 as the long-sought tumor suppressor at human *1p36* [117], a region frequently deleted in a broad range of cancers, including those of neural, epithelial, and hematopoietic origin [138]. Since this discovery, a flurry of studies have revealed CHD5 lesions, including mutation, deletion and promoter hypermethylation, in a variety of cancers such as neuroblastoma [136, 139-142], glioma [117, 143, 144], breast cancer [143, 145], lung cancer [146], ovarian cancer [147], gastric cancer [148], gallbladder carcinoma [149], colorectal cancer [143, 150], melanoma [151] and laryngeal

squamous cell carcinoma [152]. A number of studies have also demonstrated high level of CHD5 as a favorable prognostic marker for neuroblastoma [140], glioma [144], epithelial ovarian cancer [147], gallbladder carcinoma [149] and pancreatic adenocarcinoma [153]. Our lab reveals that Chd5 as a tumor suppressor controls cell proliferation, senescence and apoptosis via positively modulating the potent tumor suppressor locus *Ink4a-Arf* and the $p19^{Arf}$/p53 pathway [117]. In addition, we determined that Chd5 binds to unmodified histone H3 through its tandem PHD domains, with a preference to genomic loci lacking the active mark H3K4me3 [104]. This PHD-H3 interaction is critical for Chd5's ability to transcriptionally modulate genes implicated in cancer development and to inhibit cellular proliferation [104]. Mutation of conserved PHD residues in Chd5 abrogates the Chd5-H3 interaction, and such Chd5 mutants fail to suppress cell proliferation *in vitro* and tumor growth *in vivo* [104]. Similarly, Oliver *et al.* showed that both PHD domains of CHD5 display similar binding preferences for histone H3, where modifications such as methylation, acetylation, and phosphorylation at H3R2, H3K4, H3T3, H3T6, and H3S10 disrupt high-affinity binding of CHD5. These findings provide the first evidence that Chd5, as a chromatin remodeler, binds to histone H3 and such histone interaction is essential role for Chd5's tumor suppressor function.

CHD5 was first shown to be preferentially expressed in the nervous system, thus leading to the assumption that it plays important roles in development and/or functions of the nervous system [136, 154]. Indeed, our lab revealed that Chd5 is induced during neuronal differentiation in the developing mouse brain [155]. Chd5 is expressed broadly in mouse brain. The sub-cellular localization of Chd5 undergoes a switch from the cytoplasm to the nucleus during mid-gestation, and Chd5 is highly expressed in nuclei of differentiated neurons of the adult [155]. Consistently, Egan *et al.* reported that depletion of Chd5 in the developing mouse neocortex blocks neuronal

differentiation and leads to an accumulation of undifferentiated progenitors [121]. CHD5 binds to a large cohort of genes including Polycomb targets in brain and is required for facilitating the activation of neuronal genes [121]. Furthermore, the chromodomains of CHD5 directly bind H3K27me3 in neurons and are required for maintenance of H3K27me3 at the Polycomb targets that are bound by CHD5 [121]. Similarly, Potts *et al.* also showed that CHD5 mediates expression of neuronal genes in rat [156]. Depletion of CHD5 in rat primary neuron leads to transcriptional induction and repression of neuronal genes, transcription factors and brain-specific subunits of the SWI/SNF remodeling enzyme. Chromatin immunoprecipitation revealed that CHD5 binds to these target loci [156]. In addition, CHD5 protein isolated from mouse brain is associated with HDAC2, p66ß, MTA3 and RbAp46 in a NurD-like megadalton complex [156]. Altogether, these findings demonstrate Chd5's ability to interact with both chromatin modifications and chromatin modifying proteins/complex, and to mediate gene expression important for biological processes such as neurogenesis.

Besides of the current understanding of CHD5's roles in cancer and neurogenesis, little is known about CHD5's functions in other biological processes, partially because research regarding CHD5 has been focused on cancer and neural functions. In addition, although recent studies demonstrated the interactions of CHD5 with histone H3, Chd5's ability to mediate chromatin remodeling remains poorly understood. Here, I revealed that Chd5 was highly expressed in testis and played essential roles in sperm development and male fertility. I generated a Chd5-deficient mouse model and identified Chd5 as the first chromatin remodeler shown to orchestrate the remarkable chromatin remodeling process during spermiogenesis.

Chapter 2

Chd5 was critical for sperm development and male fertility

2.1 Chd5 was specifically expressed in spermatid nuclei and was enriched in heterochromatin

Previous studies showed that Chd5 is preferentially expressed in the central nervous system [136]. However, these studies examined Chd5 expression at the mRNA level and did not analyze Chd5 expression in all tissue types. I thus analyzed Chd5 expression in a range of mouse tissues at the protein level through Western blot, using a validated antibody against Chd5 [104]. Consistent with previous reports, Chd5 protein was highly expressed in brain as well as spinal cord and eye (Figure 1). In addition, I found that Chd5 protein was also highly expressed in testis, suggesting Chd5 protein could play an important role in testis. To determine where Chd5 protein was expressed within testis, I analyzed Chd5 protein expression through immunostaining and found that it was expressed specifically in haploid spermatids during spermiogenesis. Chd5 protein was first detected in the nuclei of step 4 spermatids, with particularly intense expression in a focal region near the edge of chromocenter, a cluster of centromeres and pericentromeric heterochromatin (Figure 2). Chd5 expression peaked at steps 7-8 of spermatid maturation, when it was expressed robustly throughout the nucleus and enriched in the chromocenter, where it co-localized with the heterochromatin marker H3K9me3 (Figure 2, 3) and showed similar pattern as H3K27me3 (Figure 2, 4). Chd5 expression started to decrease from step 9, while it remained enriched in heterochromatin, and was not detected after step 10 (Figure 3). Notably, the Chd5-intense spot around the edge of chromocenter remained from early round spermatids to step 8 spermatids, but was H3K9me3 negative (Figure 2-3). Higher magnification analyses revealed

that the Chd5-intense spot located near the edge of the junction between chromocenter and post-meiotic sex chromosome, both of which were DAPI-intense heterochromatin regions in spermatid nuclei (Figure 5a). Unlike the chromocenter, this spot was DAPI-weak and negative for H3K9me3 (Figure 3, 5a), suggesting that it could be a more active chromatin area. However, it was not clear whether this Chd5-intense spot represents a specific structure within the spermatid nucleus, given the scarcity of knowledge of spermatid nuclear structure. I speculated that the spot may be within the nucleolus. Co-immunostaining of Chd5 with the nucleolus markers fibrillarin indicated that the Chd5-intense signal was close to fribrillarin signal in many spermatid nuclei, whereas it was clearly separated from fribrillarin signal in other spermatids (Figure 5b), suggesting Chd5 may transiently associate with nucleolus and have a function in ribosomal RNA (rRNA) biogenesis (See Chapter 4). Together, these findings revealed that Chd5 was expressed specifically in the nuclei of round and early elongating spermatids during spermiogenesis, and was primarily enriched in heterochromatin region in spermatid nuclei (Figure 6).

2.2 Chd5 deficiency impaired post-meiotic sperm development and male fertility

Given the extensive chromatin remodeling activity during spermiogenesis and the putative chromatin remodeling function of Chd5, the unique dynamics of Chd5 expression during spermiogenesis indicated that it could play a role in chromatin remodeling during male gamete maturation. To explore this possibility, I generated a Chd5-deficient mouse model, which was termed as *Chd5*^{Aam1} mouse (*Aam* stands for Alea A. Mills and is a designation assigned by the mouse depository organization Jackson Laboratory for mouse models generated by the Mills lab), using gene targeting (Figure 7). *Chd5*$^{Aam1-/-}$ mice were viable and had no gross

developmental abnormality. Both immunoblotting and immunostaining analyses of testes demonstrated that Chd5 protein was not detected in *Chd5*^{Aam1} homozygotes (Figure 8). Mating tests revealed that male *Chd5*$^{Aam1-/-}$ mice were either sterile or subfertile, whereas female homozygous mice and heterozygotes of both genders were fertile (Table 1). Male *Chd5*$^{Aam1-/-}$ mice had significantly lower sperm counts (Table 2). The sperm that were produced by *Chd5*$^{Aam1-/-}$ mice showed compromised motility and a higher proportion of morphological abnormalities, and failed to fertilize wild type oocytes *in vitro* (Figure 9-10; Table 2-4). These sperm defects demonstrated that Chd5 was essential for normal sperm development.

To further understand how Chd5 deficiency impaired sperm development, I asked whether Chd5 deficiency caused perturbation of sex hormone levels, which were known to lead to abnormal sperm development. No significant alteration in serum sex hormone levels was detected in male *Chd5*$^{Aam1-/-}$ mice (Figure 11). Histological analyses of testes revealed fewer elongated spermatids in *Chd5*$^{Aam1-/-}$ seminiferous tubules than in wild type tubules at the same spermatogenic stages (Figure 12-13). Condensed spermatids were normally released into tubular lumen from epithelium by stage IX tubules, but abnormal retention of condensed spermatids in stage IX and X tubular epithelium was observed in *Chd5*$^{Aam1-/-}$ testes (Figure 12-13). The extent of histological abnormalities varied among individual *Chd5*$^{Aam1-/-}$ testes (Figure 13 and detailed description in figure legend), in agreement with the variable severity of infertility of male *Chd5*$^{Aam1-/-}$ mice. In contrast to post-meiotic defects, I did not detect significant difference between *Chd5*$^{Aam1-/-}$ and wild type testes in either earlier phases of spermatogenic cells (spermatogonia, spermatocytes and round spermatids) or in somatic cells (Sertoli cells and Leydig cells) (Figure 12-13). Furthermore, DNA content profiling of cellular populations of wild type and *Chd5*$^{Aam1-/-}$ testes showed a significant reduction of the haploid population of elongating

and elongated spermatid in *Chd5*$^{Aam1-/-}$ testes, but no significant change in the population of haploid round spermatids, diploid, or tetraploid cells (Figure 14). These findings indicated that Chd5 deficiency specifically compromised the post-meiotic elongation and condensation phase of spermatid maturation, consistent with its peak expression in step 7-8 round spermatids, the phase that immediately precedes the initiation of spermatid elongation and condensation.

2.3 CHD5 deficiency correlated with male infertility in humans

Consistent with the impaired fertility of male Chd5-deficient mice, analyses of a published gene expression data set of human testis biopsies from 39 men (29 men with defined spermatogenic defects and 10 normal controls), revealed that *CHD5* expression correlated inversely with spermatogenic defects in humans (Figure 15). This observation suggested that CHD5 deficiency could correlate with male infertility in humans as well.

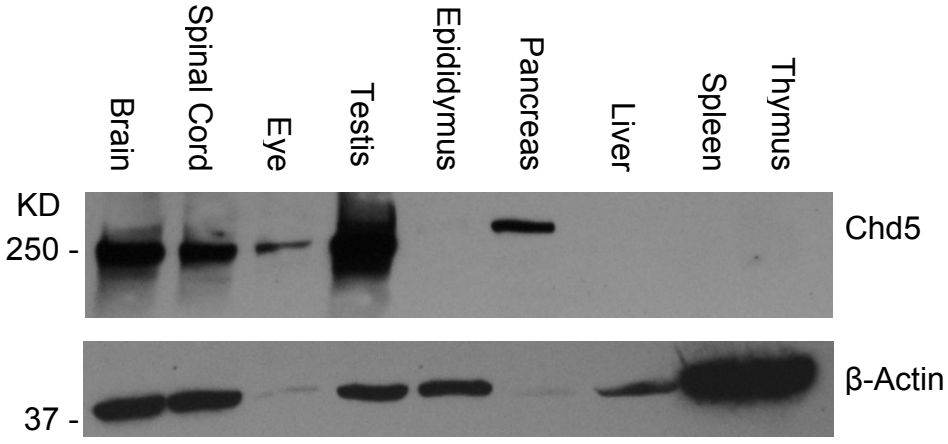

Figure 1. Chd5 protein was highly expressed in testis.

Western blot analyses of Chd5 across a panel of wild type mouse tissues confirmed that Chd5 protein was detected in neural tissues (brain, spinal cord and eye) as previously reported. Meanwhile, it revealed that Chd5 was also highly expressed in testis and pancreas. Equal amount of total protein was loaded for each tissue which however showed uneven β-Actin expression.

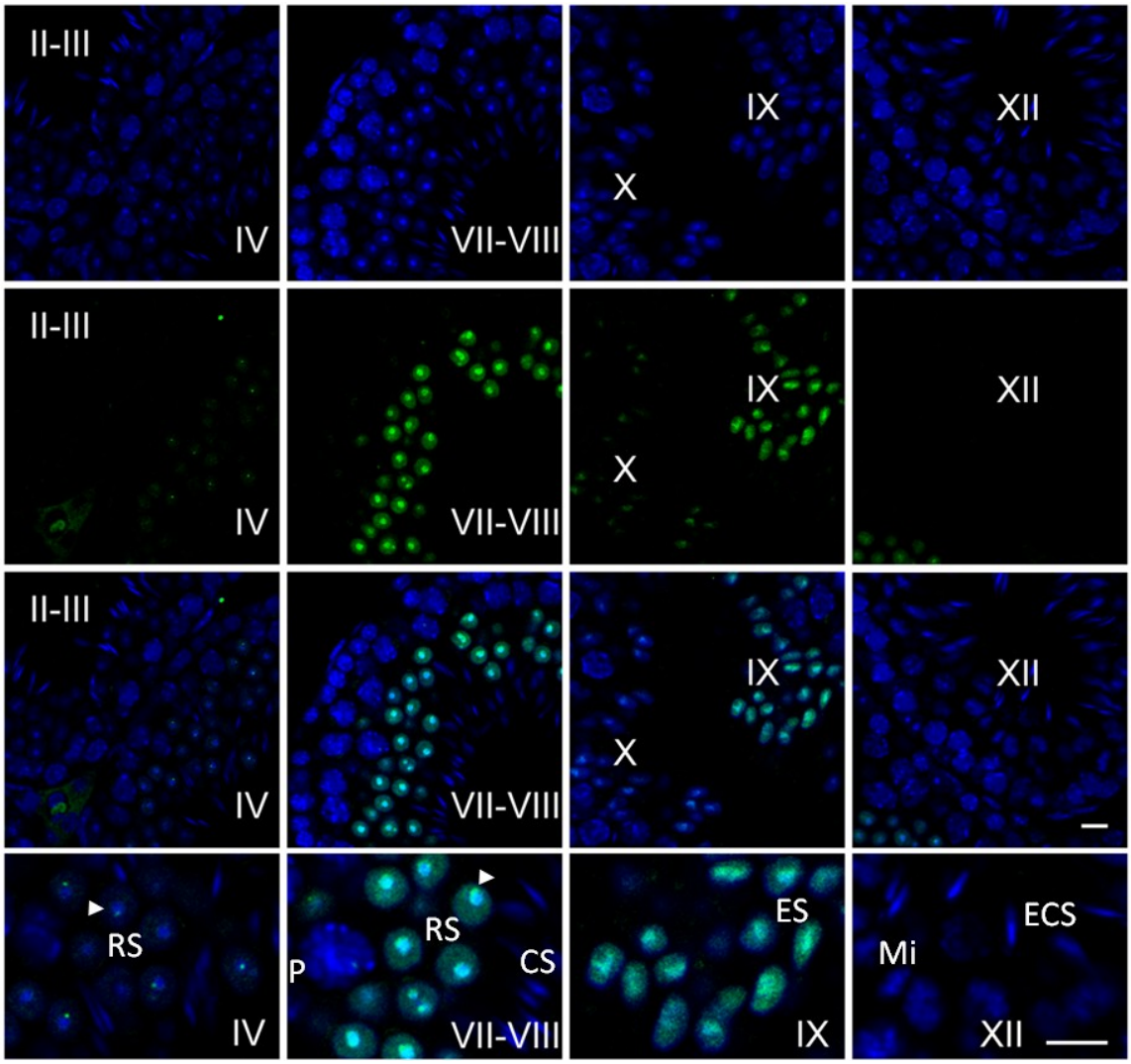

Figure 2. Chd5 was specifically expressed from step 4 to step 10 spermatids in testis.

Immunostaining of wild type testes showed that Chd5 was specifically expressed from step 4 to 10 spermatids and was enriched in heterochromatic chromocenter in testis. Roman numerals indicated the spermatogenic stages of the tubules. Blue, DAPI; Green, Chd5; RS, round spermatids; ES, elongating spermatids; ECS, elongating and condensing spermatids; CS, condensed spermatids; P, pachytene spermatocytes; Mi, meiotic figure. Arrow heads marked chromocenter, a cluster of centromeres and pericentrric heterochromatin. Scale bar, 10 μm.

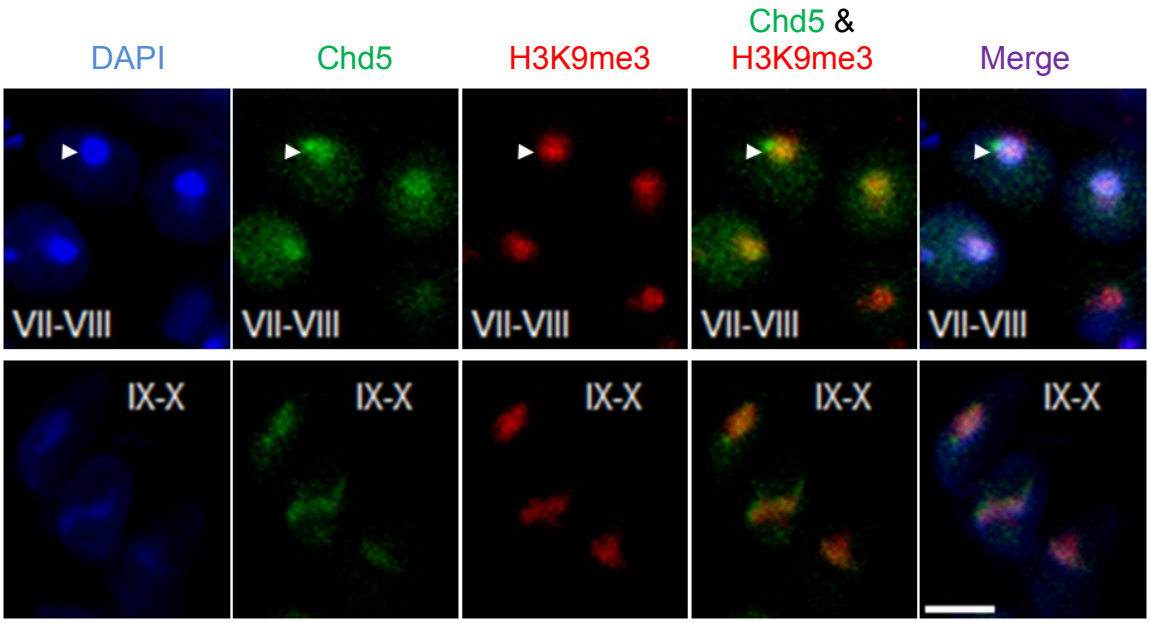

Figure 3. Chd5 was enriched in heterochromatin and co-localized with H3K9me3 in round and elongating spermatids.

Immunostaining of wild type testes revealed that Chd5 was enriched in DAPI-intense heterochromatin region and co-localized with heterochromatin marker H3K9me3 in round and elongating spermatids. Roman numerals indicated the spermatogenic stages of the tubules. Top panel, step 7-8 round spermatids; bottom panel, step 9-10 elongating spermatids. Arrow heads marked chromocenter. Scale bar, 5 μm.

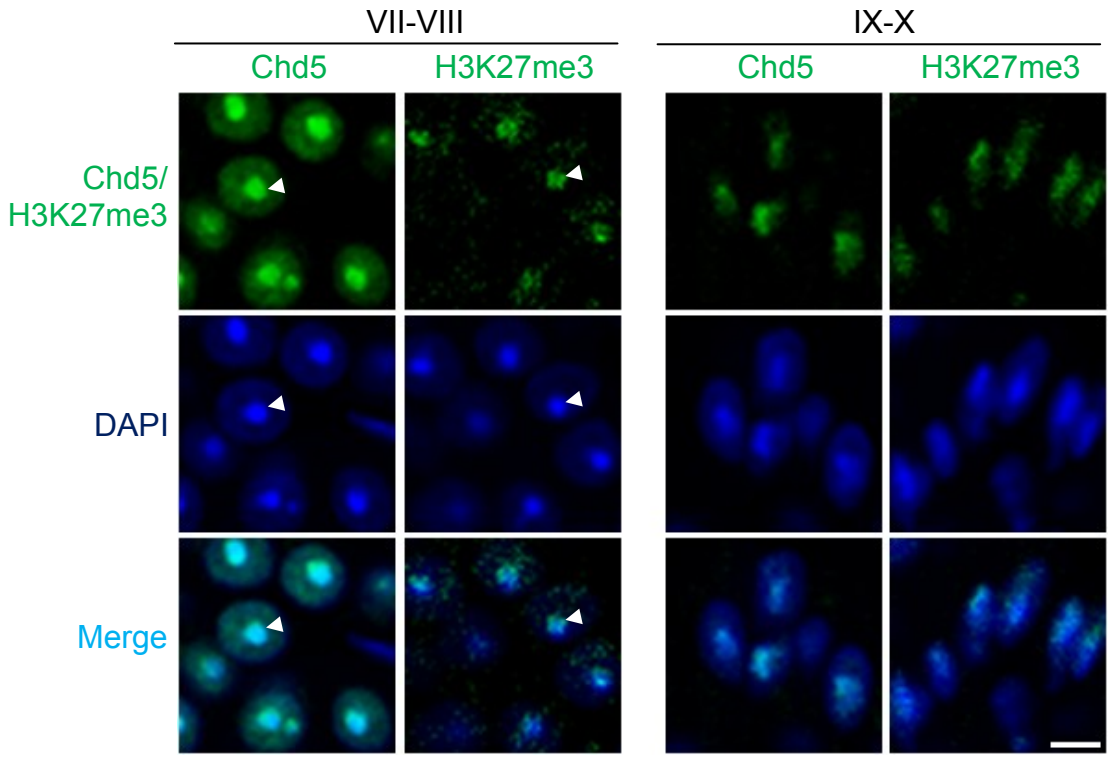

Figure 4. Chd5 was expressed in a similar pattern as H3K27me3 in round and elongating spermatids.

Immunostaining of wild type testes showed that both Chd5 and H3K27me3 were enriched in the heterochromatic chromocenter of round spermatids and DAPI-intense heterochromatic region of early elongating spermatids in wild type testes. Roman numerals indicated spermatogenic stages. Arrow heads marked chromocenter. Scale bar, 5 μm.

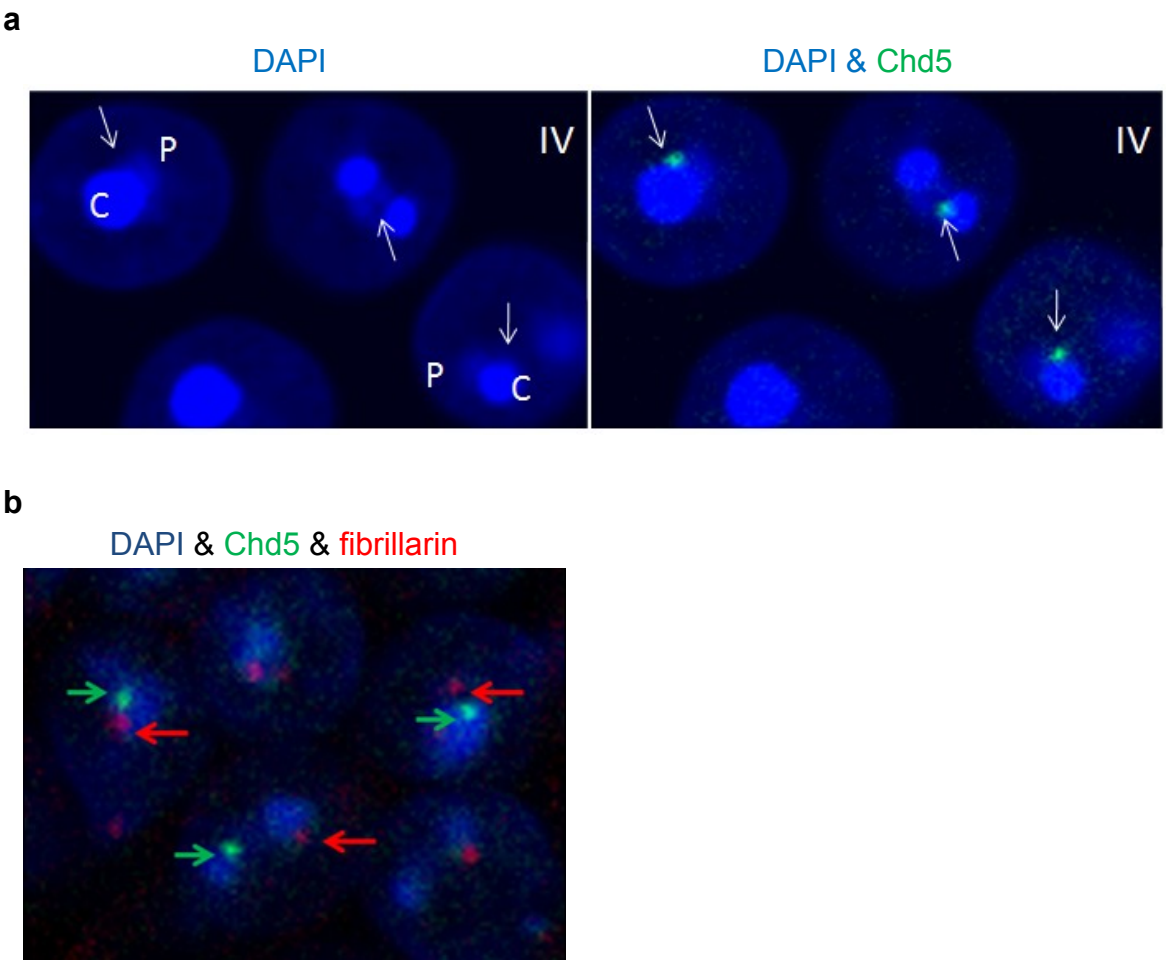

Figure 5. Intense Chd5 expression in proximity to nucleolus

Immunostaining of wild type testes revealed that an intense Chd5 spot was present around the junction edge of chromocenter and post-meiotic sex chromosome, both of which were heterochromatic, and appeared in proximity to nucleolus in round spermatid. **a,** Blue, DAPI; Green, Chd5; C, chromocenter; P, post-meiotic sex chromosome (PMSC); IV, spermatogenic stage IV; **b,** Blue, DAPI; Green, Chd5; Red, fibrillarin, a nucleolus marker. Arrows pointed to spots of intense Chd5 or fibrillarin expression.

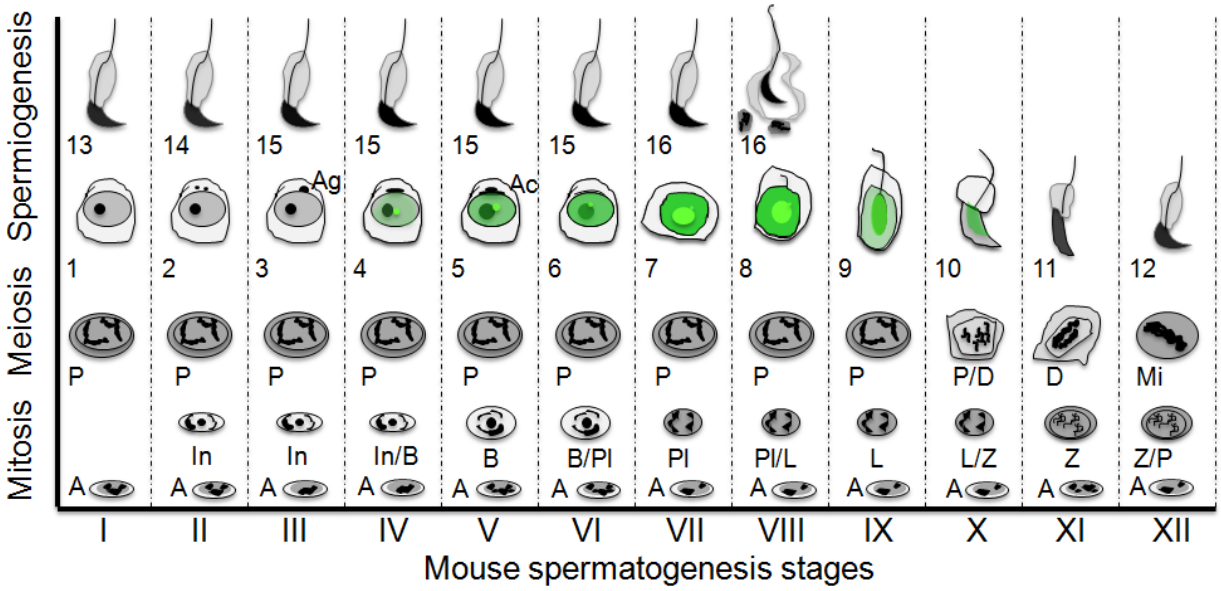

Figure 6. Schematic of Chd5 expression during spermatogenesis

Spermatogenesis is divided into twelve stages (stage I-XII) in mouse and each stage has a distinct cellular composition. Spermiogenesis, the maturation process of haploid spermatid, is further divided into 16 steps (step 1-16). Chd5 was specifically expressed in spermatids from step 4 to step 10 with peak expression in step 7-8 round spermatids, where Chd5 also showed enrichment in heterochromatic chromocenter. A spot of intense Chd5 protein expression was present around the edge of chromocenter in step 4-8 spermatids. Roman numerals indicated the spermatogenic stages. Arabic numbers (1-16) designated spermiogenic steps of the spermatids. Green marked Chd5 protein expression and brighter green indicated stronger expression. Spermatogonia (A, In, B); Spermatocyte (Pl, preleptotene; L, leptotene; Z, zygotene; P, pachytene; D, diakinesis; Mi, meiotic figure); Ag, acrosomic granule; Ac, acrosomic cap. The diagram was drawn based on the illustration of Dr. Rex Hess *et al.* in Chapter 1, *Molecular Mechanisms in Spermatogenesis*, Springer, 2008.

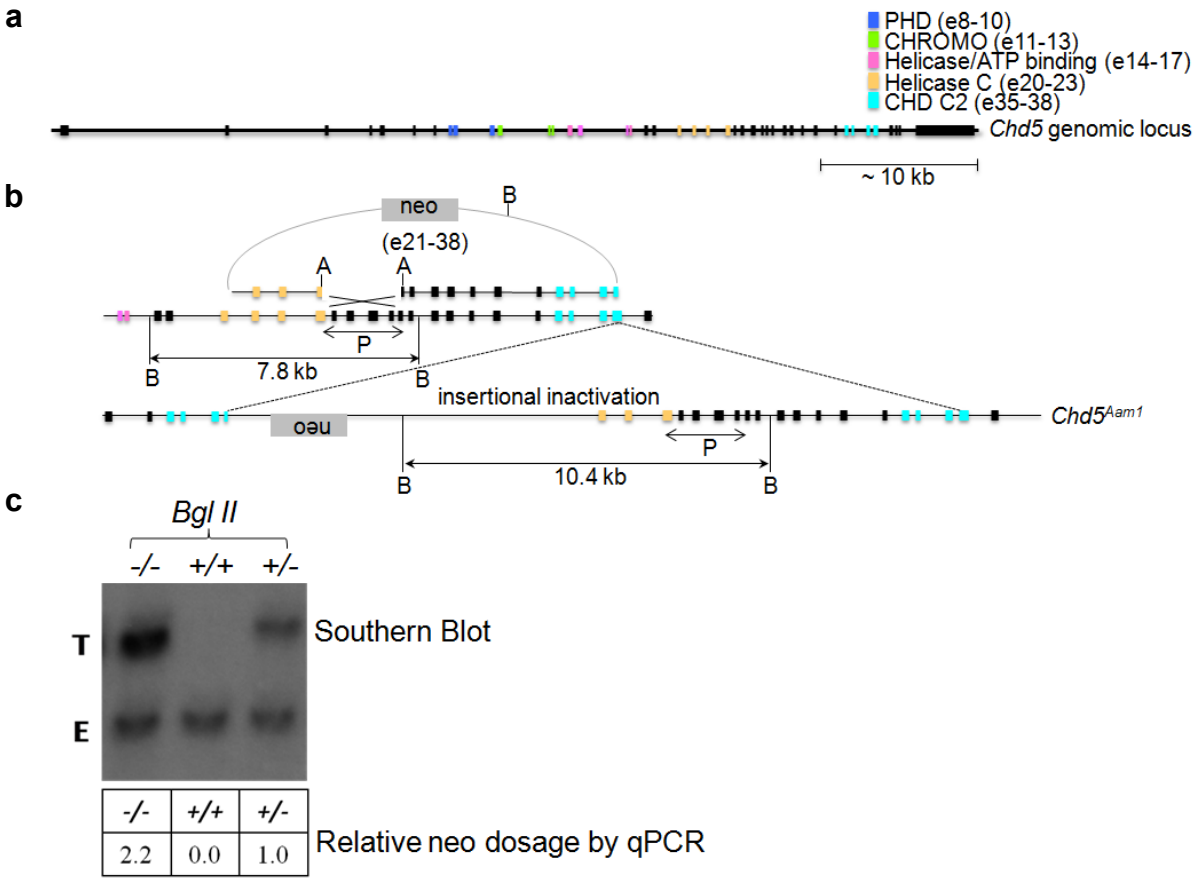

Figure 7. Generation of *Chd5*^{Aam1} mice through gene targeting

a, Genomic structure of mouse *Chd5*. Exons encoding predicted domains were marked by colors. **b,** Diagram of insertion targeting vector as well as wild-type and targeted *Chd5*^{Aam1} alleles. A, *Afl* II; B, *Bgl* II; P, location of the 2.6 kb probe for Southern blot; neo, neomycin cassette. **c,** Top panel, Southern blot analysis of *Bgl* II digested DNA from *Chd5*$^{Aam1+/+}$ *(+/+)*, *Chd5*$^{Aam1+/-}$*(+/-)* and *Chd5*$^{Aam1-/-}$*(-/-)* mice. T, targeted band (10.4 kb); E, endogenous band (7.8 kb). *Chd5*$^{Aam1-/-}$ lane had a more intense T band than *Chd5*$^{Aam1+/-}$ lane, as *Chd5*$^{Aam1-/-}$ cells had two copies of the targeted 10.4 kb band while *Chd5*$^{Aam1+/-}$ cells had only one copy. The endogenous band served as a loading control. Bottom panel, quantification of dosage of neo-cassette by qPCR was used for genotyping.

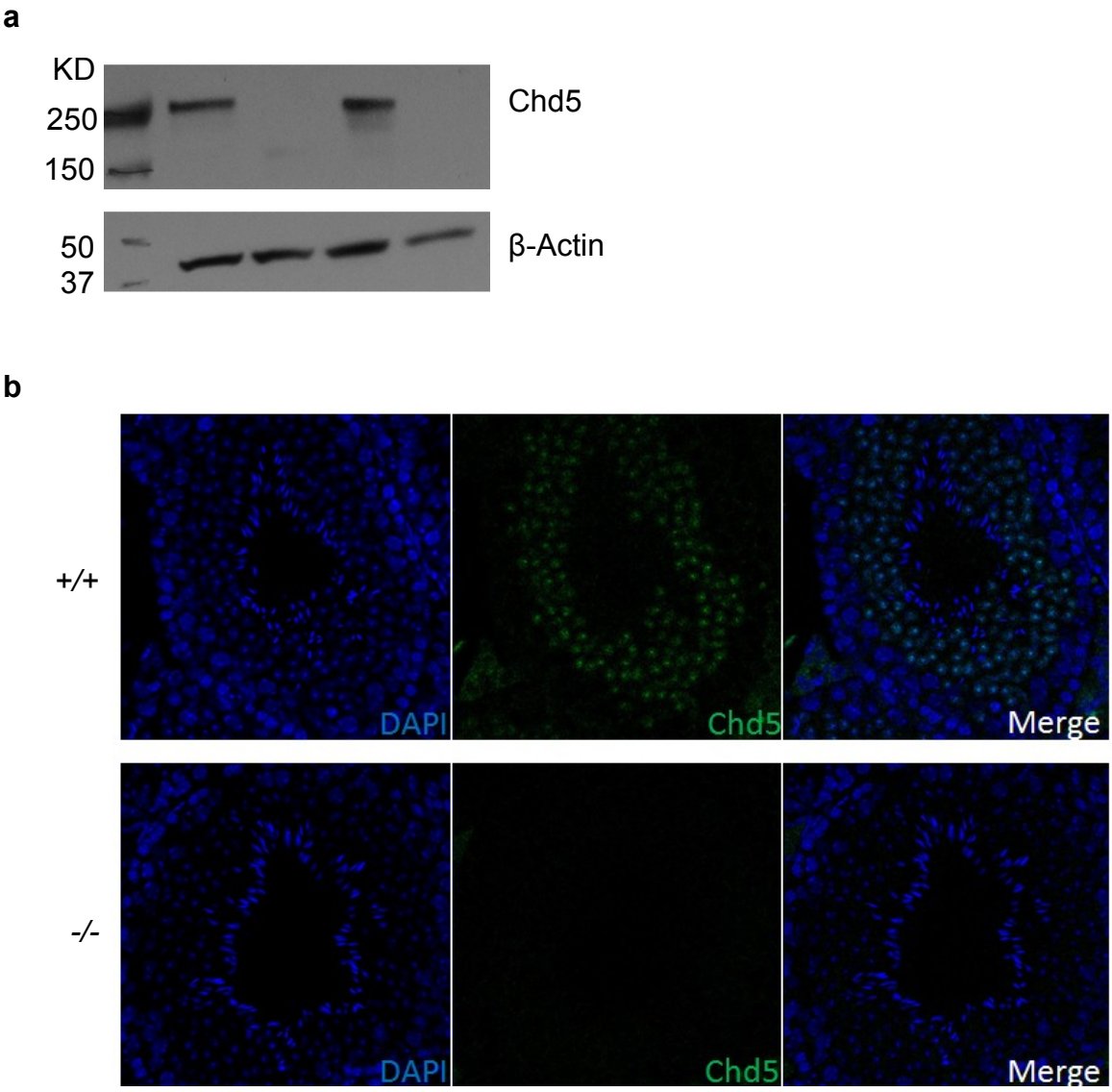

Figure 8. Chd5 protein was not detected in *Chd5*$^{Aam1-/-}$ testes by neither immunobloting nor immunostaining.

a, Western blot of Chd5 on total testis lysates from wild type and *Chd5*$^{Aam1-/-}$ mice. Wild type Chd5 protein in mouse has 1952 amino acids and a molecular weight of approximately 250 KD. **b,** Immunostaining of Chd5 on wild type and *Chd5*$^{Aam1-/-}$ testis sections. +/+, *Chd5*$^{Aam1+/+}$; -/-, *Chd5*$^{Aam1-/-}$.

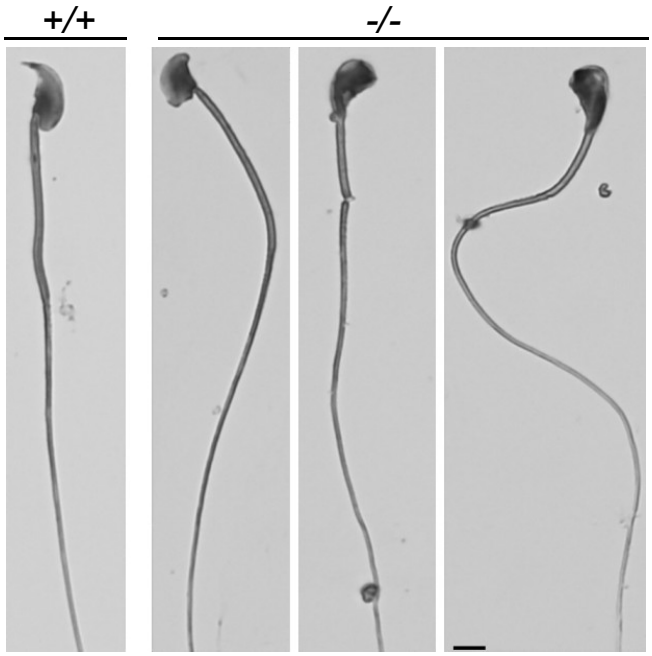

Figure 9. Abnormal head morphology of *Chd5*$^{Aam1-/-}$ sperm

Sperm collected from caudal epididymi of wild type and *Chd5*$^{Aam1-/-}$ male mice were spread on glass slides, stained with hematoxylin and examined using light microscopy at 100 fold magnification. Over 100 sperm from each mouse of three *Chd5*$^{Aam1+/+}$ and five *Chd5*$^{Aam1-/-}$ littermates were evaluated. Representative abnormal morphology observed in *Chd5*$^{Aam1-/-}$ sperm was shown. Statistics was presented in Table 3. +/+, *Chd5*$^{Aam1+/+}$; -/-, *Chd5*$^{Aam1-/-}$. Scale bar, 20 μm.

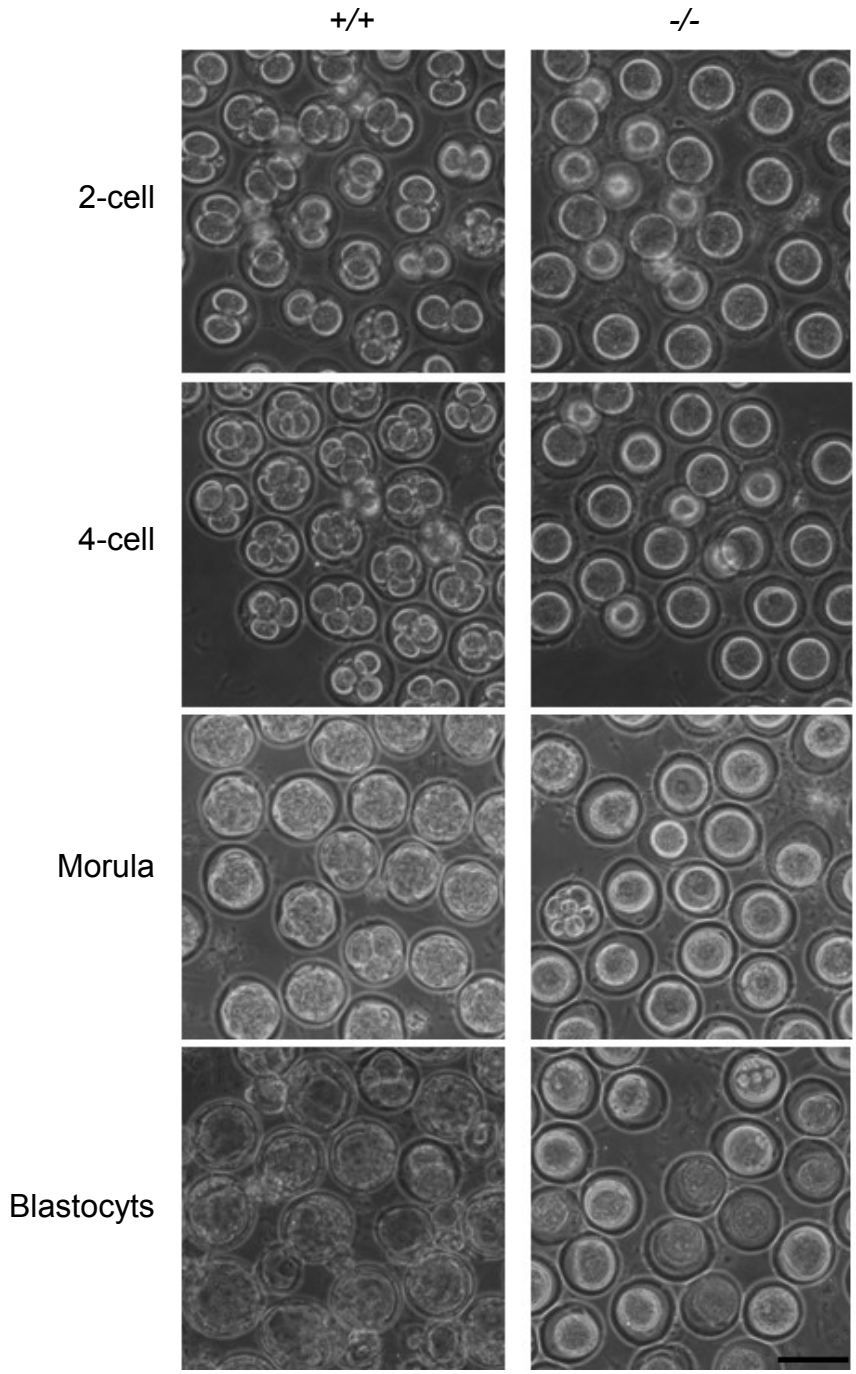

Figure 10. *Chd5*$^{Aam1-/-}$ sperm failed to fertilize wild type oocytes by *in vitro* fertilization.

Equal amount (0.35 million) of *Chd5*$^{Aam1+/+}$ and *Chd5*$^{Aam1-/-}$ sperm from three pairs of littermate mice were used to fertilize wild type oocytes *in vitro*. Oocytes were fertilized by wild type sperm and develop into blastocyts after approximately 4 days. However, *Chd5*$^{Aam1-/-}$ sperm failed to fertilize oocytes. +/+, *Chd5*$^{Aam1+/+}$; -/-, *Chd5*$^{Aam1-/-}$. Scale bar, 100 µm. (See Table 4 for statistics)

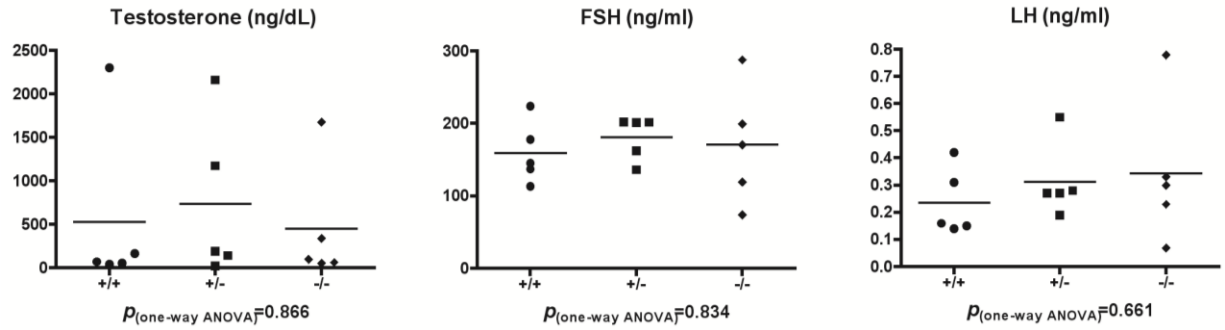

Figure 11. No significant change of serum sex hormone levels in Chd5-deficient male mice.

Serum were prepared from cohorts of male mice with indicated genotypes, and levels of follicle-stimulating hormone (FSH), leutinizing hormone (LH) and testosterone in the serum were examined by the Ligand Core Laboratory at University of Virginia. Each symbol represented an individual male mouse and the horizontal bar denoted the mean of the group. Data were analyzed by one-way ANOVA. No statistically significant difference was observed among the three genotypes. +/+, *Chd5*$^{Aam1+/+}$; +/-, *Chd5*$^{Aam1+/-}$; -/-, *Chd5*$^{Aam1-/-}$.

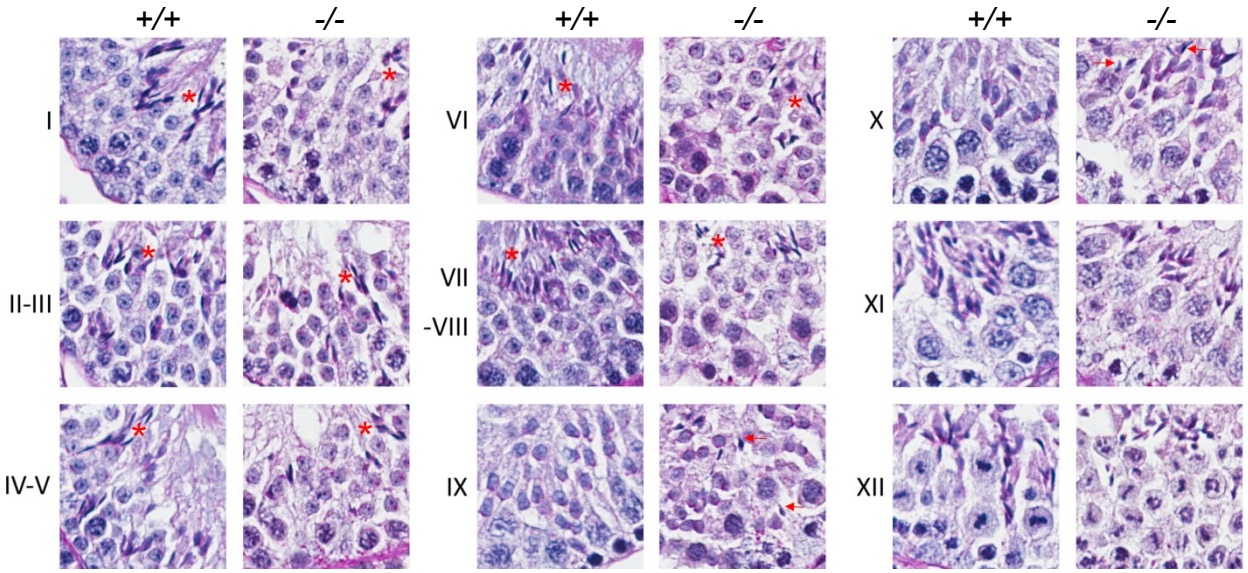

Figure 12. Staged comparison of Periodic Acid-Schiff (PAS) stained *Chd5*$^{Aam1+/+}$ and *Chd5*$^{Aam1-/-}$ testes.

Roman numerals indicated the stages of the seminiferous tubules (see Introduction and Illustration 2 for staging criteria). Decreased amount of late spermatids (marked by *), especially in stage VII-VIII, were observed in *Chd5*$^{Aam1-/-}$ tubules. Red arrows in stage IX and X tubules marked abnormal retention of condensed spermatids in the epithelium, which were normally released into the lumen by stage IX.

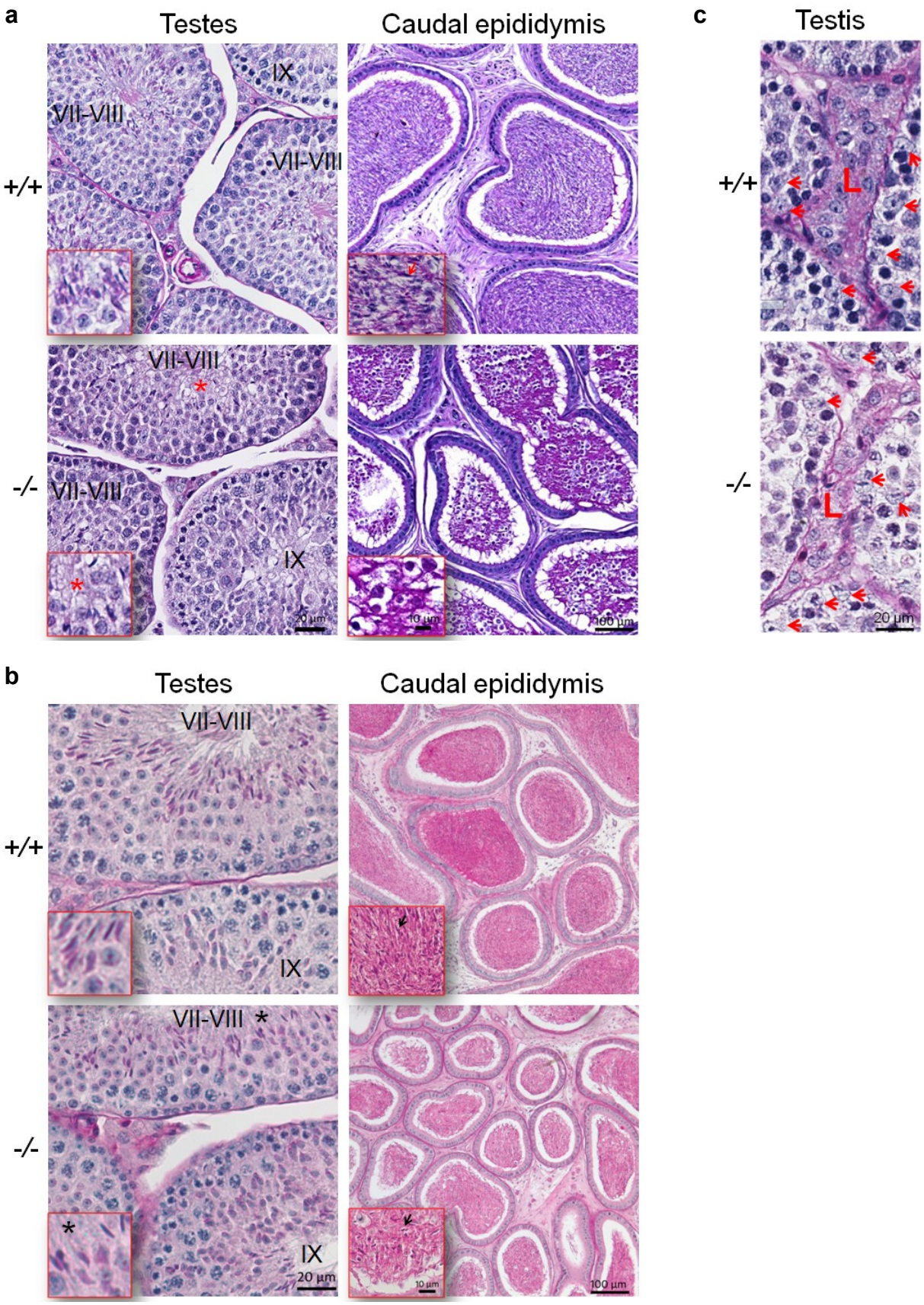
a
Testes
Caudal epididymis
+/+
-/-
VII-VIII
IX
20 µm
10 µm
100 µm
c
Testis
L
20 µm
b
Testes
Caudal epididymis
+/+
-/-
VII-VIII
IX
20 µm
10 µm
100 µm

Figure 13. Histological analyses showed a range of spermatogenic defects in individual *Chd5*$^{Aam1-/-}$ mice.

a, PAS stained testes and caudal epididymis of *Chd5*$^{Aam1+/+}$ *(+/+)* and *Chd5*$^{Aam1-/-}$ *(-/-)* mice. Roman numerals indicated the stages of the seminiferous tubules. The inserts were magnified views of representative areas. ***** indicated compromised spermatid number in *Chd5*$^{Aam1-/-}$ tubules than in *Chd5*$^{Aam1+/+}$ tubules of the same stages. The arrow pointing to a dark head indicated a sperm within the caudal epididymus. Sperm were not present in *Chd5*$^{Aam1-/-}$ caudal epididymus. **b,** Similar but less severe histopathology in a different *Chd5*$^{Aam1-/-}$ mouse. ***** indicated modestly compromised spermatid number in *Chd5*$^{Aam1-/-}$ tubules than in *Chd5*$^{Aam1+/+}$ tubules of the same stages. The arrows pointing to dark heads indicated sperm within the caudal epididymus. Sperm were present in *Chd5*$^{Aam1-/-}$ caudal epididymis but to a lower extent compared to wild type control. **c,** No significant difference was observed in Sertoli cells (the lightly stained cells indicated by arrows) or Leydig cells (the cells located within L areas) between *Chd5*$^{Aam1+/+}$ and *Chd5*$^{Aam1-/-}$ testis.

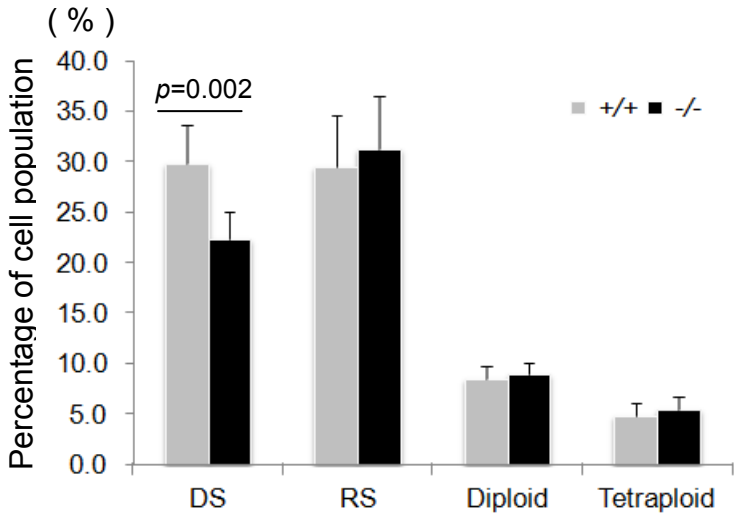

Figure 14. DNA content profiling of total testicular cells showed a reduction in the differentiated spermatid population in *Chd5*$^{Aam1-/-}$ testes.

Single-cell suspensions were prepared from whole testes of indicated genotypes, stained with propidium iodide and analyzed for DNA content through flow cytometry (LSR II, Becton Dickinson) to quantify tetraploid, diploid and haploid populations. Due to DNA condensation, haploid differentiated spermatids (DS), i.e. elongating and elongated spermatids, were stained more weakly by propidium iodide than haploid round spermatids (RS), thus giving two peaks for the haploid population. +/+, *Chd5*$^{Aam1+/+}$; -/-, *Chd5*$^{Aam1-/-}$. Data were presented as mean ± s.d. from three independent experiments using sperm prepared from three pairs of *Chd5*$^{Aam1+/+}$and *Chd5*$^{Aam1-/-}$ littermate mice. Two-tail Student's t-test was used to detect statistically significant difference in each population between *Chd5*$^{Aam1+/+}$and *Chd5*$^{Aam1-/-}$. Only the DS population showed significant difference (p=0.002).

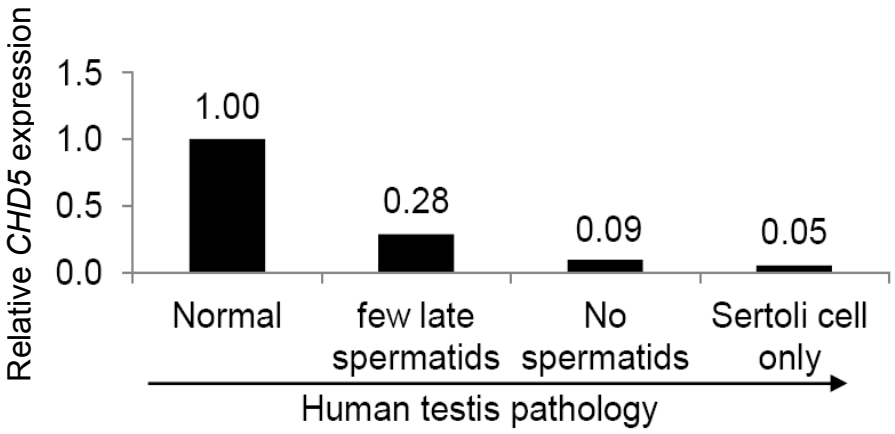

Figure 15. Low *CHD5* expression correlated with spermatogenic defects in humans.

Data were derived from published microarray expression dataset of 39 human testis samples with defined spermatogenic defects and 10 normal controls (ArrayExpress: E-TABM-234). Data were analyzed through the bioinformatics company NextBio and relative *CHD5* expressions in samples with spermatogenic defects were calculated by normalizing to the expression of normal controls. Arrow line indicated increased severity of spermatogenic defects. Normal, testis samples from fertile men with full spermatogenesis; few late spermatids, testis samples that contain few late condensed spermatids but have many spermatids of earlier steps; no spermatids, testis samples that don't have any type of spermatids but have spermatocytes, spermatogonia, Sertoli cells and other spermatogenic cells; Sertoli cell only, testis samples that only contain Sertoli cells but don't have germ cells, i.e. spermatogonia, spermatocytes and spermatids.

Table 1. Mating tests revealed infertility in *Chd5*$^{Aam1-/-}$ male mice

Sex	Genotype	Infertile mice/Total	Fertile mice/Total	Total litter#	Total progeny	Average litter size
Male	*Chd5*$^{Aam1+/+}$	0/8	8/8	24	145	6.0
	Chd5$^{Aam1+/-}$	0/8	8/8	16	104	6.5
	Chd5$^{Aam1-/-}$	4/8	4/8	7	20	2.8
Female	*Chd5*$^{Aam1+/+}$	0/4	4/4	8	52	6.5
	Chd5$^{Aam1-/-}$	0/4	4/4	7	48	6.8

When mated to wild type females for approximately 4 months, 4 out of 8 *Chd5*$^{Aam1-/-}$ male mice tested were infertile. The remaining 4 were subfertile, producing only 27.6% (20/72) of the offspring of their *Chd5*$^{Aam1+/+}$ littermates. In contrast, *Chd5*$^{Aam1+/-}$ male mice and *Chd5*$^{Aam1-/-}$ female mice were as fertile as their wild type counterparts.

Table 2. Reduced sperm counts and motility in *Chd5*$^{Aam1-/-}$ mice

Genotype	N	Sperm/caudal epididymis (X10^6)	All motile sperm (%)	Progressive motile sperm (%)
Chd5$^{Aam1+/+}$	7	5.52±1.13	62.3±5.4	48.6±11.3
Chd5$^{Aam1+/-}$	4	6.51±0.68	66.0±3.8	52.8±2.3
Chd5$^{Aam1-/-}$	11	2.74±0.68	42.4±10.3	21.0±5.7
$p_{(+/+ \text{ vs } +/-)}$		0.103	0.228	0.375
$p_{(+/+ \text{ vs } -/-)}$		0.0002*	0.0055*	0.0004*

N indicated the number of mice used for the indicated sperm analyses. *p* value was two-tail Student's t-test result between the indicated genotypes. **+/+,** *Chd5*$^{Aam1+/+}$; *-/-, Chd5*$^{Aam1-/-}$; * indicated statistical significance.

Table 3. Increased abnormal sperm morphology in *Chd5*$^{Aam1-/-}$ mice

Genotype	N	Abnormal sperm morphology	
		Total (%)	Head (%)
Chd5$^{Aam1+/+}$	3	55.7±6.1	32.5±13.6
Chd5$^{Aam1-/-}$	5	85.4±8.6	65.3±7.8
$p_{(+/+ \text{ vs } -/-)}$		0.002*	0.035*

N indicated the number of mice used for the evaluation in each genotype. For each mouse, over 100 sperm were evaluated for morphology. "Total (%)" indicated percentage of sperm with abnormal morphology in any sperm structure(s) including head, neck, mid-piece and tail. "Head (%)" indicated percentage of sperm with abnormal head morphology. *p* value was two-tail Student's t-test result between the indicated genotypes. **+/+,** *Chd5*$^{Aam1+/+}$; **-/-,** *Chd5*$^{Aam1-/-}$; ***** indicated statistical significance.

Table 4. *Chd5*$^{Aam1-/-}$ sperm failed to fertilize wild type oocytes by *in vitro* fertilization

Littermate pairs	Genotype	Sperms used for IVF (million)	Oocytes used for IVF	Oocytes fertilized	Blastocysts developed
1	*Chd5*$^{Aam1+/+}$	0.35	53	23 (43.4%)	17 (32%)
	Chd5$^{Aam1-/-}$	0.35	56	3 (5.4%)	0 (0%)
2	*Chd5*$^{Aam1+/+}$	0.35	114	46 (40.4%)	43 (37.7%)
	Chd5$^{Aam1-/-}$	0.35	108	0 (0%)	0 (0%)
3	*Chd5*$^{Aam1+/+}$	0.35	90	29 (32.2%)	26 (28.9%)
	Chd5$^{Aam1-/-}$	0.35	84	0 (0%)	0 (0%)

Approximately equal number of *Chd5*$^{Aam1+/+}$ and *Chd5*$^{Aam1-/-}$ sperm derived from 3 pairs of littermates were used to fertilize wild type oocytes *in vitro*. The sperm from two *Chd5*$^{Aam1-/-}$ mice failed to fertilize oocytes. Sperm from one *Chd5*$^{Aam1-/-}$ mouse fertilized 5.4% (3/56) of the oocytes, which developed into 2-cell stage but did not develop further. In contrast, sperm from *Chd5*$^{Aam1+/+}$ fertilized 32.2 - 43.4% of the oocytes with 28.9% - 37.7% of the oocytes developing into blastocysts (See Figure 10 for images).

Chapter 3

Chd5 deficiency impaired chromatin remodeling during spermatid maturation

To test the hypothesis that Chd5 plays an important role in the extensive chromatin remodeling process during spermiogenesis, I next investigated the chromatin remodeling aspects of spermiogenesis in Chd5-deficient mice.

3.1 Defective chromatin condensation in Chd5-deficient sperm

Abnormal chromatin remodeling during spermiogenesis could lead to impaired chromatin integrity in sperm. I thus checked whether Chd5 deficiency compromised sperm chromatin integrity using a standard technique called Sperm Chromatin Structure Assay (SCSA). SCSA stains acid-treated sperm with acridine orange, which emits green fluorescence when bound to double-strand DNA, but emits red fluorescence when bound to single-strand DNA. Sperm with impaired chromatin integrity have more DNA denatured by the acid treatment and thus emit more red fluorescence. SCSA measures the red and green fluorescence emitted by the sperm using flow cytometry and quantifies the percentage of red versus total (red + green) fluorescence, which is defined as DNA Fragmentation Index (DFI). High DFI therefore reflects impaired chromatin integrity [157]. SCSA analyses showed that *Chd5*$^{Aam1-/-}$ sperm had an approximately 3 fold increase of DFI compared to wild type sperm (Figure 16a), reflecting impaired chromatin integrity in *Chd5*$^{Aam1-/-}$ sperm. I further examined chromatin of *Chd5*$^{Aam1-/-}$ sperm and their wild type counterparts using transmission electron microscopy (TEM). TEM revealed that whereas chromatin in nuclei of normal wild type sperm were homogeneously condensed, less condensed chromatin with fibrillar texture and uneven density were observed in nuclei of *Chd5*$^{Aam1-/-}$ sperm

(Figure 16b). Abnormal vacuoles were also observed in *Chd5*$^{Aam1-/-}$ sperm nuclei (Figure 16b). In addition, abnormal retention of cytoplasm and abnormal bulges between the acrosome and nuclei were observed in *Chd5*$^{Aam1-/-}$ sperm (Figure 16b). Although abnormal vacuoles were also occasionally present in some wild type sperm, quantification revealed an approximately 3 fold increase in the number of sperm with abnormal vacuoles in *Chd5*$^{Aam1-/-}$ mice (Figure 16c). These findings revealed defective chromatin condensation in Chd5-deficient sperm, suggesting that Chd5 may play a role in chromatin compaction during sperm development.

3.2 Aberrant histone-to-protamine replacement in Chd5-deficient spermatids

Sperm chromatin condensation is achieved mainly during spermiogenesis, when somatic histones and nucleosomes are removed and temporarily replaced with transition proteins and ultimately, protamines. To define the mechanism whereby Chd5 deficiency may affect chromatin compaction during spermiogenesis, I used Western blotting to assess expression of a panel of somatic histones, transition proteins and protamines in spermatids at different steps of spermiogeneis. In order to isolate spermatids at different spermiogenic steps, I applied a technique called centrifugal elutriation, which is capable of separating cells mainly based on their sizes. Pioneered by Dr. Meistrich *et al.* in the early 1970s, centrifugal elutriation has been widely used to fractionate testicular cells into different populations with high purity, as spermatids at different spermiogenic steps have significantly different cell sizes and morphologies. With the instruction of Dr. Meistrich, I was able to master this technique and became proficient at fractionating testicular cells into subpopulations of round spermatids (RS), elongating and condensing spermatids (ECS) and condensed spermatids (CS) with over 90% purity (Figure 17). Western blot analyses of protein lysate from different steps of spermiogenic

cells showed that canonical core nucleosomal histones H4, H3, H2B, H2A and H1 were rapidly depleted after the round spermatid steps in wild type testes, with minimal retention in condensing and condensed spermatids (Figure 18). In contrast, these histones were retained to a higher extent in differentiated *Chd5*$^{Aam1-/-}$ spermatids, implying deficient histone removal in *Chd5*$^{Aam1-/-}$ testes (Figure 18). Meanwhile, transition proteins (Tnp1 and Tnp2) and protamines (Prm1 and Prm2) were both up-regulated in differentiated *Chd5*$^{Aam1-/-}$ spermatids (Figure 19). Consistent with the Western blot results, immunofluorescence analyses of Tnp1 in *Chd5*$^{Aam1+/+}$ and *Chd5*$^{Aam1-/-}$ testes revealed that Tnp1 was barely detected in step 9-10 spermatids in stage IX-X tubules of *Chd5*$^{Aam1+/+}$ testes but was detected in step 9-10 spermatids of *Chd5*$^{Aam1-/-}$ testes (Figure 20). Strong Tnp1 expression was detected in step 14 spermatids in stage II-III tubules of both *Chd5*$^{Aam1+/+}$ and *Chd5*$^{Aam1-/-}$ testes, but showed higher intensity in *Chd5*$^{Aam1-/-}$ tubules (Figure 20). Tnp1 was no longer detectable in step 15 spermatids in stage V-VI tubules of *Chd5*$^{Aam1+/+}$ testes but was still detected in a portion of step 15 spermatids of *Chd5*$^{Aam1-/-}$ testes (Figure 20). Similarly, immunofluorescent analyses of Tnp2 in *Chd5*$^{Aam1+/+}$ and *Chd5*$^{Aam1-/-}$ testes revealed that Tnp2 was first detected in step 10 spermatids in stage X tubules of *Chd5*$^{Aam1+/+}$ testes but showed stronger staining in step 10 spermatids of *Chd5*$^{Aam1-/-}$ tubules (Figure 21). Strong Tnp2 expression was detected in step 14 spermatids in stage II tubules of both *Chd5*$^{Aam1+/+}$ and *Chd5*$^{Aam1-/-}$ testes, but showed higher intensity in *Chd5*$^{Aam1-/-}$ tubules (Figure 21). Tnp2 became only weakly detectable in a small portion of step 15 spermatids in stage IV tubules of *Chd5*$^{Aam1+/+}$ testes but was still strongly expressed in step 15 spermatids of *Chd5*$^{Aam1-/-}$ tubules (Figure 21). These results indicated that Tnp1 and Tnp2 protein expression started earlier, appeared stronger and lasted longer during spermiogenesis in *Chd5*$^{Aam1-/-}$ testes than in wild type testes. Immunofluorescence analyses of Prm1 and Prm2 didn't produce good quality results

probably due to technical issue of antibody penetration into highly condensed protamines in spermatids. However, Western blot analyses (Figure 19) clearly showed elevated levels of protamines in late *Chd5*$^{Aam1-/-}$ spermatids. Abnormal levels of protamines likely contributed to impaired fertility of *Chd5*$^{Aam1-/-}$ male mice, as precise control of Prm1 and Prm2 levels is critical for male fertility [70, 158]. Consistent with the increased histone retention and elevated levels of transition proteins and protamines in *Chd5*$^{Aam1-/-}$ spermatids, Western blot analyses of mature sperm also revealed increased levels of histones H4, H3, H2A, H2B and H1 as well as protamines in *Chd5*$^{Aam1-/-}$ sperm compared to *Chd5*$^{Aam+/+}$ sperm (Figure 22). Together, these results showed that Chd5 deficiency led to abnormality of both histone disposition and homeostasis of transition proteins and protamines during spermiogenesis, suggesting that Chd5 may play important roles in the histone-to-protamine remodeling process during sperm development.

3.3 Compromised H4 acetylation in Chd5-deficient spermatids

Since Western blot analyses revealed deficient histone removal in *Chd5*$^{Aam1-/-}$ spermatids, I sought to understand the mechanism whereby Chd5 deficiency could impair histone removal. The current understanding of the molecular mechanisms underlying histone removal during spermiogenesis is limited, however H4 hyperacetylation in early elongating spermatids is believed to be a key modification to loosen up the nucleosome DNA structure to facilitate histone removal [21-23]. H4 hyperacetylation is essential for histone-to-protamine replacement in *Drosophila* [24] and considered also a prerequisite for histone-to-protamine replacement during mammalian spermiogenesis [12, 23, 24]. I noticed that Chd5 had similar expression dynamics as H4 hyperacetylation during spermiogenesis, but immediately preceded it (Figure

23a). In step 9-10 spermatids, Chd5 co-localized with acetylated H4 (H4Ac) (Figure 23a). Thus, I hypothesized that Chd5 modulates H4 hyperacetylation during spermiogenesis. Indeed, whereas more total histone H4 was retained, H4Ac was substantially reduced in differentiated *Chd5*$^{Aam1-/-}$ spermatids (Figure 23b). Since H4Ac was critical for facilitating nucleosome destabilization and histone removal during spermiogenesis, deficiency of H4Ac in *Chd5*$^{Aam1-/-}$ spermatids would likely lead to defective nucleosome destabilization and histone removal. In addition, H4Ac was recently shown to mediate degradation of histones during spermatogenesis through a testis-specific proteosome that contains bromo domain-like regions [159]. Thus, the severe deficiency of H4Ac in *Chd5*$^{Aam1-/-}$ spermatids may also lead to deficient histone degradation and thus increased histone retention.

3.4 Prolonged nucleosome retention in Chd5-deficient spermatids

It has been postulated that H4 hyperacetylation facilitates subsequent nucleosome eviction [12, 23, 24]. I therefore asked whether reduced H4 acetylation in *Chd5*$^{Aam1-/-}$ spermatids could compromise nucleosome eviction. Using an antibody specific for intact nucleosomes [160], I found that nucleosomes were detectable from step 1 to step 11 spermatids but were depleted in step 12-16 spermatids in wild type testes (Figure 24a). In contrast, nucleosomes were retained in *Chd5*$^{Aam1-/-}$ spermatids as late as step 14 (Figure 24b), implying inefficient nucleosome eviction in *Chd5*$^{Aam1-/-}$ spermatids.

3.5 Increased DNA damage in Chd5-deficient spermatids

Since DNA tightly wraps the histone octamer of a nucleosome in a left-handed supercoil, eviction of nucleosome generates DNA supercoiling tension [161]. The massive nucleosome

eviction during spermiogenesis thus produces intense supercoiling tension that need be relieved. Previous studies indicate that topoisomerase II beta (Top2β) catalyzes resolution of such supercoils in elongating spermatids. Double-strand breaks (DSBs) are generated during the resolution of supercoils, and a DNA damage response is then triggered to repair the DSBs in order to maintain genome integrity [162-165]. It has been shown that CHD family members CHD2, CHD3 and CHD4 play important roles in DSB repair and their deficiency sensitizes cells to DNA damage [110, 112, 166, 167]. I found that *Chd5* expression was induced by the DNA damaging agent adriamycin in mouse embryonic fibroblasts (Figure 25a), suggesting that Chd5 may also play a role in DNA damage response. Consistent with this speculation, Hall *et al.* recently showed that silencing of CHD5 in human pancreatic cancer cells leads to activation of DNA damage response including increased H2AX-Ser139 (γ-H2A.X, a marker for the DSB-activated DNA damage response) and CHK2-Thr68 phosphorylation and accumulation of nuclear foci [153]. I therefore hypothesized that $Chd5^{Aam1-/-}$ spermatids will have increased DNA damage. Indeed, TUNEL (Terminal deoxynucleotidyl transferase dUTP nick end labeling) analyses revealed an increased level of DNA breaks in differentiated $Chd5^{Aam1-/-}$ spermatids, most notably at step 13-14, a time point when most DNA breaks were repaired in wild type testis (Figure 25b). In agreement with this finding, immunofluorescence analyses showed that whereas γ-H2A.X was cleared in wild type spermatids after step 12, it was detected in $Chd5^{Aam1-/-}$ spermatids as late as step14 (Figure 25c). Western blot analyses further confirmed an increase in γ-H2A.X in differentiated $Chd5^{Aam1-/-}$ spermatids (Figure 25d). These findings revealed increased DNA damage during spermiogenesis in Chd5-deficient testis. The increased DNA damage in $Chd5^{Aam1-/-}$ spermatids could eventually lead to jeopardized chromatin integrity in sperm as revealed by SCSA (Figure 16a).

3.6 Altered expression of histone variants in Chd5-deficient spermatids

In addition to histone acetylation, replacement of canonical core histones of nucleosome with specific histone variants is another key mechanism facilitating the nucleosome eviction and histone removal during spermatogenesis. In mammals, each histone subtype contains from a few to dozens of non-allelic variants [168-171]. Unique to spermatogenesis, there are also a number of histone variants identified to be specifically expressed in testis and reported to have critical roles in spermatogenesis [19, 20]. I examined the expression of a panel of general and testis-specific histone variants in $Chd5^{Aam1+/+}$ and $Chd5^{Aam1-/-}$ round spermatids via quantitative RT-PCR (qRT-PCR) and discovered that Chd5 deficiency disturbed the transcription of multiple histone variants in $Chd5^{Aam1-/-}$ round spermatids (Figure 26). Most notably, expression of H2b variant *Hist1h2bc* (histone cluster 1, H2bc) was elevated over 5 fold in $Chd5^{Aam1-/-}$ round spermatids compared to wild type counterparts (Figure 26). On the other hand, a 20 - 30% decrease in expression of histone H1 variant *Hist1h1e* (histone cluster 1, H1e), testis specific H1 variant *H1t* (histone cluster 1, H1t), histone H2A variants *Hist1h2aa* (histone cluster 1, H2aa) and *Hist3h2a* (histone cluster 3, H2a), histone H3 variants *Hist1h3i* (histone cluster 1, H3i) and *Hist2h3c1*(histone cluster 2, H3c1), and histone H4 variants *Hist1h4i* (histone cluster 1, H4i), were also consistently observed in $Chd5^{Aam1-/-}$ spermatids (Figure 26). These findings showed that transcription of specific histone variants during spermiogenesis were altered in Chd5-deficient spermatids.

3.7 Increased *Prm1* transcription in Chd5-deficient spermatids

Concomitantly with defective histone removal, transition proteins and protamines were highly elevated in $Chd5^{Aam1-/-}$ spermatids. This was quite surprising, given previous reports

usually show deficiency rather than elevation of transition proteins and/or protamines in infertile mice and it is rare that all the four basic proteins are affected simultaneously [38, 39, 47, 50, 51, 54, 70, 172]. The elevated protein levels of all transition proteins and protamines in *Chd5*$^{Aam1-/-}$ spermatids suggested that their transcription may be increased in Chd5-deficient spermatids. *Tnp1*, *Tnp2*, *Prm1* and *Prm2* are transcribed in round spermatids, but their transcripts are not translated into protein until later in differentiation [56-59]. Transcriptional regulation of transition protein and protamine genes is critical for male fertility, as disruption of transcriptional regulators of *Tnps* and *Prms* can result in male sterility. For example, targeted disruption of the gene encoding the H3K9 demethylase Jhdm2a compromises *Tnp1* and *Prm1* transcription [70], and leads to post-meiotic chromatin condensation defects and infertility in male mice [70]. To determine whether Chd5 deficiency could alter transcription of transition protein and protamine genes, I used qRT-PCR to assess *Tnp1*, *Tnp2*, *Prm1* and *Prm2* expression in *Chd5*$^{Aam1-/-}$ and *Chd5*$^{Aam1+/+}$ round spermatids. Whereas only a slight increase of *Tnp1*, *Tnp2,* and *Prm2* transcription was observed, *Prm1* transcription was increased approximately 2.5 fold in *Chd5*$^{Aam1-/-}$ round spermatids (Figure 27a). Through chromatin immunoprecipitation-qPCR (ChIP-qPCR) analyses of testicular cells, I further discovered that Chd5 was enriched at the promoter region of the *Prm1* gene (region P: -77 bp to +135 bp, transcription start site was regarded as +1 bp) (Figure 27b). Less pronounced Chd5 enrichment was also observed at region A (-860 to -672bp), B (-444 bp to -239 bp) and C (+397 bp to +585 bp), but not in region 5' (-1319 bp to -1164 bp) (Figure 25b) of *Prm1* gene. These data indicated that Chd5 directly bound to the promoter of *Prm1* and its deficiency led to enhanced *Prm1* transcription.

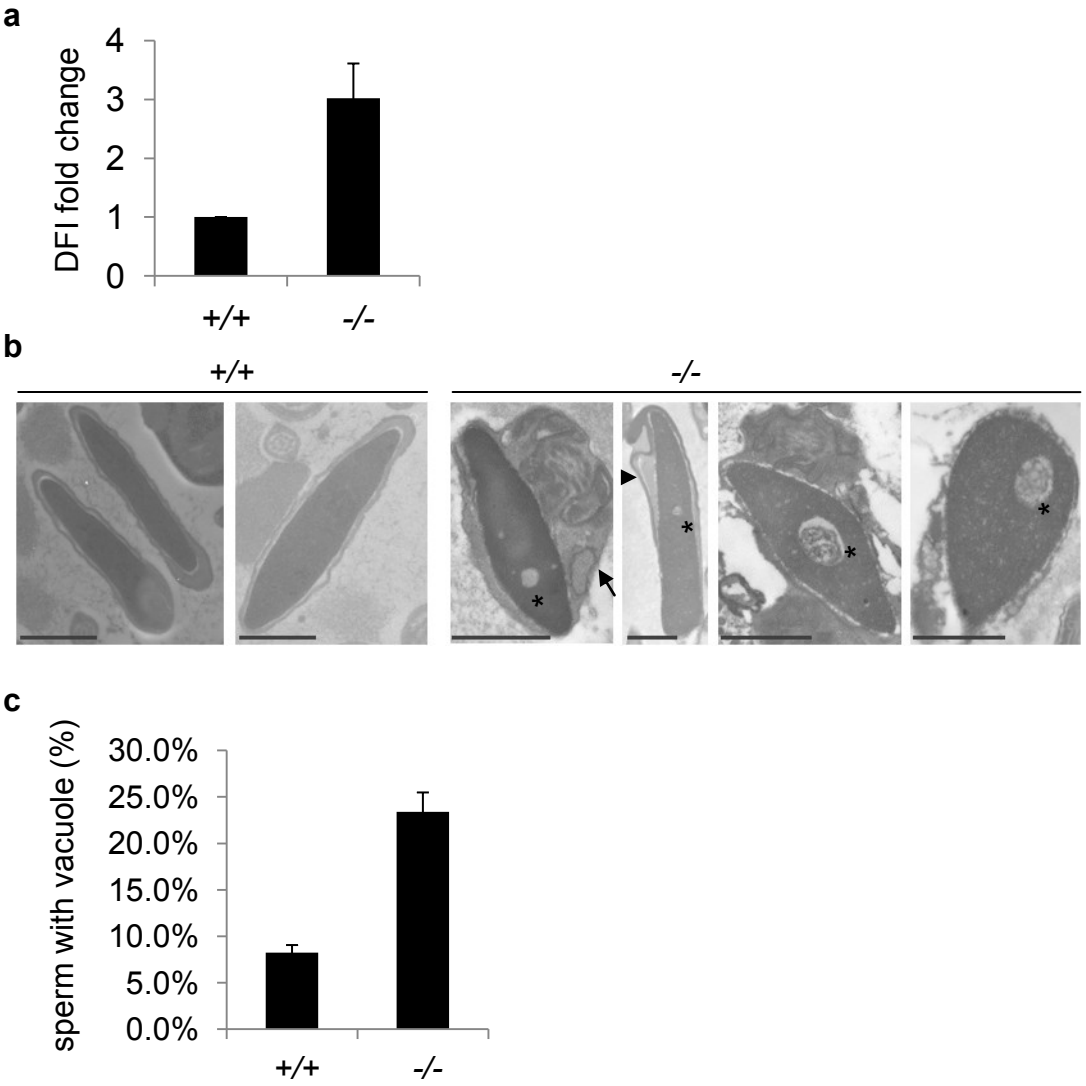

Figure 16. Impaired chromatin integrity and condensation in *Chd5*$^{Aam1-/-}$ sperm

a, Sperm chromatin structure assay (SCSA) revealed impaired chromatin integrity of *Chd5*$^{Aam1-/-}$ sperm. DFI, DNA Fragmentation Index (see Chapter 7. Materials and Methods for details). Data were presented as mean ± s.d. from four independent experiments using sperm from 4 sets of *Chd5*$^{Aam1+/+}$ and *Chd5*$^{Aam1-/-}$ littermate mice. **b,** Transmission electron microscopy (TEM) analyses of sperm from *Chd5*$^{Aam1+/+}$ and *Chd5*$^{Aam1-/-}$ caudal epididymi. Top, Chromatin appeared homogenously condensed in *Chd5*$^{Aam1+/+}$ sperm**,** but showed heterogeneous, less condensed and fibrillar texture with abnormal presence of vacuoles (marked by *) in *Chd5*$^{Aam1-/-}$ sperm nuclei. Abnormal retention of cytoplasm (arrow) and abnormal bulge (arrow head) between the acrosome and nuclei were also observed. Scale bar**,** 1 μm. **c,** Percentage of sperm with abnormal vacuoles in *Chd5*$^{Aam1+/+}$ and *Chd5*$^{Aam1-/-}$ mice. Sperm of 3 *Chd5*$^{Aam1+/+}$ mice and 4 *Chd5*$^{Aam1-/-}$ mice from two litters were examined under TEM. The percentages of sperm with abnormal vacuoles in *Chd5*$^{Aam1+/+}$ and *Chd5*$^{Aam1-/-}$ mice were determined by counting over 240 sperm from each mouse. Data were presented as mean ± s.d. +/+, *Chd5*$^{Aam1+/+}$; -/-, *Chd5*$^{Aam1-/-}$.

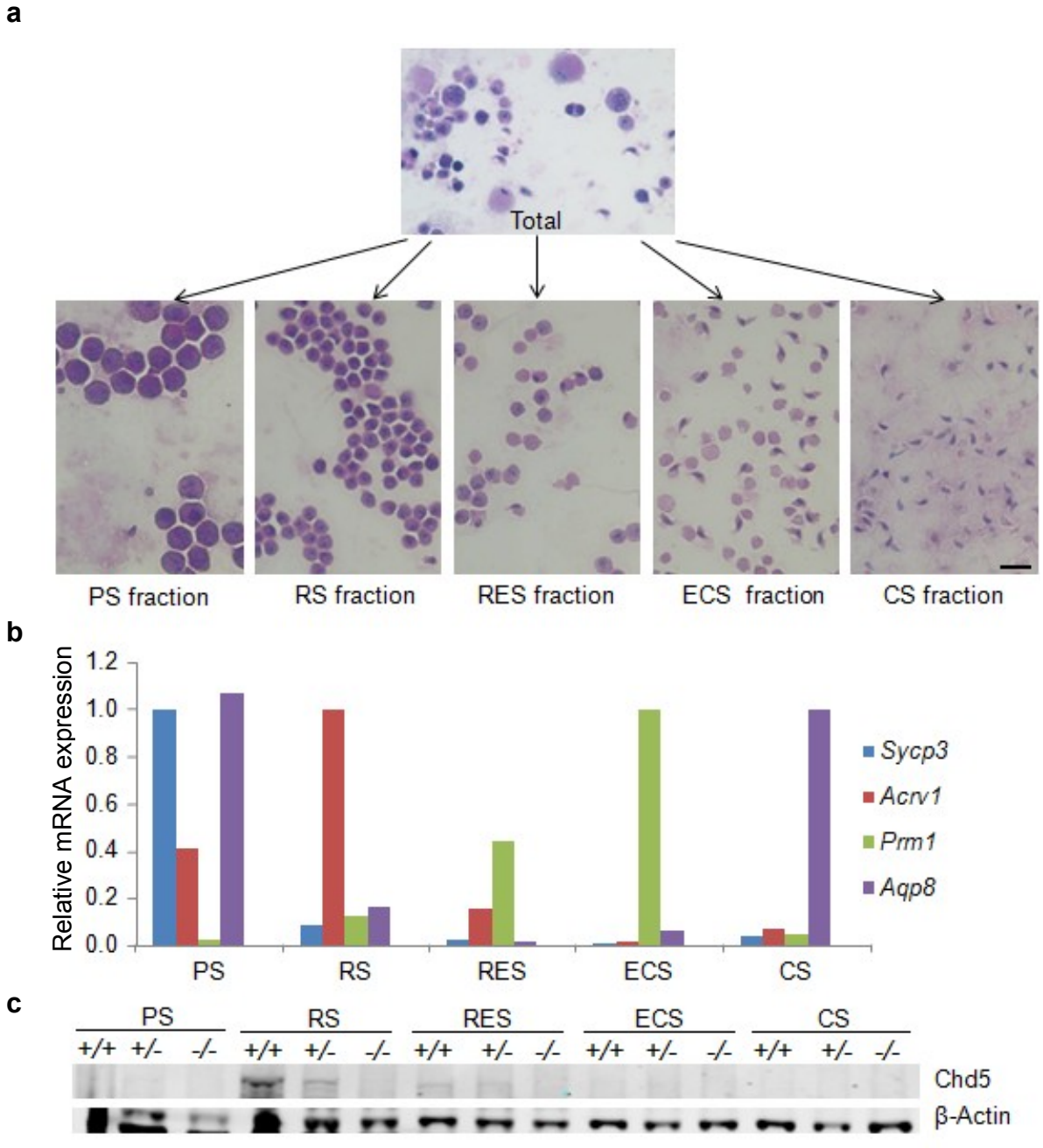
a
Total
PS fraction
RS fraction
RES fraction
ECS fraction
CS fraction
b
Relative mRNA expression
1.2
1.0
0.8
0.6
0.4
0.2
0.0
PS
RS
RES
ECS
CS
Sycp3
Acrv1
Prm1
Aqp8
c
PS
RS
RES
ECS
CS
+/+ +/- -/-
Chd5
β-Actin

Figure 17. High-purity fractions of testicular cells at different stages obtained through centrifugal elutriation

a, Periodic acid–Schiff (PAS) staining of elutriation-purified testicular cell fractions. PS, pachytene spermatocytes; RS, round spermatids; RES, round and early elongating spermatids; ECS, elongating and condensing spermatids; CS, condensed spermatids. Scale bar, 10 μm. The purities of RS, ECS and CS fractions, assessed on smears, were 91%, 91% and 90% respectively. Note that the pink round bodies in ECS fraction were not cells but residual bodies of cytoplasm shed from the nuclei of elongating and condensing spermatids. **b,** Quantitative RT-PCR (qRT-PCR) analyses of stage marker expression in purified testicular cell fractions. The expression of the marker for a specific stage, e.g. *Acrv1* expression in RS population, was defined as 1 and used to normalize expression of markers for other stages. Low expression of other stage markers indicated low contamination of cells from other spermatogenic stages. *Sycp3* (*Synaptonemal complex protein 3*), strongly expressed in spermatocytes with also very low level in spermatogonia and round spermatids [173]; Acrv1 (*Acrosomal Vesicle Protein 1*), round spermatid-specific [174]; *Prm1* (*Protamine 1*), present from late step 7 round spermatids through step 14 condensing spermatids [175]; *Aqp8* (*Aquaporin 8*), condensed spermatid-specific [176]; *β-Act* (*beta actin*), control. **c,** Western blot analyses on lysates from purified testicular cell fractions confirmed that Chd5 was specifically expressed in round spermatids and early elongating spermatids (RS and RES) of $Chd5^{Aam1+/+}$ testes, and was not detected in lysates from all the cellular fractions of $Chd5^{Aam1-/-}$ testes. *+/+,* $Chd5^{Aam1+/+}$; *+/-,* $Chd5^{Aam1+/-}$; *-/-,* $Chd5^{Aam1-/-}$.

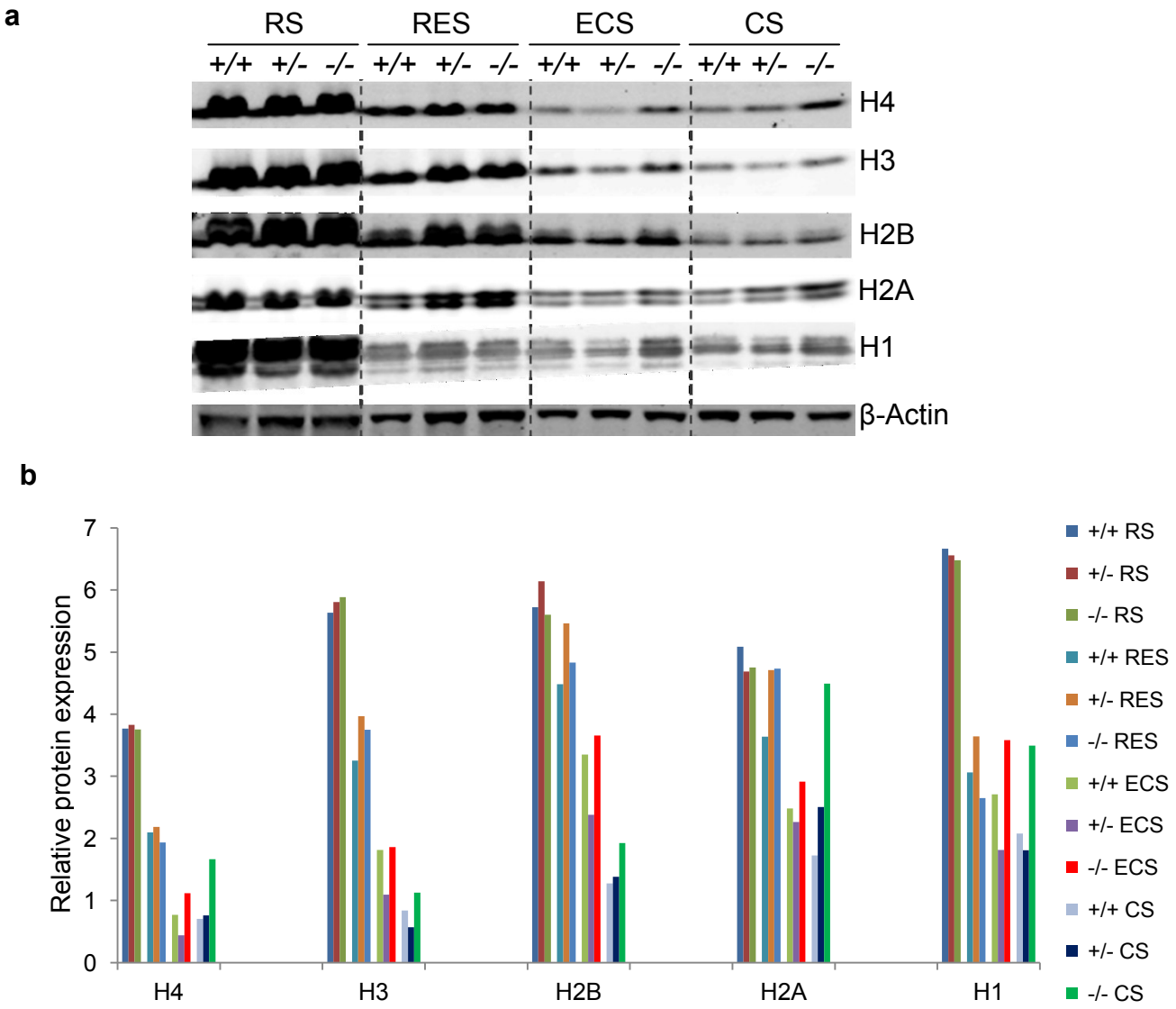

Figure 18. Increased histone retention in Chd5-deficient spermatids

a, Western blot analyses of protein lysates from purified spermatids at different spermiogenic stages. RS, round spermatids; RES, round and early elongating spermatids; ECS, elongating and condensing spermatids; CS, condensed spermatids. Increased retention of histones (H4, H3, H2B, H2A and H1) were observed in differentiated spermatids (elongating, condensing and condensed spermatids) but not in round spermatids of *Chd5*$^{Aam1-/-}$ *(-/-)* testes. β-Actin served as a loading control. Western blot was repeated multiple times on lysates from two different batches of fractionated spermatids. Each batch was elutriation-purified from a pool of 3-6 mice of indicated genotype with matched background and age. **b**, Quantification of Western blot shown in **a**. The intensities of indicated protein bands on Western blot images were quantified using the imaging analysis software Image J. The intensity values of indicated histone bands were divided by the intensity values of the β-Actin bands from the same lysates. The normalized values were plotted in the histogram to show comparison of expression levels of the indicated proteins among different samples.

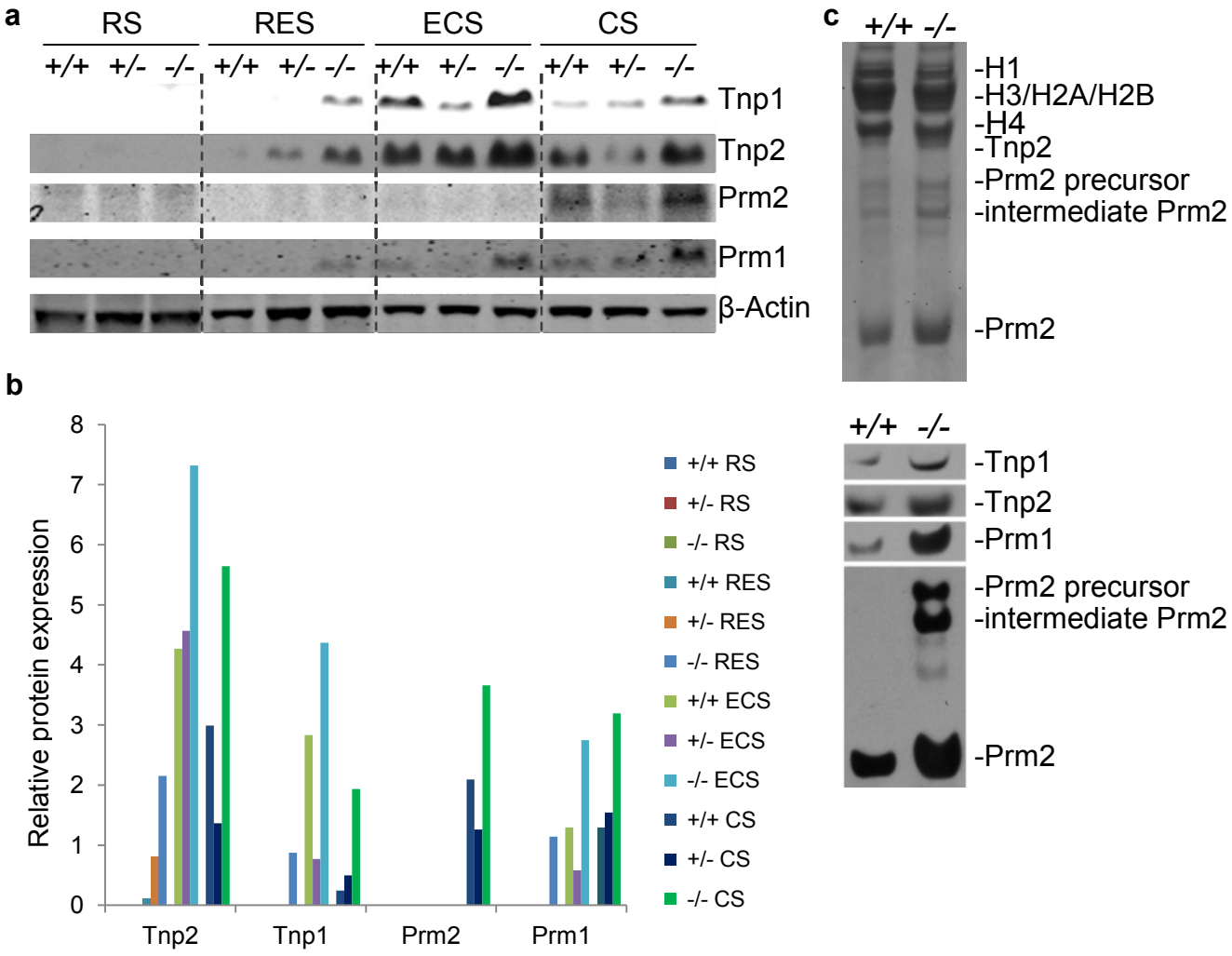
a
RS
RES
ECS
CS
+/+ +/- -/- +/+ +/- -/- +/+ +/- -/- +/+ +/- -/-
Tnp1
Tnp2
Prm2
Prm1
β-Actin
b
Relative protein expression
0
1
2
3
4
5
6
7
8
Tnp2
Tnp1
Prm2
Prm1
+/+ RS
+/- RS
-/- RS
+/+ RES
+/- RES
-/- RES
+/+ ECS
+/- ECS
-/- ECS
+/+ CS
+/- CS
-/- CS
c
+/+ -/-
-H1
-H3/H2A/H2B
-H4
-Tnp2
-Prm2 precursor
-intermediate Prm2
-Prm2
+/+ -/-
-Tnp1
-Tnp2
-Prm1
-Prm2 precursor
-intermediate Prm2
-Prm2

Figure 19. Elevated levels of transition proteins and protamines in Chd5-deficient spermatids

a, Western blot analyses of protein lysates from purified spermatids at different spermiogenic stages. RS, round spermatids; RES, round and early elongating spermatids; ECS, elongating and condensing spermatids; CS, condensed spermatids. Increased transition proteins (Tnp1 and Tnp2) and protamines (Prm1 and Prm2) were observed in *Chd5*$^{Aam1-/-}$ spermatids. β-Actin served as a loading control. Western blot was repeated multiple times on lysates from two different batches of fractionated spermatids. Each batch was elutriation-purified from a pool of 3-6 mice of indicated genotype with matched background and age. **b**, Quantification of Western blot shown in **a**. The intensities of indicated protein bands on Western blot images were quantified using the imaging analysis software Image J. The intensity values of indicated protein bands were divided by the intensity values of the β-Actin bands from the same lysates. The normalized values were plotted in the histogram to show comparison of expression levels of the indicated proteins among different samples. **c,** Top panel, Coomassie blue staining of basic protein extracts that were prepared from *Chd5*$^{Aam1+/+}$ and *Chd5*$^{Aam1-/-}$ sonication resistant spermatids (SRS) and separated through urea-acid gel electrophoresis. Equal amount of protein was loaded. Bottom panel, Western blot analyses of the same basic protein extract showed increased amount of Tnp1, Tnp2, Prm1 and Prm2 proteins in *Chd5*$^{Aam1-/-}$ SRS. The increased levels of Prm2 precursor and intermediate Prm2 indicated deficient processing of Prm2 precursor into mature Prm2 in *Chd5*$^{Aam1-/-}$ SRS.

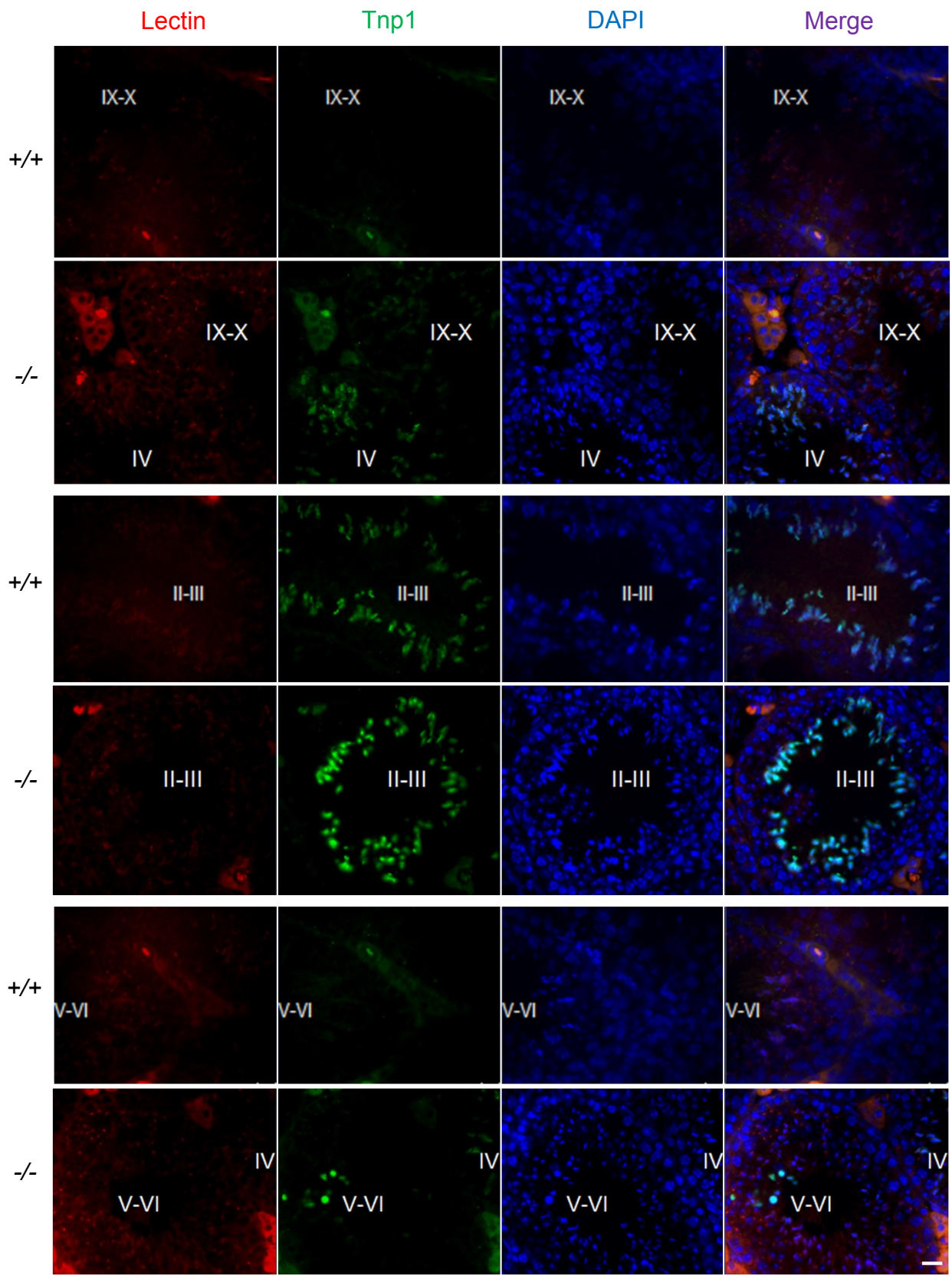
Lectin
Tnp1
DAPI
Merge
+/+
-/-
+/+
-/-
+/+
-/-
IX-X
IV
II-III
V-VI

Figure 20. Enhanced Tnp1 expression in Chd5-deficient spermatids

Immunofluorescence analyses of Tnp1 in *Chd5*$^{Aam1+/+}$ (+/+) and *Chd5*$^{Aam1-/-}$(-/-) seminiferous tubules. Roman numerals indicated spermatogenic stages of the marked areas. Red, Lectin (visualizing acrosome for staging seminiferous tubules); Green, Tnp1; Blue, DAPI. Top panel, Tnp1 was barely detected in step 9-10 spermatids in stage IX-X tubules of *Chd5*$^{Aam1+/+}$ testes but was detected in step 9-10 spermatids in stage IX-X tubules of *Chd5*$^{Aam1-/-}$ testes; middle panel, Tnp1 was detected in step 14 spermatids in stage II-III tubules of both *Chd5*$^{Aam1+/+}$ and *Chd5*$^{Aam1-/-}$ testes but showed stronger staining in *Chd5*$^{Aam1-/-}$ tubules; bottom panel, Tnp1 was no longer detectable in step 15 spermatids in stage V-VI tubules of *Chd5*$^{Aam1+/+}$ testes but was still detected in some step 15 spermatids in stage V-VI tubules of *Chd5*$^{Aam1-/-}$ testes. Scale bar, 20 μm.

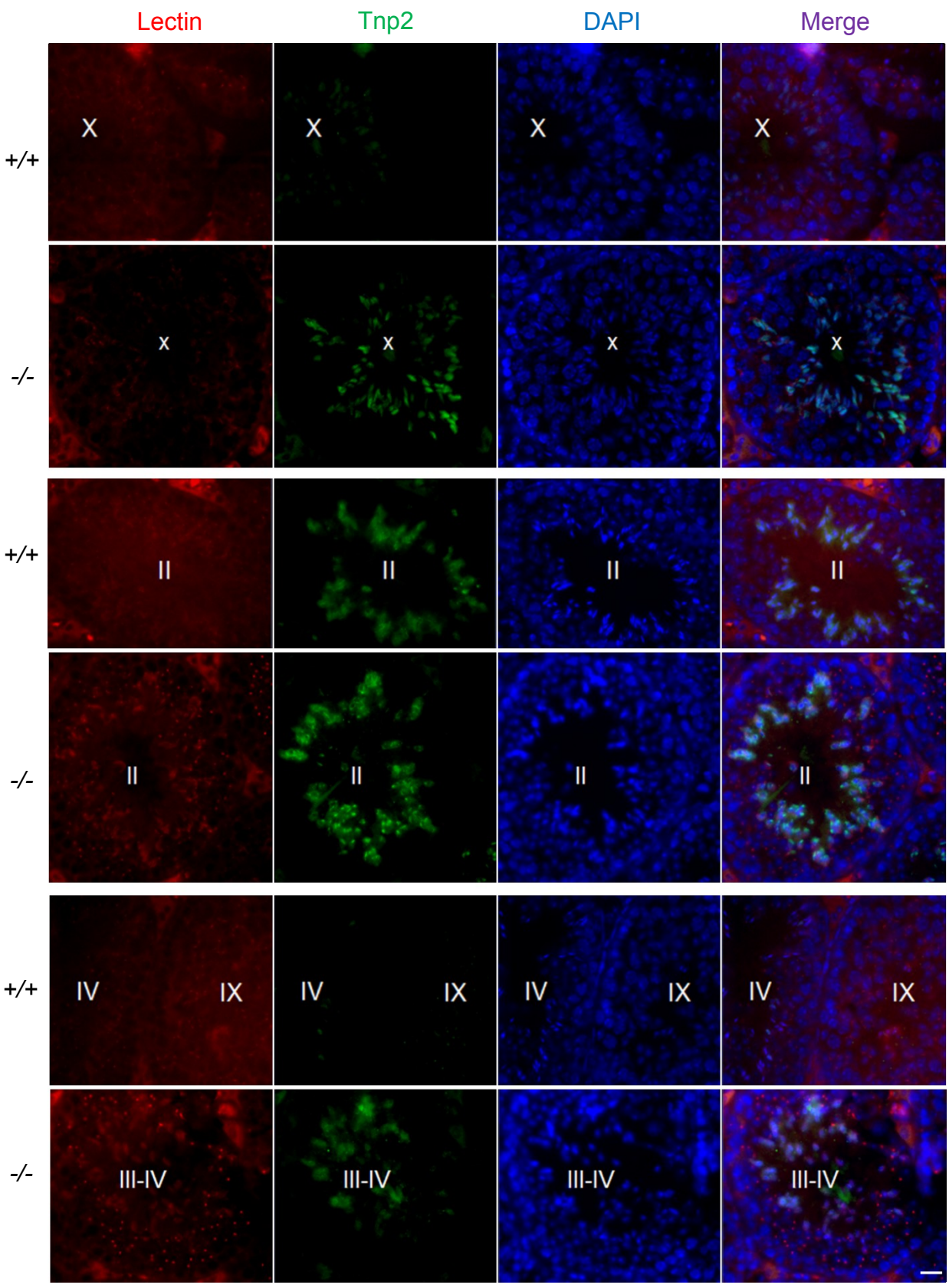
Lectin
Tnp2
DAPI
Merge
+/+
X
-/-
x
+/+
II
-/-
II
+/+
IV
IX
-/-
III-IV

Figure 21. Enhanced Tnp2 expression in Chd5-deficient spermatids

Immunofluorescence analyses of Tnp2 in *Chd5*$^{Aam1+/+}$ (+/+) and *Chd5*$^{Aam1-/-}$(-/-) seminiferous tubules. Roman numerals indicated spermatogenic stages of the marked areas. Red, Lectin (visualizing acrosome for staging seminiferous tubules); Green, Tnp2; Blue, DAPI. Top panel, Tnp2 was first detected in step 10 spermatids in stage X tubules of *Chd5*$^{Aam1+/+}$ testes but showed stronger staining in step 10 spermatids in stage X tubules of *Chd5*$^{Aam1-/-}$ tubules; middle panel, High Tnp2 expression was detected in step 14 spermatids in stage II tubules of both *Chd5*$^{Aam1+/+}$ and *Chd5*$^{Aam1-/-}$ testes but showed stronger staining in *Chd5*$^{Aam1-/-}$ tubules; bottom panel, Tnp2 became only weakly detectable in a small portion of step 15 spermatids in stage IV tubules of *Chd5*$^{Aam1+/+}$ testes but was still highly detected in step 15 spermatids in stage III-IV tubules of *Chd5*$^{Aam1-/-}$ testes. Scale bar, 20 μm.

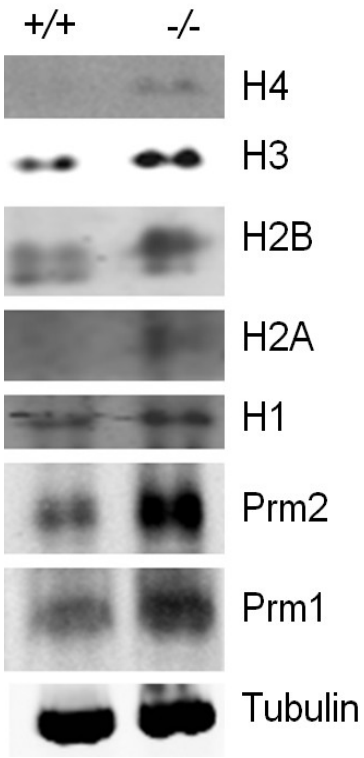

Figure 22. Elevated levels of histones and protamines in Chd5-deficient sperm

Western blot analyses of protein lysates of sperm prepared from caudal epididymi of *Chd5*$^{Aam1+/+}$ (+/+) and *Chd5*$^{Aam1-/-}$ (-/-) mice revealed increased levels of histones H4, H3, H2B, H2A and H1 as well as protamines Prm1 and Prm2 in *Chd5*$^{Aam1-/-}$ sperm. Tubulin served as a loading control.

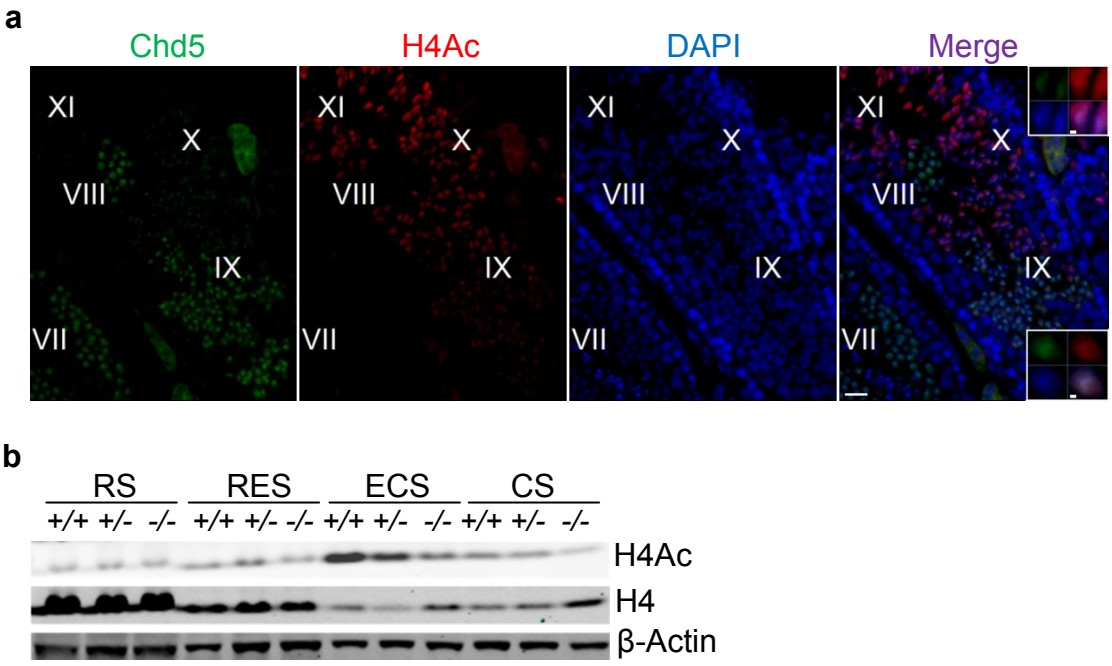

Figure 23. Compromised H4 acetylation in Chd5-deficient spermatids

a, Roman numerals indicated spermatogenic stages of the marked areas. Top insert, co-staining of Chd5 and H4 acetylation (H4Ac) in step 10 spermatids; Bottom insert, co-staining of Chd5 and H4Ac in step 9 spermatids. Both Chd5 and H4Ac showed enrichment in DAPI-intense regions in the nuclei of step 9 and 10 spermatids in wild type testes. Scale bars, 20 μm and 1 μm (inside inserts) respectively. H4Ac was detected by a mouse monoclonal antibody against pan-H4K5/8/12/16Ac. **b,** Western blot analyses of purified spermatids at different spermiogenic stages. Histone H4 became transiently hyperacetylated in ECS of *Chd5*$^{Aam1+/+}$ testes but not in ECS of *Chd5*$^{Aam1-/-}$ testes. H4Ac was detected by a rabbit polyclonal antibody against pan-H4 acetylation. β-Actin served as a loading control. RS, round spermatids; RES, round and early elongating spermatids; ECS, elongating and condensing spermatids; CS, condensed spermatids.

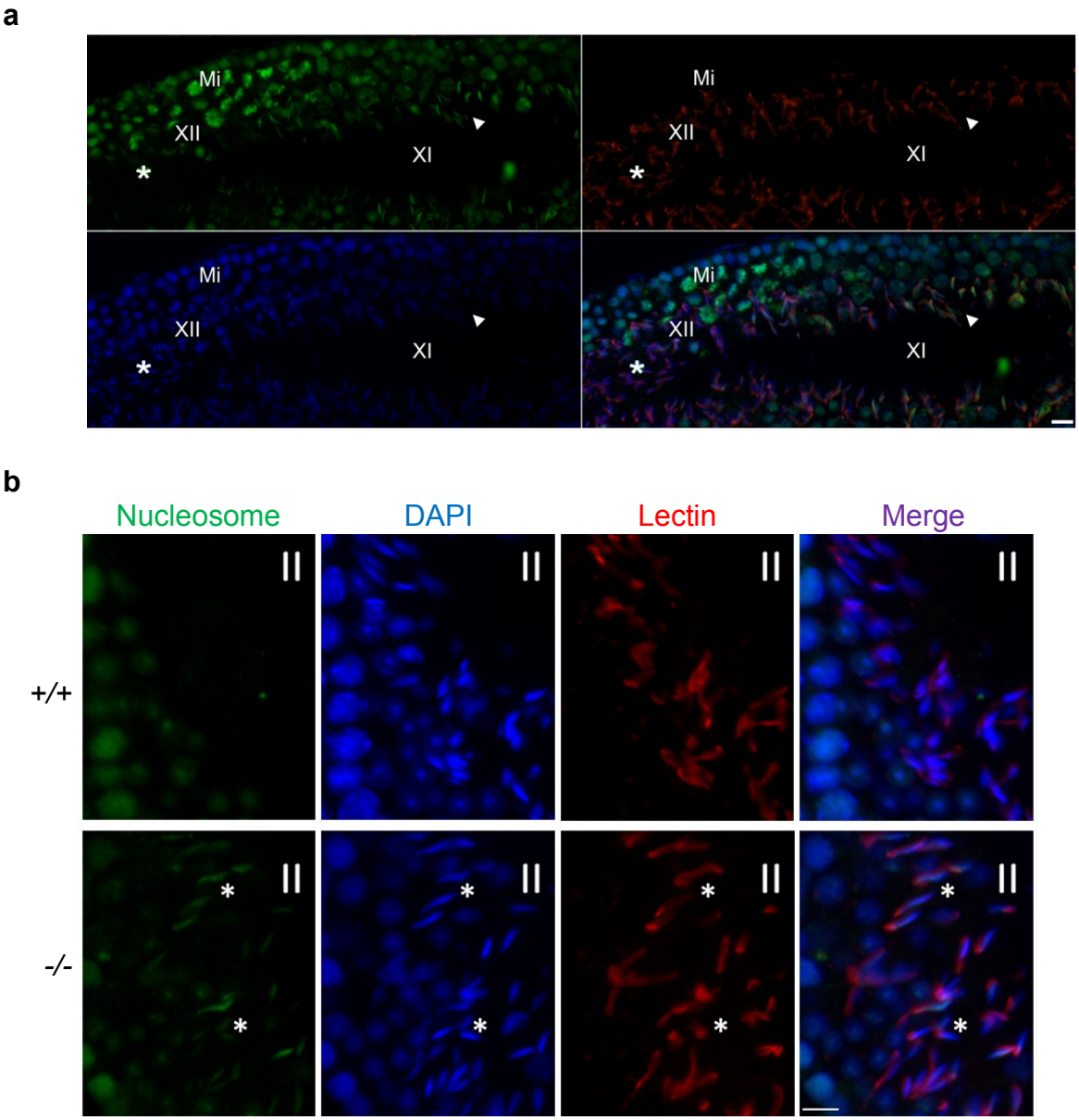

Figure 24. Inefficient nucleosome eviction in Chd5-deficient spermatids

Roman numerals indicated the spermatogenic stages of tubular areas. **a,** Nucleosomes were detected in step 11 spermatids (indicated by arrow head) in Stage XI tubules of wild type testes, but were depleted afterwards and not detectable in step 12 spermatids (indicated by *) of stage XII tubule. Green, nucleosome; Red, Lectin (visualizing acrosome for staging seminiferous tubules); Blue, DAPI; Mi, meiotic figure, a hallmark of stage XII tubules. **b,** Immunostaining of nucleosome showed that nucleosomes were retained as late as in step 14 spermatids in stage II seminiferous tubules of *Chd5*$^{Aam1-/-}$ testes. Asterisks (*) marked nucleosome-positive condensing spermatids (step 14) in *Chd5*$^{Aam1-/-}$ tubules. Scale bar, 10 μm.

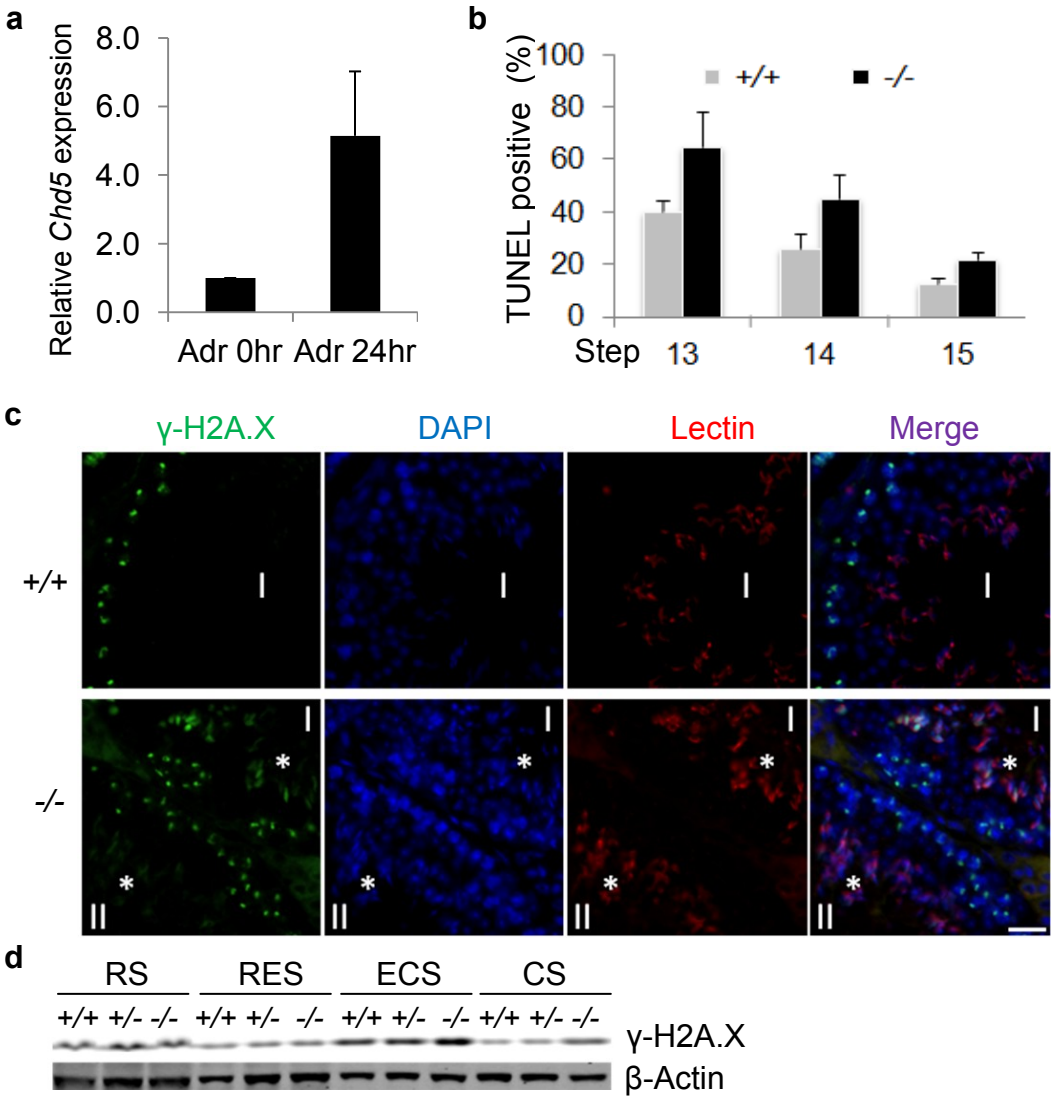

Figure 25. Increased DNA damage in Chd5-deficient spermatids

a, qRT-PCR analyses showed that *Chd5* expression was induced approximately 5 fold when wild type mouse embryonic fibroblasts were treated with DNA damaging agent adriamycin (0.4 μg/ml) for 24 hours. Results were normalized to *Actb* and the expression level at 0 hour was defined as 1. Data were presented as mean ± s.d. from three independent experiments. Adr, Adriamycin. **b,** Increased TUNEL-positive condensing spermatids (step 13-15) in $Chd5^{Aam1-/-}$ testis. Data were presented as mean ± s.d. from three independent experiments. **c,** Immunofluorescence analyses of γ-H2A.X in $Chd5^{Aam1+/+}$ (+/+) and $Chd5^{Aam1-/-}$(-/-) seminiferous tubules. Asterisks (*) marked γ-H2A.X-positive spermatids (step 13 in stage I and step 14 in stage II tubules) in $Chd5^{Aam1-/-}$ testis. Scale bar, 20 μm. **d,** Western blot analyses of purified spermatids at different spermiogenic stages showed transient up-regulation of γ-H2A.X in wild type ECS, and increased accumulation of γ-H2A.X in $Chd5^{Aam1-/-}$ ECS and CS compared to wild type counterparts. β-Actin served as a loading control. RS, round spermatids; RES, round and early elongating spermatids; ECS, elongating and condensing spermatids; CS, condensed spermatid.

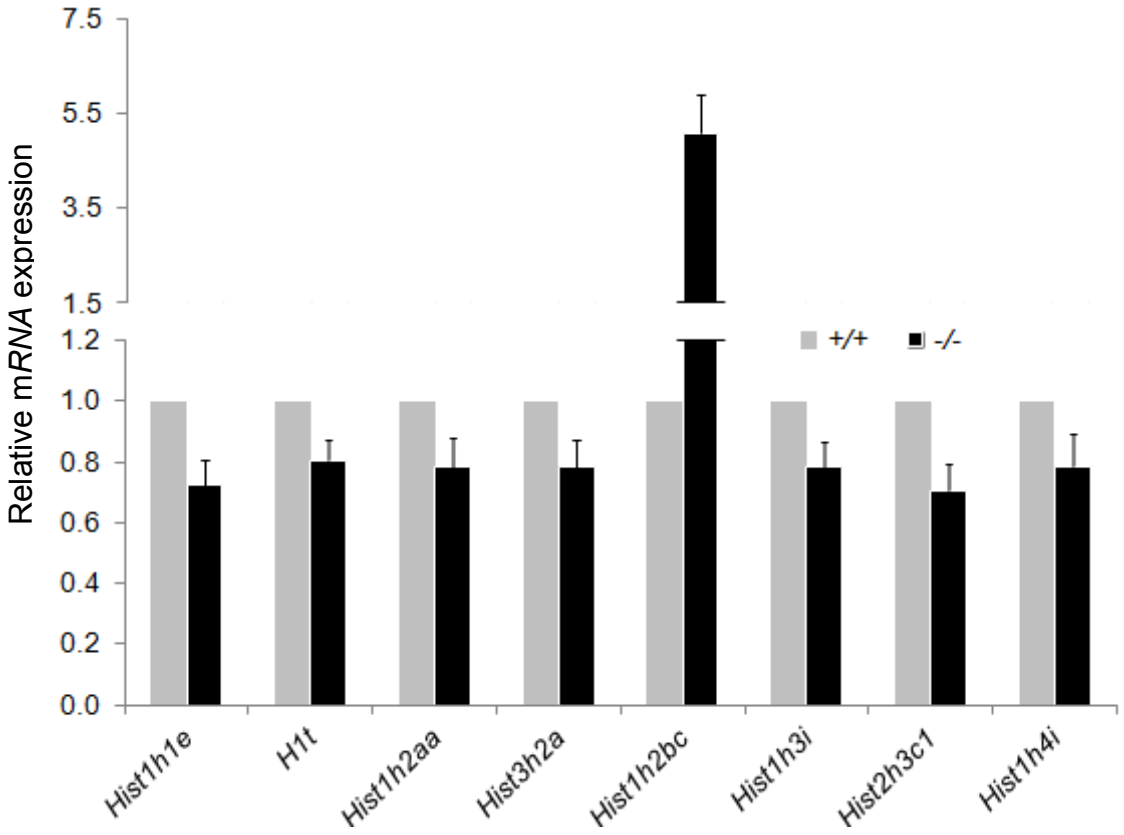

Figure 26. Altered expression of histone variants in Chd5-deficient spermatids

qRT–PCR analyses of histone variants revealed an approximately 5.5 fold increase in expression of histone H2B variant *Hist1h2bc* (histone cluster 1, H2bc) and modest decreases in expression of histone H1 variants *Hist1h1e* (histone cluster 1, H1e) and *H1t* (histone cluster 1, H1t), histone H2A variants *Hist1h2aa* (histone cluster 1, H2aa) and *Hist3h2a* (histone cluster 3, H2a), histone H3 variants *Hist1h3i* (histone cluster 1, H3i) and *Hist2h3c1*(histone cluster 2, H3c1), and histone H4 variants *Hist1h4i* (histone cluster 1, H4i) in $Chd5^{Aam1-/-}$ (-/-) round spermatids. Results were normalized to *Actb* expression. Data were presented as mean ± s.d. from three to five independent experiments.

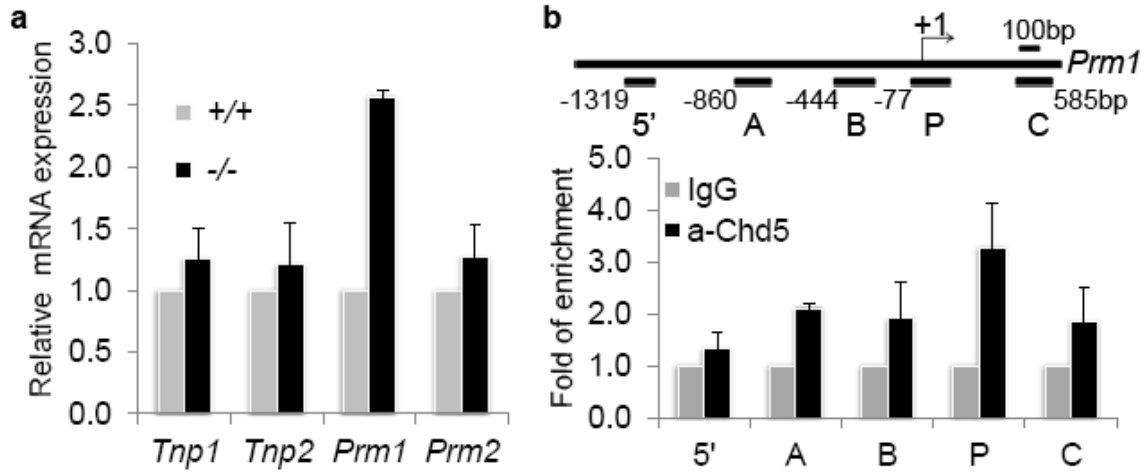

Figure 27. Increased *Prm1* transcription in Chd5-deficient spermatids

a, qRT–PCR analyses of transition protein and protamine genes in *Chd5*$^{Aam1+/+}$ and *Chd5*$^{Aam1-/-}$ round spermatids. Results were normalized to *Actb* expression. *Prm1* expression was increased approximately 2.5 folds in *Chd5*$^{Aam1-/-}$ round spermatids. Data were presented as mean ± s.d. from four independent experiments. **b,** Top panel, diagram of mouse *Prm1* gene and locations of primer sets used for ChIP-qPCR. Bottom panel, ChIP-qPCR analyses revealed enrichment of Chd5 at promoter region P (-77 bp to +135 bp) of *Prm1* gene. The results were normalized to IgG control and were shown as fold of enrichment. Data were presented as mean ± s.d. from four or five independent experiments.

Chapter 4

Chd5 deficiency altered gene expression in spermatids

In order to understand how Chd5 deficiency may affect H4 acetylation, DNA damage and homeostasis of transition proteins and protamines, and also to gain insights on Chd5 functions in spermiogenesis from a global perspective, I sought to perform RNA Sequencing (RNA-Seq), a method using next-generation sequencing technologies to reveal the expression and quantity of the entire RNA transcriptome of a given sample, in order to detect global gene expression changes in Chd5 deficient testes and identify candidate Chd5 targets. Chd5 was primarily expressed in round spermatids, where transcription is most active during spermiogenesis as transcription is globally ceased during spermatid elongation and condensation. Thus, it would be ideal to perform RNA-Seq on round spermatids from $Chd5^{Aam1+/+}$, $Chd5^{Aam1+/-}$ and $Chd5^{Aam1-/-}$ littermate mice. To purify round spermatids through elutriation, testes from at least 3 mice need be pooled. To prepare 3 biological replicates for RNA-Seq experiment, at least 9 sets of $Chd5^{Aam1+/+}$, $Chd5^{Aam1+/-}$ and $Chd5^{Aam1-/-}$ littermate mice with matched background and age are needed. It would require months of mouse breeding to fully obtain such a number (~30) of littermate mice. In addition, it would be quite physically challenging to perform 9 elutriations, as the elutriation purification process is very laborious and exhausting. Due to these limitations, I took a less ideal but more practical design. I performed RNA-Seq on 1 set of pooled round spermatids (1 $Chd5^{Aam1+/+}$: 1 $Chd5^{Aam1+/-}$:1 $Chd5^{Aam1-/-}$) that were elutriation-purified from 5 sets of $Chd5^{Aam1+/+}$, $Chd5^{Aam1+/-}$ and $Chd5^{Aam1-/-}$ littermate mice with matched background and age. Meanwhile, I also performed RNA-Seq on 3 biological replicates of total testes from 3 sets of $Chd5^{Aam1+/+}$, $Chd5^{Aam1+/-}$ and $Chd5^{Aam1-/-}$ littermates with matched background and age. RNA-

Seq was performed using Illumina HiSeq 2000. RNA-Seq data were analyzed mainly using the widely used RNA-Seq data analysis tool Cufflinks package (v2.0.2) [177] by Dr. Jie Wu, a collaborating bioinformatician previously at Professor Michael Zhang's lab at Cold Spring Harbor Laboratory (see Chapter 7. Materials and Methods). Cufflinks assembles transcripts, estimates their abundances, and tests for differential expression in RNA-Seq samples. It aligns RNA-Seq reads to the reference genome and assembles the alignments into a set of transcripts. Cufflinks then estimates the relative abundance of the transcripts based on the number of fragments per kilobase of transcript per million mapped reads (FPKM). Briefly, Cufflinks was first used to calculate transcript expression levels represented by FPKM for all the samples. Cuffdiff, a component of the Cufflinks package that can compare differences of transcript FPKMs between samples and evaluate their statistical significance, was then run to detect differential expression between $Chd5^{Aam1+/+}$ and $Chd5^{Aam1-/-}$ samples. Differential expression of protein-coding transcripts with at least a 2 fold change between $Chd5^{Aam1-/-}$ samples and $Chd5^{Aam1+/+}$ controls were selected for downstream analyses. After this pipeline of data analyses and filtration, a list of 61 hits were identified from total testis RNA-Seq data (called "total testis gene list" onwards), among which 30 showed down-regulated expression and 31 showed up-regulated expression (Table 5). A list of 240 hits (called "round spermatid gene list" onwards) were identified from round spermatid RNA-Seq data, among which 146 showed down-regulated expression and 94 showed up-regulated expression (Table 5). The two lists shared 18 common hits, whereas there were 222 genes that uniquely showed expression changes in $Chd5^{Aam1-/-}$ round spermatids but not in total testes (Figure 28). Such larger gene expression changes in round spermatids than in total testes revealed by RNA-Seq were not surprising, since Chd5 protein was specifically expressed in round and early elongating spermatids and its deficiency was expected

to affect gene expression in those cellular populations. In total testis, such gene expression changes may be masked, as round spermatids only account for a fraction of the total testicular cells. I next performed qRT-PCR validation for 10 hits revealed by RNA-Seq using both the same round spermatid RNA samples used for RNA-Seq and a different batch of round spermatid RNA samples prepared from a different set of mice. qRT-PCR results confirmed similar expression changes of these genes in *Chd5*$^{Aam1-/-}$ round spermatids as RNA-Seq revealed (Figure 29), confirming the reliability of the RNA-Seq data and analyses.

I next performed gene ontology analyses using The Database for Annotation, Visualization and Integrated Discovery (DAVID v6.7), a widely used gene ontology analysis tool [178], on both the total testis and round spermatid gene lists selected above to uncover the biological processes, functions and pathways that were affected in Chd5-deficient samples. For the total testis gene list, the main biological processes and functions affected were phosphate metabolic process, protein phosphorylation, tissue morphogenesis and cell membrane-related activity especially vesicle secretion (Table 6). Phosphoprotein and vesicle functions were also two gene ontology terms affected in the round spermatid gene list (Table 7). In addition, gene ontology analyses revealed that a range of biological processes, molecular functions and cellular components were affected in Chd5-deficient round spermatids, including acetylation, N-acetyltransferase activity, alternative splicing, adenyl ribonucleotide binding, nuclear export, ubiquitin conjugation, protein transport, ribosomal structure and biogenesis, nucleotide binding, ATP binding, chromosome, nuclear lumen, cell cycle, lipid transporter activity and fatty acid metabolism (Table 7). Many of the gene ontology changes were in agreement with the impacts of Chd5 deficiency on histone acetylation, DNA damage response and homeostasis of transition proteins and protamines, as discussed in previous chapters. Using qRT-PCR, I have validated the

expression changes of a number of RNA-Seq hits implicated in acetylation, DNA damage, RNA metabolism, translation and nuclear structure maintenance.

4.1 Gene expression changes and candidate Chd5 targets implicated in acetylation

As discussed in Chapter 3.3, severely compromised H4 acetylation occurred during spermiogenesis in Chd5-deficient testis, suggesting that Chd5 may play a role in modulating H4 hyperacetylation during spermiogenesis. Given that Chd5 does not have acetyltransferase or deacetylase activity itself, Chd5 may indirectly affect H4 acetylation through interacting partners or downstream targets that have the capability of directly acetylating or deacetylating H4. Currently, no histone acetyltransferase (HAT) or deacetylase has been identified as responsible for the H4 hyperacetylation during spermiogenesis. However, acetyltransferases Cdyl (chromodomain protein, Y chromosome-like) and Kat6b (lysine acetyltransferase 6B), also known as Myst4 [33-35], and deacetylases HDAC1 (histone deacetylase 1) and HDAC2 (histone deacetylase 2) [33, 36] have been implicated in histone hyperacetylation during spermiogenesis. I compared expression of *Cdyl* and *Kat6b* as well as several other acetyltransferases potentially implicated in H4 hyperacetylation, such as *Cdyl2* (chromodomain protein, Y chromosome-like 2), *Kat2a* (lysine acetyltransferase 2A) and *Kat2b* (lysine acetyltransferase 2B), in $Chd5^{Aam1-/-}$ round spermatids with that in $Chd5^{Aam1+/+}$ round spermatids using qRT-PCR. No change was observed for *Cdyl* and only an approximately 20% decrease was observed for *Cdyl2*, *Kat6b*, *Kat2a* and *Kat2b* (Figure 30). However, RNA-Seq and gene ontology analyses revealed expression changes of 4 N-acetyltransferases and another 35 genes implicated in acetylation in $Chd5^{Aam1-/-}$ round spermatids (Table 7). Particularly, expression of *1700019G17Rik* (RIKEN cDNA 1700019G17 gene) that encodes a putative N-acetyltransferase , was reduced by over 80% in $Chd5^{Aam1-/-}$ round

spermatids. The expression reduction of *1700019G17Rik* in *Chd5*$^{Aam1-/-}$ round spermatids was validated by repeated qRT-PCR on both the same round spermatid RNA samples used for RNA-Seq and another batch of round spermatid RNA samples prepared from a different set of mice (Figure 30). Although very little is known about 1700019G17Rik, its primary protein sequence indicates that it could have N-acetyltransferase activity. NCBI EST profile showed that *1700019G17Rik* ESTs were highly enriched in mouse testis but not detected in most of other tissues (NCBI UniGene/ESTProfile: Mm.24454). These data suggested *1700019G17Rik* as a potential acetyltransferase that may play a role in H4 acetylation during spermiogenesis. RNA-Seq and qRT-PCR validation also revealed that expression of *Nat10* (N-acetyltransferase 10), a N-alpha acetyltransferase showed an approximately 35% decrease in *Chd5*$^{Aam1-/-}$ round spermatids (Figure 30). Nat10 is a component of NatA complex shown to acetylate histones and implicate in de-condensation of mitotic chromosomes and DNA damage response [179-181]. It is possible that Nat10 may also involve in H4 acetylation during spermiogenesis.

4.2 Gene expression changes and candidate Chd5 targets implicated in DNA damage response

As discussed in Chapter 3.5, increased DNA damage was observed in *Chd5*$^{Aam1-/-}$ spermatids and *Chd5* expression was induced by DNA damaging agent in MEFs, suggesting that Chd5 may play a role in DNA damage response. Chd3, Chd4 and many other chromatin remodelers have been shown to mediate DNA damage response through remodeling chromatin structure, modulating histone modifications and interacting with other partners critical for DNA damage and repair [106-110, 182, 183]. Given that Chd5 belongs to the same subfamily of Chd3 and Chd4, it may play a similar role. Meanwhile, histone acetylation has been shown to be

crucial for DNA damage repair [183-185]. The severely deficient H4 acetylation in *Chd5*$^{Aam1-/-}$ spermatids thus could compromise DNA repair. Meanwhile, RNA-Seq and qRT-PCR validation revealed that expression of several genes known to play important roles in DNA damage and repair, such as *Top2b* (topoisomerase (DNA) II beta), *Rif1* (Rap1 interacting factor 1 homolog (yeast)), *Wrnip1* (Werner helicase interacting protein 1), *Rad51ap2* (RAD51 associated protein 2) and *Trp53inp1* (transformation related protein 53 inducible nuclear protein 1) were compromised in *Chd5*$^{Aam1-/-}$ spermatids (Figure 31). *Top2b* encodes Top2β which induces DSB to release supercoil tension generated along nucleosome eviction during spermiogenesis [162-165, 186]. Rif1 is essential for 53BP1 (transformation related protein 53 binding protein 1)-dependent nonhomologous end joining (NHEJ) and suppression of double-strand DNA break resection [187-193]. Given the haploid nature of spermatids, the DSBs generated in spermatids must be repaired through non homologous recombination based mechanisms, such as NHEJ, which may require Rif1. Compromised expression of *Top2b*, *Rif1* and other DNA damage response genes thus could contribute to the increased DNA damage in *Chd5*$^{Aam1-/-}$ spermatids. Furthermore, transition proteins and protamines are also important for DNA repair during spermiogenesis [47, 51, 194-197], thus the abnormal homeostasis of transition proteins and protamines in *Chd5*$^{Aam1-/-}$ spermatids may jeopardize DNA damage repair as well.

4.3 Gene expression changes and candidate Chd5 targets implicated in RNA metabolism

As discussed in Chapter 3.7, Chd5 deficiency led to significant elevation of Tnp1, Tnp2 and Prm2 protein levels but minimal increase in their transcription, suggesting that the homeostasis of Tnp1, Tnp2, and Prm2 were affected mainly post-transcriptionally in Chd5-deficient spermatids. Following transcription in round spermatids, the mRNAs of transition

proteins and protamines are stored in translationally repressed ribonucleoprotein particles (RNPs) before they are translated into protein later in elongating spermatids [56-60]. The underlying mechanisms regulating the translational delay remain poorly understood, but post-transcriptional processing, transport, and storage of mRNAs play important roles in controlling translation of specific mRNA at specific timing during spermatogenesis [55, 58, 60, 74, 75, 77, 198-200]. After transcription, mRNAs are assembled in to RNPs within both sequence-specific and sequence-independent mechanisms, transported into the cytoplasm and sequestered in RNPs in confined compartments, primarily the chromatoid body, a male-germ-cell specific RNA processing center, and loaded onto polyribosomes for translation when activated [55, 58, 60, 74, 75, 77, 198-202]. Y-box protein Ybx2 (also known as Contrin in human and Msy2 in mouse) and Tsn (Translin) are important translation regulators for RNAs sequestered in the RNPs [72-75]. Ybx2-deficient male mice are sterile [76], whereas male mice lacking Translin have reduced sperm production [77]. Other RNA binding proteins are also identified as critical translational regulators during spermatogenesis. For example, protamine 1 RNA-binding protein (Prbp) and its human homologue TAR RNA-binding protein (TRBP) regulate *Prm1* mRNA translation, as they contain two RNA-binding domains that bind to the 3′-UTR of protamine 1 [78]. Depletion of Prbp in male mice leads to defective translation of both *Prm1* and *Prm2* mRNA, delayed replacement of transition proteins and eventually severe oligozoospermia and infertility [79]. To determine whether Chd5 could mediate any of the genes known to regulate mRNA processing or translation, I used qRT-PCR to examine their expression changes in $Chd5^{\Delta am1-/-}$ round spermatids. qRT-PCR revealed that the expression of *Tarbp2,* which encodes Prbp, decreased by approximately 30% in $Chd5^{\Delta am1-/-}$ round spermatids (Figure 32). Given Prbp's role in regulating

translation of *Prm1* and *Prm2* mRNA, compromised *Prbp* expression may contribute to the abnormal protein expression of Prm1 and Prm2 in *Chd5*$^{Aam1-/-}$ spermatids.

In addition, RNA-Seq and gene ontology analyses revealed expression changes in *Chd5*$^{Aam1-/-}$ spermatids of 73 genes implicated in alternative splicing, 25 genes implicated in adenyl ribonucleotide binding and 3 genes implicated in nuclear export (Table 7). This suggested a broad alteration of gene expression for multiple aspects of RNA metabolism in *Chd5*$^{Aam1-/-}$ spermatids, which may lead to abnormal post-transcriptional metabolism of spermatid mRNAs such as *Tnp1*, *Tnp2* and *Prm2* mRNAs. Using qRT-PCR, I validated a number of candidate Chd5 targets implicated in RNA metabolism including *Phax* (phosphorylated adaptor for RNA export), *Lsm3* (LSM3 homolog, U6 small nuclear RNA associated (S. cerevisiae)), *Cstf2t* (cleavage stimulation factor, 3' pre-RNA subunit 2, tau), *Drosha* (drosha, ribonuclease type III) and *Mov10* (Moloney leukemia virus 10) (Figure 32). Phax is a mediator required for U snRNA nuclear export [203]. Lsm3 is a component of the Lsm complexes that play critical roles in both pre-mRNA splicing and RNA degradation [204, 205]. *Cstf2t* encodes the RNA polyadenylation protein tauCstF-64, which is expressed during meiosis and haploid differentiation in testis [206]. Depletion of tauCstF-64 encoded by *Cstf2t* in mice specifically disrupts meiotic and postmeiotic development, resulting in male infertility [206]. *Drosha* encodes the RNase processing pri-miRNA into pre-miRNA and is essential for microRNA (miRNA) biogenesis [207]. It has been shown that Drosha-mediated miRNA production is essential for normal spermatogenesis and male fertility, as conditional knockout of Drosha in mouse testis depletes spermatocytes and spermatids, leading to male infertility with few or no sperm production [208]. MOV10 is a putative RNA helicase and a component of the RNA-induced silencing complex (RISC) [209]. MOV10 has been shown to interact with Argonaute 1 (AGO1) and AGO2 in mRNA processing

bodies and stress granules that participate in mRNA decay and sequester stalled mRNA translation complexes during times of cellular stress [209]. Notably, TRBP, the human homologue of mouse Prbp, is also an integral part of the RNA-induced silencing complex [210]. Together, these data revealed that the expression of three genes (*Prbp*, *Drosha* and *Mov10*) implicated in the miRNA biogenesis pathway were reduced in *Chd5*$^{Aam1-/-}$ spermatids, suggesting that miRNA biogenesis may be compromised in *Chd5*$^{Aam1-/-}$ round spermatids.

4.4 Compromised rRNA biogenesis in Chd5-deficient spermatids and candidate Chd5 targets implicated in translation

As described in Chapter 2, a Chd5-intense signal near the edge of chromocenter in round spermatids showed proximity to nucleolus marker fibrillarin (see Figure 5), suggesting that Chd5 may play a role in rRNA biogenesis. To test this hypothesis, I used qRT-PCR to determine whether Chd5 deficiency could affect production of 45S rRNA precursor and 28S mature rRNA in *Chd5*$^{Aam1-/-}$ round spermatids. Indeed, I found that expression of 45S rRNA was reduced approximately 30% in *Chd5*$^{Aam1-/-}$ round spermatids compared to wild type counterparts, and 28S rRNA expression was reduced over 50% (Figure 33). Considering the high abundance of rRNA in spermatids, the 30-50% reduction of rRNAs in *Chd5*$^{Aam1-/-}$ spermatids represented a very significant decrease and could substantially affect ribosomal assembly. These findings revealed compromised rRNA biogenesis in Chd5-deficient spermatids. How Chd5 deficiency may affect rRNA biogenesis requires further investigation, however a role for Chd5 in rRNA biogenesis would be consistent with the known function of other CHD proteins such as CHD4 and CHD7 in positively regulating rRNA biogenesis [113, 114]. Indeed, RNA-Seq and gene ontology analyses revealed that expression of 5 genes implicated in translation and ribosomal structure and

biogenesis were changed in *Chd5*$^{Aam1-/-}$ spermatids (Table 7). For example, expression of *Rptor* (regulatory associated protein of mTOR) showed over 50% reduction in *Chd5*$^{Aam1-/-}$ spermatids compared to *Chd5*$^{Aam1+/+}$ spermatids (Figure 34). Rptor is a defining component of the mTOR complex 1 (mTORC1), which directly regulates protein synthesis in mammals [211]. Thus, compromised *Rptor* expression may affect protein synthesis in *Chd5*$^{Aam1-/-}$ spermatids.

4.5 Gene expression changes and candidate Chd5 targets implicated in nuclear structure

Gene ontology analyses of round spermatid RNA-Seq data also identified 10 genes implicated in chromosome structure and 15 genes implicated in nuclear lumen (Table 7). Notably, expression of *Syne3* (spectrin repeat containing, nuclear envelope family member 3), previously known as *4831426l19Rik*, was reduced over 80% in *Chd5*$^{Aam1-/-}$ spermatids (Figure 29). Syne3 is a nuclear envelope component tethering the nucleus to the cytoskeleton and is critical for maintaining nuclear organization and structural integrity as well as sperm head development [212-216]. Thus, the compromised expression of *Syne3* in *Chd5*$^{Aam1-/-}$ spermatids may contribute to the abnormal head morphology of *Chd5*$^{Aam1-/-}$ sperm.

Altogether, the RNA-Seq results revealed gene expression changes with functional implications consistent with prior discoveries of the impacts of Chd5 deficiency on histone acetylation, DNA damage response and homeostasis of transition proteins and protamines, and identified candidate targets through which Chd5 may mediate these processes. The RNA-Seq results also provided new insights on how Chd5 deficiency may lead to abnormal sperm nuclear morphology. Although I have prioritized and validated the expression changes of a number of targets identified from the RNA-Seq data, more work is needed to determine whether Chd5 directly regulates the expression of these targets, to functionally characterize the relationships

between these targets and Chd5, and to investigate many other interesting Chd5 targets identified. Findings from such studies will not only provide more comprehensive and mechanistic details about Chd5's functions during spermatogenesis, but could also provide valuable implications for studying Chd5 functions in non-spermatogenic cells.

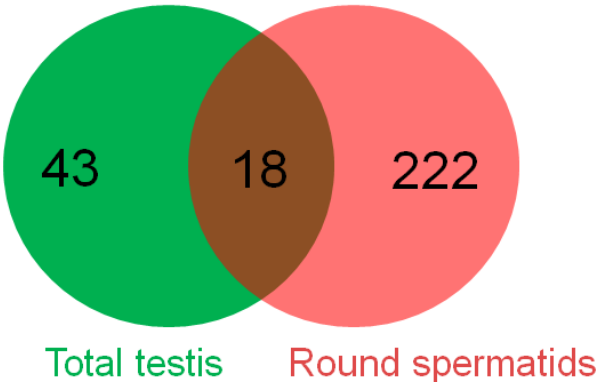

Figure 28. Statistics of common and unique hits between total testis and round spermatid RNA-Seq results

Transcript expression levels represented by FPKM (fragments per kilo bases per mapped million reads) were calculated by Cufflinks [177] for all the samples. Cuffdiff was then run to detect differential expression between *Chd5*$^{Aam1+/+}$and *Chd5*$^{Aam1-/-}$ samples. Differential expressions of protein-coding transcripts with at least a 2 fold change between *Chd5*$^{Aam1-/-}$ samples and *Chd5*$^{Aam1+/+}$ controls were selected. 61 hits were identified from total testis RNA-Seq and 240 hits were identified from round spermatid RNA-Seq. 18 hits were commonly identified in both total testis and round spermatid RNA-Seq results.

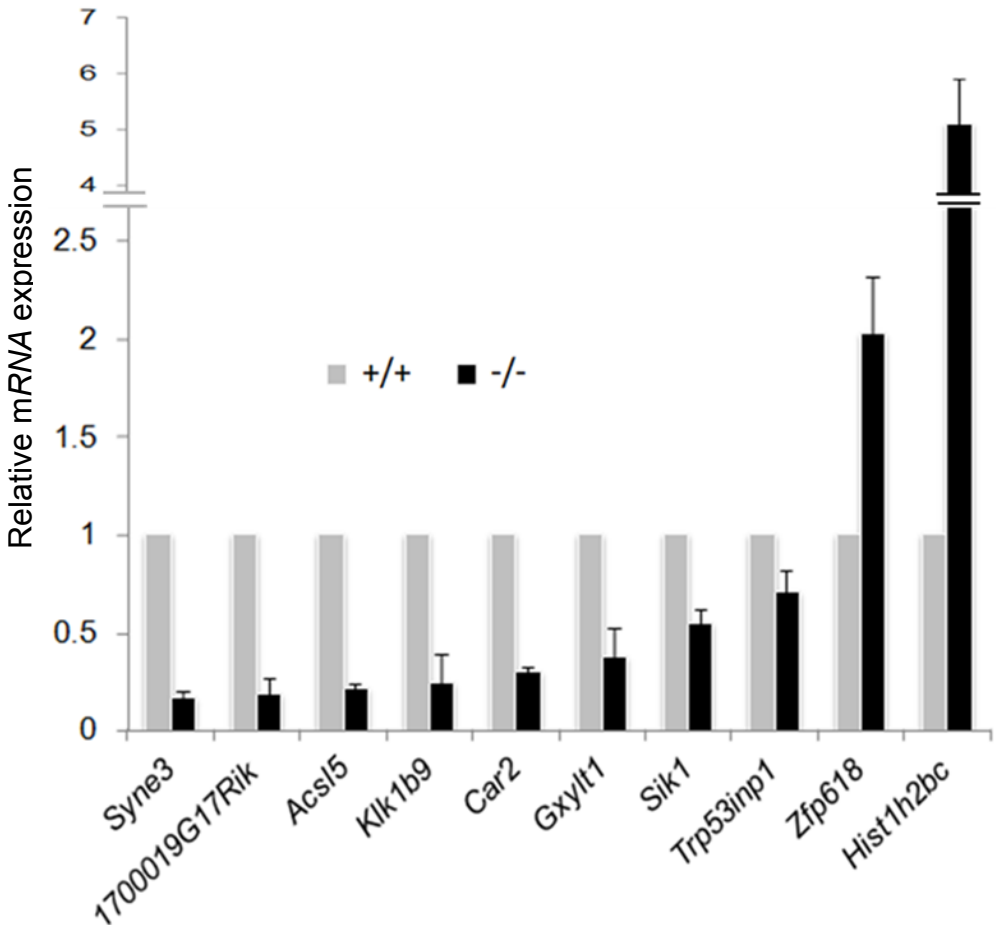

Figure 29. qRT-PCR validation of RNA-Seq hits in round spermatid samples

qRT-PCR was first performed and repeated on the same round spermatid RNA samples used for RNA-Seq. Each RNA sample was prepared from round spermatids elutriation-purified from a pool of 5 *Chd5*$^{Aam1+/+}$ (+/+) or *Chd5*$^{Aam1-/-}$ (-/-) mice with matched background and age (approximately 10 months old). The results validated the expression changes of the indicated genes revealed by RNA-Seq. qRT-PCR was then performed and repeated on another batch of round spermatid RNA samples prepared from a different set of mice with different age. In this batch of RNA samples, each RNA sample was prepared from round spermatids elutriation-purified from a pool of 3 *Chd5*$^{Aam1+/+}$ or *Chd5*$^{Aam1-/-}$ mice with matched background and age (approximately 3 months old). qRT-PCR results showed consistent results between the two batches of pooled RNA samples. All the qRT-PCR results were pooled together and data were presented as mean ± s.d. from five independent experiments. *Syne3* (spectrin repeat containing, nuclear envelope family member 3), previously known as *4831426l19Rik*; *1700019G17Rik* (RIKEN cDNA 1700019G17 gene), *Acsl5* (acyl-CoA synthetase long-chain family member 5), *Klk1bp* (kallikrein 1-related peptidase b9), *Car2* (carbonic anhydrase 2), *Gxylt1* (glucoside xylosyltransferase 1), *Sik1* (salt inducible kinase 1), *Trp53inp1* (transformation related protein 53 inducible nuclear protein 1), *Zfp618* (zinc finger protein 618), *Hist1h2bc* (histone cluster 1, H2bc).

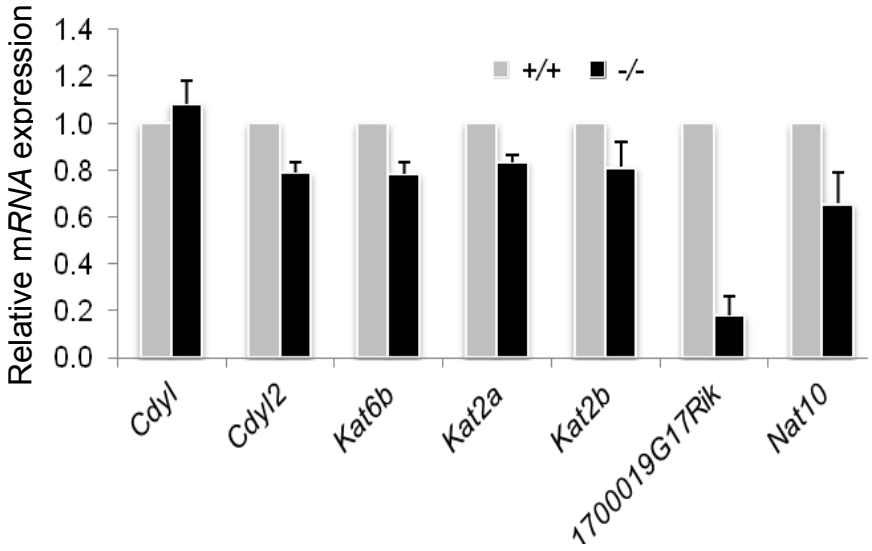

Figure 30. Compromised expression of candidate H4 acetyltransferases in Chd5-deficient spermatids

qRT-PCR analyses of indicated genes in *Chd5*$^{Aam1+/+}$ (+/+) and *Chd5*$^{Aam1-/-}$ (-/-) round spermatids. Results were normalized to *Actb* expression. Data were presented as mean ± s.d. from three to five independent experiments. *Cdyl* (chromodomain protein, Y chromosome-like); *Cdyl2* (chromodomain protein, Y chromosome-like 2); *Kat6b* (lysine acetyltransferase 6B), *Kat2a* (lysine acetyltransferase 2A), *Kat2b* (lysine acetyltransferase 2B), *1700019G17Rik* (RIKEN cDNA 1700019G17 gene), *Nat10* (N-acetyltransferase 10), *Acsl5* (acyl-CoA synthetase long-chain family member 5).

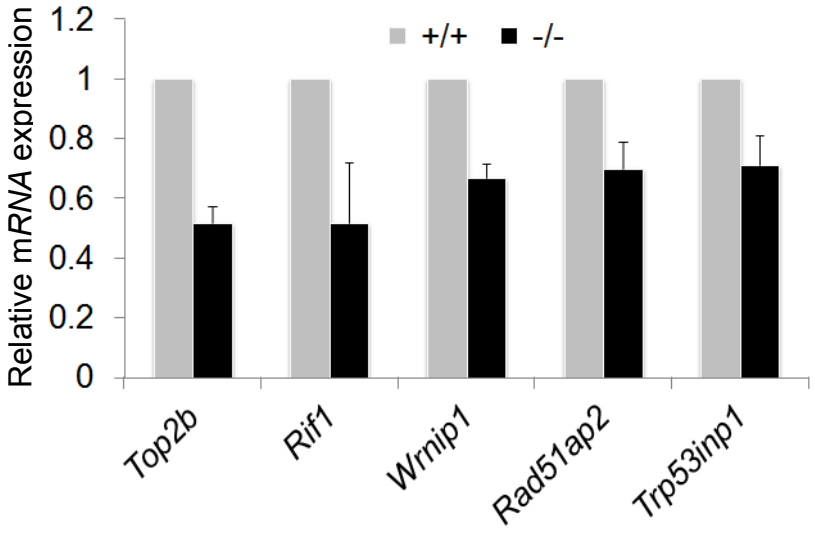

Figure 31. Compromised expression of DNA damage response genes in Chd5-deficient spermatids

qRT-PCR analyses of indicated genes in *Chd5*$^{Aam1+/+}$ (+/+) and *Chd5*$^{Aam1-/-}$ (-/-) round spermatids. Results were normalized to *Actb* expression. Data were presented as mean ± s.d. from five independent experiments. *Top2b* (topoisomerase (DNA) II beta), *Rif1* (Rap1 interacting factor 1 homolog (yeast)), *Wrnip1* (Werner helicase interacting protein 1), *Rad51ap2* (RAD51 associated protein 2) *and Trp53inp1* (transformation related protein 53 inducible nuclear protein 1).

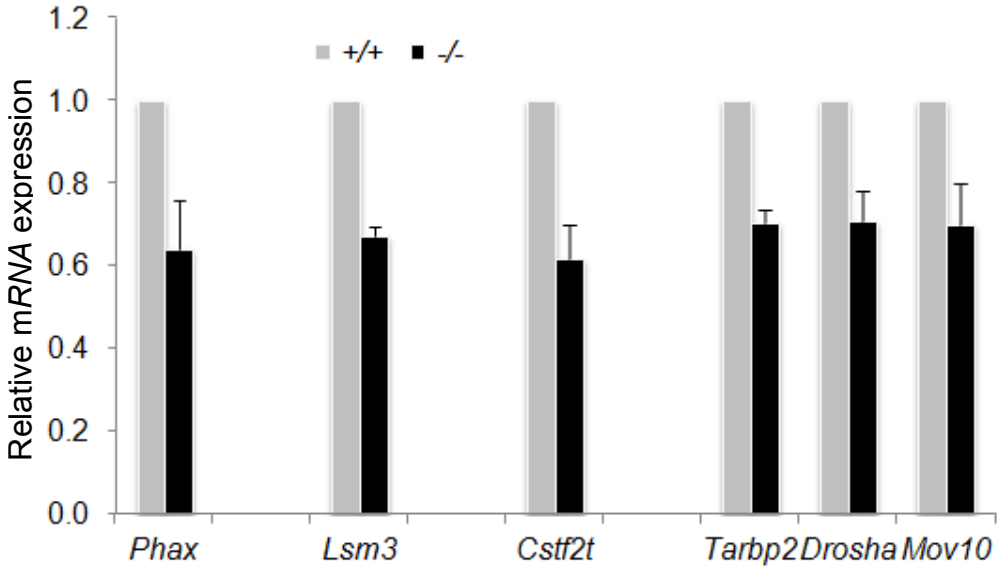

Figure 32. Compromised expression of genes implicated in RNA metabolism in Chd5-deficient spermatids

qRT-PCR analyses showed decreased expression of *Phax* (phosphorylated adaptor for RNA export), *Lsm3* (LSM3 homolog, U6 small nuclear RNA associated (S. cerevisiae)), *Cstf2t* (cleavage stimulation factor, 3' pre-RNA subunit 2, tau), *Tarbp2* (TAR (HIV) RNA binding protein 2), *Drosha* (drosha, ribonuclease type III) and *Mov10* (Moloney leukemia virus 10) in $Chd5^{Aam1-/-}$ (-/-) round spermatids. Results were normalized to *Actb* expression. Data were presented as mean ± s.d. from three to five independent experiments. *Tarbp2* encodes Prm1-RNA binding protein, i.e. Prbp.

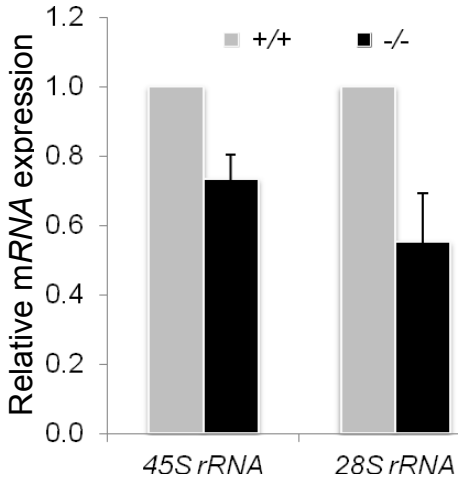

Figure 33. Compromised rRNA biogenesis in Chd5-deficient spermatids

qRT-PCR analyses showed reduced production of 45S rRNA precursor and 28S mature rRNA in *Chd5*$^{Aam1-/-}$ (-/-) round spermatids. Results were normalized to *Actb* expression. Data were presented as mean ± s.d. from five independent experiments.

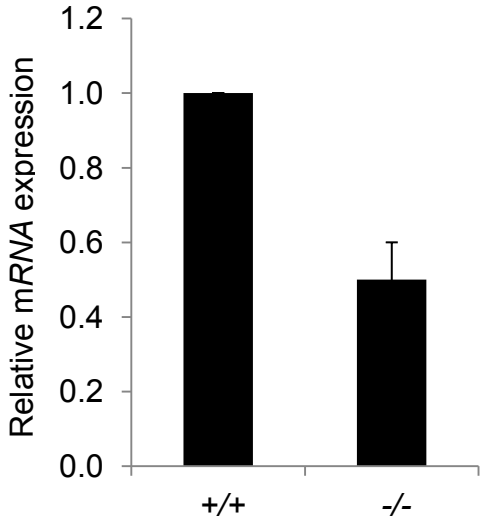

Figure 34. Compromised expression of *Rptor* in Chd5-deficient spermatids

qRT-PCR analyses revealed compromised expression of *Rptor* (regulatory associated protein of mTOR) in *Chd5*$^{Aam1-/-}$ (-/-) round spermatids. Results were normalized to *Actb* expression. Data were presented as mean ± s.d. from five independent experiments.

Table 5. Summary of gene expression changes revealed by RNA-Seq

	Total testis	Round spermatids
Down regulated	30	146
Up regulated	31	94
Total	61	240

Cufflinks was first used to calculate transcript expression levels represented by FPKM (fragments per kilo bases per mapped million reads) for all the samples. Cuffdiff was then run to detect differential expression between $Chd5^{Aam1+/+}$ and $Chd5^{Aam1-/-}$ samples. Genes whose expressions in $Chd5^{Aam1-/-}$ samples were 50% or less of the expression in $Chd5^{Aam1+/+}$ controls were selected as down-regulated genes. Genes whose expressions in $Chd5^{Aam1-/-}$ samples were 2 fold or more of the expression in $Chd5^{Aam1+/+}$ controls were selected as up-regulated genes.

Table 6. Gene ontology classification of total testis RNA-Seq gene list

Gene Ontology Category	Term	Gene Counts	% of Total	P-Value
GOTERM_BP_FAT	phosphate metabolic process	7	12.1	7.90E-03
GOTERM_BP_FAT	tissue morphogenesis	4	6.9	1.50E-02
GOTERM_BP_FAT	regulation of secretion	3	5.2	3.00E-02
GOTERM_BP_FAT	protein amino acid phosphorylation	5	8.6	4.10E-02
GOTERM_BP_FAT	regulation of Ras protein signal transduction	3	5.2	4.80E-02
SP_PIR_KEYWORDS	cell membrane	11	19	6.00E-03
SP_PIR_KEYWORDS	membrane	20	34.5	3.30E-02

The 61 genes showing at least a 2 fold expression change between *Chd5*$^{Aam1+/+}$ and *Chd5*$^{Aam1-/-}$ total testis samples were analyzed for gene ontology classification using DAVID (v6.7) [178]. GOTERM_BP_FAT, GOTERM_MF_FAT, SP_PIR_KEYWORDS, SP_PIR_KEYWORDS and COG_ONTOLOGY categories were selected for the gene ontology analyses. The top ontology terms identified were presented. Gene Counts, number of genes enriched in the term; % of Total, the percentage of genes enriched in the specific ontology term among the total 61 genes.

Table 7. Gene ontology classification of round spermatid RNA-Seq gene list

Gene Ontology Category	Term	Gene Counts	% of total	P-Value
SP_PIR_KEYWORDS	phosphoprotein	105	44.7	1.00E-09
SP_PIR_KEYWORDS	alternative splicing	73	31.1	5.80E-06
SP_PIR_KEYWORDS	acetylation	39	16.6	3.00E-03
GOTERM_MF_FAT	nucleotide binding	34	14.5	1.70E-02
GOTERM_MF_FAT	ATP binding	25	10.6	1.40E-02
GOTERM_MF_FAT	adenyl ribonucleotide binding	25	10.6	1.60E-02
GOTERM_CC_FAT	nuclear lumen	15	6.4	3.80E-02
GOTERM_BP_FAT	cell cycle	13	5.5	1.60E-02
GOTERM_BP_FAT	protein transport	13	5.5	2.40E-02
SP_PIR_KEYWORDS	ubl conjugation	13	5.5	9.60E-03
GOTERM_CC_FAT	vesicle	11	4.7	2.90E-02
GOTERM_CC_FAT	chromosome	10	4.3	8.60E-03
KEGG_PATHWAY	Endocytosis	6	2.6	2.40E-02
COG_ONTOLOGY	Translation, ribosomal structure and biogenesis	5	2.1	1.10E-02
GOTERM_MF_FAT	lipid transporter activity	4	1.7	1.10E-02
GOTERM_MF_FAT	N-acetyltransferase activity	4	1.7	1.70E-02
SP_PIR_KEYWORDS	fatty acid metabolism	4	1.7	2.60E-02
GOTERM_BP_FAT	nuclear export	3	1.3	3.10E-02

The 240 genes showing at least a 2 fold expression change between *Chd5*$^{Aam1+/+}$ and *Chd5*$^{Aam1-/-}$ round spermatid samples were analyzed for gene ontology classification using DAVID (v6.7) [178]. GOTERM_BP_FAT, GOTERM_MF_FAT, SP_ PIR _KEYWORDS, and COG_ONTOLOGY categories were selected for the gene ontology analyses. The top ontology terms identified were presented. Gene Counts, number of genes enriched in the term; % of Total, the percentage of genes enriched in the specific ontology term among the total 240 genes.

Chapter 5

Validation in a second Chd5-deficient mouse model

As I observed variations from infertility to subfertility among *Chd5*$^{Aam1-/-}$ male mice and variable extent of histological abnormalities in *Chd5*$^{Aam1-/-}$ testes, I asked whether genetic background variations could be an underlying contributor to the phenotypic variations, given that the *Chd5*$^{Aam1-/-}$ mouse model analyzed was in a mixed C57BL/6 and 129S7 background. To determine whether the genetic background was responsible, we generated a different Chd5-deficient mouse model termed as *Chd5*$^{Tm1b-/-}$ mouse (*Tm1b* stands for targeted mutation 1 b) using *Chd5*-targeted ES cell lines purchased from EUCOMM (European Conditional Mouse Mutagenesis). One advantage of this model was that the targeted ES cells and resulting *Chd5*^{Tm1b} mice were on a 100% C57BL/6 background. The model also used a targeting strategy distinct from the one we used for generating the *Chd5*^{Aam1} mouse model. For the *Chd5*^{Aam1} model, an insertional targeting strategy was used to disrupt exon 38 of *Chd5* to inactivate Chd5 expression (Figure 7). In *Chd5*^{Tm1b} mice, a conditional *Cre-LoxP* knockout strategy was applied to excise exon 2 of *Chd5* locus (Figure 35). Western blot confirmed depletion of Chd5 protein in *Chd5*$^{Tm1b-/-}$ testes (Figure 36). Similar to *Chd5*$^{Aam1-/-}$ male mice, mating tests showed that *Chd5*$^{Tm1b-/-}$ male mice were also either sterile or subfertile (Table 8), suggesting that the variability of infertility in Chd5-deficient mice was inherent to Chd5 loss and not likely due to genetic background variation. I also observed lower sperm counts and lower sperm motility in *Chd5*$^{Tm1b-/-}$ male mice as in *Chd5*$^{Aam1-/-}$ male mice. Furthermore, histone H4 acetylation was compromised in *Chd5*$^{Tm1b-/-}$ testes as observed in *Chd5*$^{Aam1-/-}$ testes (Figure 37). These phenotypic and molecular resemblances between the two distinct Chd5-deficient mouse models (*Chd5*$^{Aam1-/-}$

and *Chd5*$^{Tm1b-/-}$) confirmed that the spermatogenetic phenotypes and molecular changes revealed in Chd5-deficient male mice are not likely affected by genetic background or gene targeting strategy, but rather are the phenotypic consequences of Chd5 deficiency.

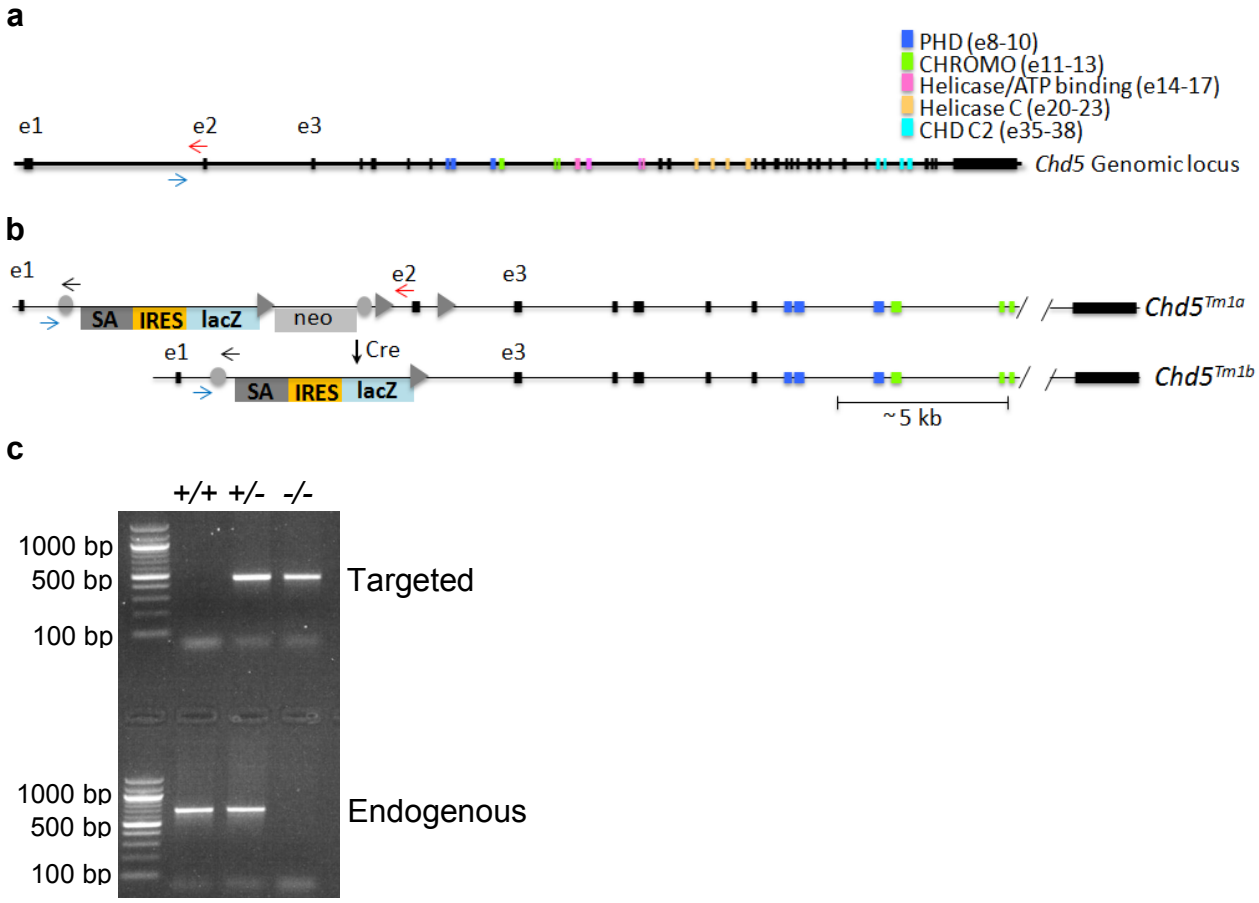

Figure 35. Generation of *Chd5*^{Tm1b} mice through gene targeting

a, Genomic structure of mouse *Chd5*. Exons (e1, e2, e3…e42) encoding predicted domains were marked by colors. Blue and red arrows indicated PCR genotyping primers to detect a 674 bp endogenous band specific for wild type *Chd5* allele. **b,** Diagram of targeted *Chd5* alleles prior to Cre excision (*Chd5*^{Tm1a}) and after Cre excision (*Chd5*^{Tm1b}). Excision of exon 2 also led to a frameshift. Grey circle, *Frt* site; grey triangle, *LoxP* site; SA, splicing acceptor site; IRES, Internal ribosome entry site; lacZ, β-galactosidase; Neo, neomycin cassette. Blue and black arrows indicated PCR genotyping primers to detect a 456 bp band from *Chd5*^{Tm1b} allele. **c,** Genotyping of *Chd5*$^{Tm1b+/+}$, *Chd5*$^{Tm1b+/-}$ and *Chd5*$^{Tm1b-/-}$ mice through PCR using the primers indicated in **a, b.** Blue forward primer, Tm1b-F; black reverse primer, Tm1b-R; red reverse primer, Tm1b-WT-R. **+/+,** *Chd5*$^{Tm1b+/+}$; +/-, *Chd5*$^{Tm1b+/-}$; -/-, *Chd5*$^{Tm1b-/-}$.

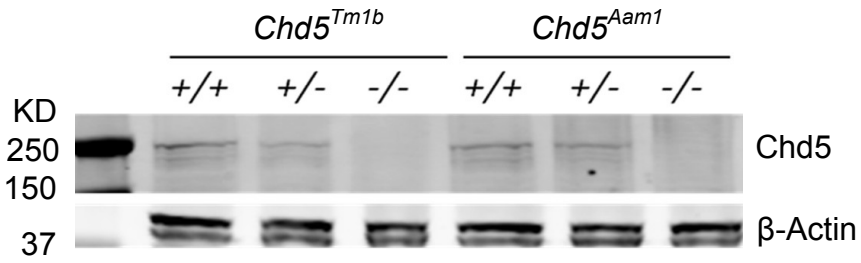

Figure 36. Depletion of Chd5 protein in *Chd5$^{Tm1b-/-}$* testes

Western blot against Chd5 on total testis lysates from *Chd5$^{Tm1b-/-}$* and *Chd5$^{Aam1-/-}$* mice showed that Chd5 protein was not detected in both *Chd5$^{Tm1b-/-}$* and *Chd5$^{Aam1-/-}$* testes, whereas it was detected in wild type as well as *Chd5$^{Tm1b+/-}$* and *Chd5$^{Aam1+/-}$* testes. β-Actin served as a loading control.

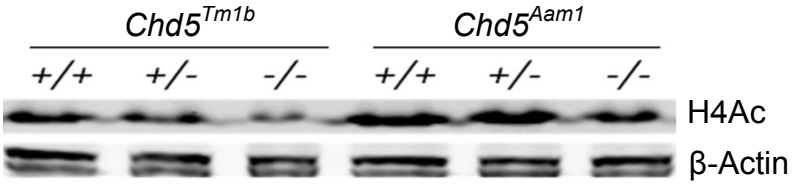

Figure 37. Compromised histone H4 acetylation in *Chd5*$^{Tm1b-/-}$ testes

Western blot of total testis lysates showed compromised H4 acetylation (H4Ac) in both *Chd5*$^{Tm1b-/-}$ and *Chd5*$^{Aam1-/-}$ testes compared to wild type or *Chd5*$^{Tm1b+/-}$ or *Chd5*$^{Aam1+/-}$ testes. H4Ac was detected by a rabbit polyclonal antibody against pan-H4 acetylation. β-Actin served as a loading control.

Table 8. Mating tests revealed infertility in *Chd5*$^{Tm1b-/-}$ male mice.

Sex	Genotype	Infertile mice/Total	Fertile mice/Total	Total litter#	Total progeny	Average litter size
Male	*Chd5*$^{Tm1b+/+}$	0/4	4/4	28	220	7.9
	Chd5$^{Tm1b-/-}$	3/5	2/5	5	11	2.2

When mated to wild type females for over 5 months, 3 out of 5 *Chd5*$^{Tm1b-/-}$ male mice tested were infertile. The remaining 2 were subfertile, producing only 5.0% (11/220) of the offspring of their *Chd5*$^{Tm1b+/+}$ littermates. The average 2.2 progeny per litter produced by subfertile *Chd5*$^{Tm1b-/-}$ male mice was similar to the 2.8 progeny per litter produced by subfertile *Chd5*$^{Δam1-/-}$ male mice (Table 1).

Chapter 6

Discussion and Perspectives

Remarkable chromatin remodeling activities take place during spermiogenesis, a fascinating process that dramatically reorganizes the spermatid genome and provides an excellent system to study chromatin remodeling *in vivo*. Given its dramatic chromatin reorganization, chromatin remodelers have been expected to be essential for the process but had not been identified. Here, I identified Chd5 as the first chromatin remodeler that played essential roles during spermiogenesis, and revealed surprising functions in male reproduction for Chd5, whose roles have been assumed to be in the nervous system. I further discovered that Chd5 exerts multifaceted roles in the extensive histone-to-protamine remodeling process during spermiogenesis. Chd5 deficiency led to disruption of a cascade of processes underlying the removal of histones during spermiogenesis, including H4 hyperacetylation, nucleosome eviction, DNA damage and repair, and histone variant production. Meanwhile, Chd5 deficiency led to abnormal homeostasis of protamines and transition proteins, including increased transcription of *Prm1* and post-transcriptional expression of Prm2, Tnp1 and Tnp2. Together, Chd5 seems to play a role in orchestrating the remarkable histone-to-protamine remodeling process. Thus, Chd5 could provide an excellent access point to unravel the molecular networks underlying histone removal and regulation of homeostasis of transition proteins and protamines during spermiogenesis. Indeed, RNA-Seq experiments revealed that Chd5 deficiency altered expressions of a diverse molecular network implicated in a range of molecular functions and biological processes that could mediate histone removal and/or homeostasis of transition proteins and protamines, such as acetylation, nucleotide binding, ATP binding, chromosome and nuclear

structure, RNA transport, processing and translation, rRNA biogenesis as well as protein synthesis, transport, modification and degradation (Table 7). The RNA-Seq results thus provided an excellent starting point for follow-up projects to identify and characterize Chd5 targets that may directly mediate histone removal and homeostasis of transition proteins and protamines as well as other proteins.

Notably, I showed that rRNA biogenesis was compromised in Chd5-deficient spermatids, an observation further supported by RNA-Seq results revealing expression changes of 5 genes implicated in ribosomal structure and biogenesis in Chd5-deficient spermatids. These findings suggested that Chd5 may play a role in mediating rRNA biogenesis. Such a role would be in agreement with my earlier observation that an intense Chd5 signal was present in proximity to the nucleolus. It would also be consistent with the known function of other CHD proteins such as CHD4 and CHD7 in rRNA biogenesis [113-115]. Further studies to determine whether Chd5 directly regulates rRNA production will be highly warranted. If confirmed, validation of the candidate Chd5 targets revealed by RNA-Seq and further investigation of how Chd5 may modulate rRNA biogenesis in both spermatogenic cells and somatic cells will shed more light on Chd5's function in rRNA biogenesis and also add insights into how the CHD family proteins commonly regulate rRNA biogenesis.

Meanwhile, I have identified a number of candidate Chd5 target genes that are implicated in H4 acetylation and DNA damage response during spermiogenesis. In particular, the enzymes responsible for H4 hyperacetylation remain unidentified and it has been of great interest for the field. My findings suggested that the acetyltransferases and deacetylases modulated by Chd5 could be high-potential candidates responsible for H4 hyperacetylation during spermiogenesis. Specifically, the expression of *1700019G17Rik*, which encodes a putative N-

acetyltransferase, was substantially reduced in *Chd5*$^{Aam1-/-}$ spermatids in which H4 acetylation was severely compromised. Along with the high expression of *1700019G17Rik* in elongating spermatids, these data suggested 1700019G17Rik as a high-potential candidate acetyltransferase that may play a role in H4 hyperacetylation during spermiogenesis. In addition, expression of the acetyltransferase-encoding genes *Nat10*, *Cdyl2, Myst4*, and *Kat2a* were also modestly compromised in Chd5-deficient spermatids, providing hints that these acetyltransferases may play roles in H4 acetylation during spermiogenesis. Further studies to demonstrate and characterize the roles of these enzymes in histone acetylation during spermiogenesis would be valuable. In addition, revealing interacting partners of Chd5 in round and early elongating spermatids through proteomics approaches will present another opportunity for identifying potential acetyltransferases and/or deacetylases responsible for H4 acetylation during spermiogenesis.

H4 hyperacetylation in early elongating spermatids is essential for histone-to-protamine replacement in *Drosophila* [24] and has been widely considered to be also a prerequisite for the nucleosome eviction and histone removal during mammalian spermiogenesis [12, 23, 24]. In my study, I discovered that Chd5 deficiency led to severely compromised H4 acetylation in elongating spermatids, and subsequent defects in nucleosome eviction and histone removal, supporting the idea that H4 hyperacetylation is critical for efficient nucleosome eviction and histone removal during mouse spermiogenesis. However, most nucleosomes and histones eventually got disposed in late *Chd5*$^{Aam1-/-}$ spermatids. In addition, Western blot analyses of fractionated wild type spermatids also revealed that large amount of histones were already removed in the fraction of round and early elongating spermatids before the appearance of H4 hyperacetylation (Figure 23), suggesting H4 hyperacetylation-independent histone removal in

those spermatids. These findings suggested that whereas H4 hyperacetylation is important for efficient nucleosome eviction and histone removal during mammalian spermiogenesis, it seems non-essential, countering the current general view. Thus, whether H4 hyperacetylation is required for histone-to-protamine replacement during mammalian spermiogenesis warrants further investigation.

I discovered that Chd5 expression was stimulated in somatic cells by DNA damage such as adriamycin treatment and revealed increased DNA damage in Chd5-deficient spermatids during spermiogenesis. Consistent with previous reports [162-165], my study revealed extensive DNA break and repair during spermiogenesis. Such DNA damage, however, is normally repaired by the time of late spermatid steps. Given the haploid nature of the spermatid genome, its DNA repair must rely on error-prone nonhomologous recombination mechanisms. Thus, the spermiogenesis process could be potentially mutagenic. Indeed, a transgenic mouse model for Huntington Disease showed that the CAG trinucleotide expansion occurs specifically during spermiogenesis, but not during mitosis or meiosis [217]. Whereas such mutagenesis could provide a source for evolution selection, it is critical to repair such DNA damage properly and in a timely manner in order to maintain genomic integrity, ensure normal functionality of the sperm and prevent transmission of detrimental genomic lesions to the next generation. Increasing evidence indicate aberration of chromatin integrity in male gametes as a cause of male infertility as well as *de novo* genetic disorders and developmental defects in the offspring [196, 218-220]. In my study, I demonstrated that abnormalities in the chromatin remodeling process during spermiogenesis in $Chd5^{Aam1-/-}$ testes led to increased DNA damage. The increased DNA damage may lead to higher genomic mutagenesis, and contribute to the defective sperm production and infertility of $Chd5^{Aam1-/-}$ male mice. The intrinsically variable extent of DNA damage may

contribute to the observed variability of infertility among individual *Chd5*$^{Aam1-/-}$ male mice. Moreover, it suggested that aberrations in the chromatin remodeling and/or DNA repair processes during spermiogenesis, due to either lesions in genes critical for the processes or aging effects, could significantly increase genomic lesions in the sperm and thus may predispose the next generation to higher risk of *de novo* genetic disorders, developmental defects and neuropsychiatric diseases that were shown to be associated with *de novo* genomic lesions [221-224]. To test this hypothesis, it would be interesting to investigate whether sperms from *Chd5*$^{Aam1-/-}$ mice, compared to *Chd5*$^{Aam1+/-}$ and *Chd5*$^{Aam1+/+}$ controls, have increased genomic lesion such as copy number variations (CNVs) and mutations through genomic studies. It will be also interesting to follow up the progenies from subfertile *Chd5*$^{Aam1-/-}$ male mice to determine whether these progenies show signs of increased and/or accelerated pathogenesis compared to progenies produced from *Chd5*$^{Aam1+/-}$ and *Chd5*$^{Aam1+/+}$ controls.

The cascade of defects in H4 hyperacetylation, nucleosome eviction, and DNA damage and repair during *Chd5*$^{Aam1-/-}$ spermatid maturation provided functional evidence revealing the sequential order of these events, and suggested a model for the molecular events underlying the histone-to-protamine replacement process during spermiogenesis: H4 is first hyperacetylated, which along with other epigenetic modifications, leads to chromatin loosening and nucleosome eviction to facilitate histone removal and exposure of the DNA to allow for deposition of transition proteins and eventually protamines. Top2β resolves the supercoiling that is introduced by nucleosome eviction, and DSBs are generated during this process. A DNA damage response is then activated to repair the DSBs, ensuring integrity of the sperm genome. This sequence of molecular events is in agreement with a model proposed by Leduc *et al.* from observation of the expression pattern of H4 hyperacetylation, Top2β and γ-H2A.X during spermiogenesis [162].

My findings established functional evidence revealing the cascade of major molecular events underlying the histone-to-protamine replacement process, and provided a guiding model to further elucidate this critical process.

Chapter 7

Materials and Methods

Generation of *Chd5*$^{Aam1-/-}$ mice and genotyping

The *Chd5* locus was disrupted in AB2.2 ES cells using the MHPN20h05 MICER vector through gap-induced insertional targeting, and targeted ES cells were injected into C57BL/6 blastocysts through standard procedures. Progeny resulting from germline transmission were backcrossed to wild type C57BL/6 mice and *Chd5*$^{Aam1+/-}$ mice were intercrossed to obtain homozygotes. For Southern blot genotyping, the MHPN20h05 MICER vector was cut with *Afl* II and the 2.6 kb fragment was gel purified and used as a probe. Southern blot of genomic DNA cut with *Bgl* II using the 2.6 kb probe yielded the expected 7.8 kb endogenous band and 10.4 kb targeted bands. Genotypes were differentiated based on dosage of the targeted allele (*Chd5*$^{Aam1+/+}$, 0 copy; *Chd5*$^{Aam1+/-}$, 1 copy; *Chd5*$^{Aam1-/-}$, 2 copies). All genotypes had 2 copies of the endogenous band, which serve as an internal loading control and reference for dosage. For PCR-based genotyping, relative dosage of the neo-cassette in different genotypes (*Chd5*$^{Aam1+/+}$, 0 copy; *Chd5*$^{Aam1+/-}$, 1 copy; *Chd5*$^{Aam1-/-}$, 2 copies) was quantified by qPCR. Neo-cassette dosage was normalized to dosage of the *Actb* locus to differentiate genotype.

Antibodies

Antibodies used for immunostaining, Western blot and ChIP are as follows: anti-H3K27me3(Cell Signaling, 9756), anti-H2A (Cell Signaling, 2578), anti-H4 (Cell Signaling, 2935), y-H2A.X (Cell signaling, 9718), anti-H3K9me3 (Active Motif, 39385), anti-H1 (Active Motif, 39707), anti-H2B (Active Motif, 39125), anti-H4Ac-pan (Active Motif, 39243), anti-H3

(Abcam, ab1791), anti-Chd5 (Santa Cruz Biotechnology, sc-68389), anti β-Actin (Sigma, A2228), anti-H4K5/8/12/14Ac (Millipore, 05-1335), lectin PNA Alex Fluor 568 (Invitrogen, L32458), anti-Prm1 and Prm2 (Briar Patch Biosciences, Hup1N and Hup2B), anti-Tnp1 and Tnp2 (gift from Dr. Stephen Kistler, University of South Carolina), anti-Nucleosome (mab #32, gift from Dr. Jo H.M. Berden, Radboud University Nijmegen Medical Center).

Histology

Testes were fixed in Bouin's fixative or 4% paraformaldehyde, embedded in paraffin, and sectioned at 5 μm. Sections were deparaffinized in xylene and subjected to Periodic acid-Schiff (PAS) staining for histological analysis using Sigma PAS staining kit (#395B-1KT) according to the manufacturer's instructions.

Immunostaining

Sections were deparaffinized in xylene and heated in either Tris-EDTA buffer pH 9.0 or 10 mM Sodium Citrate buffer pH 6.0 or Trilogy buffer (Cell Marque # 920P-10) for 15 minutes at boiling temperature under high pressure in a pressure cooker for antigen retrieval. Sections were cooled, washed in 1X PBS, blocked with 10% goat serum in 1X PBS for 1 hour at room temperature, incubated with indicated primary antibody in 1% goat serum in 1X PBS for 2 hours at room temperature or overnight at 4 °C, washed 3 times with 1X PBS, incubated with Alex Fluro® secondary antibodies for 1 hour at room temperature, counterstained with DAPI and mounted for microscopic examination and imaging.

Centrifugal elutriation

Fractionation of spermatogenic cells through centrifugal elutriation was performed as previously described [225] using a Beckman Coulter Avanti J-26XP centrifuge with JE-5.0 rotor. Briefly, testes from 3 to 6 male mice of the same genotype with matched background and age were pooled, testes were decapsulated and digested with collagenase (0.5 mg/ml) and DNase I (200 μg/ml) for 15 min with shaking at 32.5 °C in enriched DMEM/F12 (GIBCO), to which 0.1 mM non-essential amino acids (GIBCO), 1 mM L-glutamine (GIBCO), 1 mM sodium pyruvate (GIBCO), and 5 mM sodium lactate (Sigma-Aldrich, St. Louis, MO) were added. Testes dispersed into spaghetti-like tubules after collagenase digestion. The dispersed tubules were then allowed to settle and resuspended in 8 ml of enriched DMEM/F12 solution, which was then gently layered onto 40 ml of 5% Percoll solution. The tubules were allowed to settle through the Percoll solution. The supernatants were removed and the settled tubules were washed with 40ml enriched DMEM/F12 solution and then digested with trypsin (1 mg/ml) and DNase I (200 μg/ml) in enriched DMEM/F12 for 15-20 min at 32.5 °C with shaking until most tubules were dissociated into cells. Fetal bovine serum was added to 10% to quench trypsin, and the cells were dispersed by pipetting. The single cell suspensions were spun down, washed, resuspended in 1X PBS with 1.5% BSA, 5 mM NDA (Dipotassium 2-Naphthol-6,8-disulfonate), 200 μg/ml DNase I and 0.02% Soybean Trypsin Inhibitor, filtered through 30 μm nylon mesh and separated by centrifugal elutriation (JE-5.0 rotor, Beckman Coulter Avanti J-26XP) to obtain fractions enriched in condensed spermatids (flow rate: 9.6 ml/min, rotor speed: 3000 rpm), elongating and condensing spermatids (17.5 ml/min, 3000 rpm), mixture of early elongating spermatids and round spermatids (12.4 ml/min, 2250 rpm), round spermatids (17.5 ml/min, 2250 rpm), and pachytene primary spermatocytes (36.9 ml/min, 2250 rpm). Elutriated cell fractions were then

pelleted by centrifugation, washed in 1X PBS and kept for molecular or biochemical analyses. Cell smears were also prepared on glass slides for PAS staining and counted under microscope to calculate cellular purity. qRT-PCR of stage-specific markers were applied to confirm purity of elutriated cell fractions.

Western blot

Tissues or cells were homogenized and lysated in 2X Laemmli sample buffer (0.12 M Tris pH 6.8, 20% glycerol, 4% SDS, 0.2 M DTT). Lysates were subjected to SDS-Polyacrylamide Gel Electrophoresis (SDS-PAGE) and transferred to Whatman® nitrocellulose membranes. The membranes were then blocked in 5% nonfat milk or 5% BSA for 1 hour at room temperature, and incubated with indicated primary antibodies diluted in 5% nonfat milk or 5% BSA for 2 hours at room temperature or overnight at 4 °C, washed in 1X TBS with 1% Tween-20, and incubated with LI-COR IRDye® fluorescence-conjugated secondary antibodies diluted in LI-COR blocking buffer (#927-40000) for 1 hour at room temperature. Fluorescent signals and images were acquired using LI-COR Odyssey Infrared Imaging System.

qRT-PCR and ChIP

Total RNA was purified from whole testis or elutriation-purified testicular cell populations using RNeasy kit (Qiagen) with DNase I treatment. cDNA was synthesized using SuperScript III (Invitrogen), and qPCR was performed using LightCycler 480 and SYBR Green I Master mix (Roche). ChIP was performed using SimpleChIP Enzymatic Chromatin IP Kit (Cell Signaling #9003) according to the manufacturer's instructions with the indicated antibodies. Primers for qRT-PCR and ChIP-qPCR are listed in Table 9.

Basic protein extraction from sonication-resistant spermatids (SRS) and acid-urea gel electrophoresis

Testes were surgically decapsulated and homogenized in buffer (10 mM Tris-HCl pH7.2, 0.32 M sucrose, 5 mM $MgCl_2$, 0.1% Triton-X100, 0.5 mM PMSF). After centrifugation, cell pellets were resuspended in sonication buffer (10 mM Tris-HCl, pH7.5, 25 mM 2-mercaptoethanol) and sonicated in a Diagenode Bioruptor UCD-200 to obtain SRS, which represent step 12 to 16 spermatids. After centrifugation, SRS pellets were resuspended in 10 mM Tris-HCl pH 7.5 by brief vortexing and HCl was added to a final concentration of 0.5 M. Samples were incubated on ice for 30 minutes to extract basic proteins. After centrifugation, the supernatant was transferred to a clean tube and 20% trichloroacetic acid (final concentration) was added to precipitate basic proteins. Protein pellets were washed with acetone, dried, and dissolved in buffer containing 5 M urea, 0.5% acetic acid and 1% -2-mercaptoethanol. Proteins were separated by electrophoresis in acid-urea-15% polyacrylamide gels and were subjected to either staining with Coomassie brilliant blue or Western blot using the indicated antibodies.

Sperm chromatin structure assay (SCSA)

SCSA was carried out as previously described [226] using a LSR II flow cytometer (Becton Dickinson). Briefly, 200 µl approximately 1.5 x 10^6/ml fresh or frozen sperm in TNE buffer (0.1 M Tris pH 7.5, 0.15 M NaCl, 1 mM EDTA) were mixed with 400ul acid detergent solution (0.08 N HCl, 0.15 M NaCl, 0.1% Triton X-100, pH 1.2), after 30 seconds incubation exactly, 1.2 ml acridine orange staining solution (860 µg/ml acridine organge, 5 mM citric acid, 18 mM Na2HPO4, 21 mM NaCl, 0.15 mM EDTA, pH 6.0) was added to the mixture. The

mixture was then loaded into LSR II. Data recording was started after 3 minutes of running the sample in LSR. Acid treatment denatures sperm DNA into single strand if chromatin integrity is impaired. Acridine orange emits red fluorescence when binds to single strand DNA, whereas emits green fluorescence when binds to double strand DNA. SCSA quantifies the red and green fluorescence emitted by flow cytometry. Sperm with impaired chromatin have DNA that is more easily denatured by the acid treatment and thus emit more red fluorescence. The percentage of red/(green + red) fluorescence is defined as DNA Fragmentation Index (DFI) which serves as a readout for sperm chromatin integrity. The higher DFI is, the more impaired the chromatin integrity.

DNA content assay

Single-cell suspensions were prepared from whole testis through mild homogenization with a Polytron homogenizer, filtered through 70 μm nylon mesh, and fixed in ice-cold 70% ethanol for 2 hours. After washes, cells were resuspended in 0.5% pepsin in PBS (pH 2.0) for 10 minutes at 37 °C, and stained with propidium iodide solution (5 mM Tris pH 8, 0.5 mM NaCl, 0.05% Nonidet P-40, 0.35 mg/ml RNase A, 0.025 mg/ml propidium iodide) for 20 minutes at room temperature. Cells were kept on ice or at 4°C prior to flow cytometry analysis with the LSR II (Becton Dickinson).

TUNEL assay

TUNEL assay was performed with the *In Situ Cell Death Detection* Fluorescein *Kit (*Roche), following the manufacturer's instruction. Briefly, testes sections were deparaffinized, rehydrated, and digested with 20 μg/ml Proteinase K in 10 mM Tris pH 7.5 for 30 minutes at

37°C. After washes, sections were incubated with TUNEL reaction mixture for 1 hour at 37°C, followed by staining with lectin PNA (1:4000, 1 hr) and DAPI (1:5000, 5 minutes) to visualize acrosomes and DNA.

Sperm counts and motility analysis

Individual caudal epididymi were minced in 200 µl HTF medium (Irvine Scientific). After 30 minutes incubation at 37 °C, the tissue pieces were separated from sperm by pipetting and passaging through a 70 µm nylon filter. Sperm counts and motility assessment were performed using the DRM-600 CELL-VU Sperm Counting Cytometer under microscopy. Sperm that showed movement were counted as motile sperm, among which those progressively moved forward were counted as progressive motile sperm. Sperm that didn't show movement were counted as immotile sperm.

Sperm morphology assessment

Air-dried smears were prepared from sperm in PBS, stained with hematoxylin, and examined using light microscopy at 100 X magnification. Head, neck, and tail morphology were determined independently for each individual mouse with counts of at least 100 sperm per sample.

Transmission Electron Microscopy

Testes were fixed with 2% paraformaldehyde and 2% glutaraldehyde in 0.1 M sodium phosphate buffer (pH 7.4), dehydrated, and embedded in Epon. Sections were contrasted and imaged in a Hitachi H7000T transmission electron microscope.

Hormone quantification

Blood were collected from mice through tail bleeding and clotted at room temperature for 30 min. Serum were separated from clotted cells through centrifugation. Levels of follicle-stimulating hormone, leutinizing hormone, and testosterone in the serum were determined by the Ligand Core Laboratory at University of Virginia.

RNA-Seq

RNA-Seq was performed for both whole testes and elutriation-purified round spermatids. For whole testes, 3 sets of $Chd5^{Aam1+/+}$: $Chd5^{Aam1+/-}$: $Chd5^{Aam1-/-}$ littermate male mice with matched background and age were used. Total RNA was prepared from testis of each individual mouse (3 $Chd5^{Aam1+/+}$: 3 $Chd5^{Aam1+/-}$: 3$Chd5^{Aam1-/-}$) using RNeasy kit (Qiagen) with DNase I treatment. RNA-Seq libraries were then prepared from the 9 RNA samples using Illumina TruSeq protocol with oligo-dT primer for reverse transcription. For round spermatids, 5 sets of $Chd5^{Aam1+/+}$: $Chd5^{Aam1+/-}$: $Chd5^{Aam1-/-}$ littermate male mice with matched background and age were used. Ten testes from 5 mice of the same genotype were pooled together for elutriation fractionation, and the purified round spermatid population was thus a pooled sample from 5 individual mice of the same genotype. Total RNAs and RNA-Seq libraries were prepared from pooled round spermatid samples using the same methods for total testis samples. RNA-Seq libraries were barcoded and sequenced on Illumina HiSeq 2000.

RNA-Seq data analyses

The quality of raw data was assessed and passed by FastQC. The reads were then mapped to mm9 genome reference with OLego [227]. Known junctions were provided to OLego for

maximized sensitivity. The junctions were derived from TXdb [228], which is an exon trio database constructed with transcript annotations from RefSeq [229], UCSC known genes [230] and dbCASE [231]. For the other options of OLego, default parameters were used. The alignment results were first compared to ensembl transcript structures and Repeatmasker annotations downloaded from UCSC genome browser to evaluate library quality. Bedtools [232] was used to locate the reads onto the features, including CDS, UTR/non-coding, intron, gene flanking (2k bp upstream or downstream of known gene boundaries) and deep intergenic regions. Cufflinks (v2.0.2) [177] was used to estimate transcript expression levels represented by FPKM (fragments per kilo bases per mapped million reads) for all the samples. GTF annotations of ensembl transcripts were provided with option -G. Cuffdiff was then run to detect differential expression between different samples. Cuffdiff tests differences in the summed FPKM of transcripts sharing each gene ID or protein ID to detect differential expression. Differential expression of transcripts sharing each protein ID with at least a 2 fold change between two different samples were selected for further gene ontology analyses using DAVID (v6.7) [178]. GOTERM_BP_FAT, GOTERM_MF_FAT, SP_PIR_KEYWORDS, SP_PIR_KEYWORDS and COG_ONTOLOGY categories were selected for gene ontology analyses.

qRT-PCR validation of RNA-Seq hits

qRT-PCR was first performed and repeated on the same round spermatid RNA samples used for RNA-Seq. Each RNA sample was prepared from round spermatids elutriation-purified from a pool of 5 *Chd5*$^{Aam1+/+}$ or *Chd5*$^{Aam1-/-}$ mice with matched background and age (approximately 10 months old). Validated targets was then re-validated on another batch of round spermatid RNA samples prepared from a different set of mice of different ages. In this

batch of RNA samples, each RNA sample was prepared from round spermatids elutriation-purified from a pool of 3 *Chd5*$^{Aam1+/+}$ or *Chd5*$^{Aam1-/-}$ mice with matched background and age (approximately 3 months old). All the qRT-PCR results were pooled together and data are presented as mean ± s.d.

Generation of *Chd5*$^{Tm1b-/-}$ mice and genotyping

ES clones with *Chd5*$^{Tm1a(EUCOMM)Wtsi}$ allele, which has exon 2 of *Chd5* locus flanked by *LoxP* sites, were purchased from EUCOMM (European Conditional Mouse Mutagenesis) (http://www.mousephenotype.org/martsearch_ikmc_project/martsearch/ikmc_project/36581). The ES clones were on C57BL/6N-A/a background and were injected into albino B6 (C57BL/6J-Tyr c-2J) blastocysts through standard procedures by the Gene Targeting Facility at Cold Spring Harbor Laboratory. Progeny resulting from germline transmission were called F1 *Chd5*$^{Tm1a+/-}$ mice which had the exon 2 of *Chd5* locus flanked by *LoxP* sites but not excised yet. F1 *Chd5*$^{Tm1a+/-}$ mice were crossed to wild type C57BL/6 mice to obtain more *Chd5*$^{Tm1a+/-}$ progeny, which were then intercrossed to obtain *Chd5*$^{Tm1a-/-}$ mice. Chd5 $^{Tm1a+/-}$ mice were also crossed to *CMV-Cre* line on a C57BL/6 background to obtain *Chd5* $^{Tm1b+/-}$ mice which had exon 2 of *Chd5* excised. *Chd5* $^{Tm1b+/-}$ mice were then intercrossed to obtain *Chd5* $^{Tm1b-/-}$ mice. Genotyping was done by PCR using primers (Figure 35) that amplify a 674 bp endogenous band specifically from wild type *Chd5* allele and a 456 bp targeted band specifically from *Chd5* ^{Tm1b} allele.

Table 9. List of primers used for qRT-PCR, ChIP-qPCR and genotype PCR

Primer	Application	Sequence
Actin-F	qRT-PCR	GATCTGGCACCACACCTTCT
Actin-R	qRT-PCR	GGGGTGTTGAAGGTCTCAAA
Acrv1-F	qRT-PCR	TCAGCAACTTTCAAGCGAGTAT
Acrv1-R	qRT-PCR	CTCCTGAAGAGTGCTCACCTG
Acsl5-F	qRT-PCR	TCCTGACGTTTGGAACGGC
Acsl5-R	qRT-PCR	CTCCCTCAATCCCCACAGAC
Aqp8-F	qRT-PCR	GGATGTCTATCGGTCATTGAG
Aqp8-m	qRT-PCR	GAATTAGCAGCATGGTCTTGA
Car2-F	qRT-PCR	TCCCACCACTGGGGATACAG
Car2-R	qRT-PCR	CTCTTGGACGCAGCTTTATCATA
Cdyl-F	qRT-PCR	ATGGGCATAGGCAATAGCCAG
Cdyl-R	qRT-PCR	GGGTTCTGAGACTGTTGCAGG
Cdyl2-F	qRT-PCR	CTTATCCGATGGAAAGGCTACG
Cdyl2-R	qRT-PCR	GGAGCCCGTTGAACTCGTC
Drosha-F	qRT-PCR	ATGCAAGGCAATACGTGTCAT
Drosha-R	qRT-PCR	TTTTGGGGTCTGAAAGCTGGT
Gxylt1-F	qRT-PCR	GACGGGCAGGTATGATATGAAAA
Gxylt1-R	qRT-PCR	AAAGCTATCGTGCAGTTGGTC
H1t-F	qRT-PCR	CTGTGGAGGAGAAACCTTCATC
H1t-R	qRT-PCR	GCACCAGGACTCCTTTATTCAC
Hist1h1e-F	qRT-PCR	AGGCAAAGGCAACTAAGGCTA
Hist1h1e-R	qRT-PCR	CTTTAGGCTTTACCGTTTTCGC
Hist1h2aa-F	qRT-PCR	ATGTCTGGTCCTACAAAGCGG
Hist1h2aa-R	qRT-PCR	CCAATTCGTTGTGCGTAGTTCC
Hist3h2a-F	qRT-PCR	TGTAGCTGCTCAAACGCTTG
Hist3h2a-R	qRT-PCR	TAGTACACCTCCCTCCACGA
Hist1h2bc-F	qRT-PCR	GAGGAGCAGACCTGACATCG
Hist1h2bc-R	qRT-PCR	CACTGTCTTGAGGTTACAGCAT
Hist1h3i-F	qRT-PCR	CTCGTGGGTCTGTTTGAGGA
Hist1h3i-R	qRT-PCR	GGAATTACGCCCTCTCCCC
Hist2h3c1-F	qRT-PCR	AGGACTTCAAGACGGACCTG
Hist2h3c1-R	qRT-PCR	TTTGTGGGGAATGGATGGGA
Hist1h4i-F	qRT-PCR	GACAACATCCAGGGCATCAC
Hist1h4i-R	qRT-PCR	AAACTGAGCAGCTTAACCGC
Kat2a-F	qRT-PCR	AAGGCCAATGAAACCTGCAAG
Kat2a-R	qRT-PCR	CTCACAGCTACGGCACAACTC
Kat2b-F	qRT-PCR	CGGATCGCCGTGAAGAAGG

Kat2b-R	qRT-PCR	CATTGCATTTACAGGACTCCTCT
Kat6b-F	qRT-PCR	AGAAGAAAAGGGGTCGTAAACG
Kat6b-R	qRT-PCR	GTGGGAATGCTTTCCTCAGAA
Klk1b9-F	qRT-PCR	CAACCTATACGAAGAGGAACCCT
Klk1b9-R	qRT-PCR	AGGATGTCGGATGTGGTTTCTA
Nat10-F	qRT-PCR	GCGGCAGAGGTCTCTTTTTGT
Nat10-R	qRT-PCR	GTGACTGCTAAATCCCAGCTC
Prm1-F	qRT-PCR	ACAAAATTCCACCTGCTCACA
Prm1-R	qRT-PCR	GTTTTTCATCGGCGGTGGC
Prm2-F	qRT-PCR	GCTGCTCTCGTAAGAGGCTACA
Prm2-R	qRT-PCR	AGTGATGGTGCCTCCTACATTT
Rif1-F	qRT-PCR	TTCTTTACCAAATTGTGGTGGCT
Rif1-R	qRT-PCR	CTCCGACTTGTAGGCTGTGG
Rtel1-F	qRT-PCR	TTGCCAGTCGGACCTTGTC
Rtel1-R	qRT-PCR	GTTAGCTGGGAGTGCGTTCTA
Sik1-F	qRT-PCR	TCATGTCGGAGTTCAGTGCG
Sik1-R	qRT-PCR	ACCTGCGTTTTGGTGACTCG
Sycp3-F	qRT-PCR	AGCCAGTAACCAGAAAATTGAGC
Sycp3-R	qRT-PCR	CCACTGCTGCAACACATTCATA
Syne3-F	qRT-PCR	TGGAGGCAAGGCTTCGAGA
Syne3-R	qRT-PCR	TTCTGGAACCAGCGGTAAAAC
Tarbp2-F	qRT-PCR	CTGCTCACCGCAAAGAGTTCA
Tarbp2-R	qRT-PCR	CCAGCTTTTTGGAAGTGCCA
Tnp1-F	qRT-PCR	GAGAGGTGGAAGCAAGAGAAAA
Tnp1-R	qRT-PCR	CCCACTCTGATAGGATCTTTGG
Tnp2-F	qRT-PCR	GAAGGGAAAGTGAGCAAGAGAA
Tnp2-R	qRT-PCR	GCATAGAAATTGCTGCAGTGAC
Top2b-F	qRT-PCR	CTGACCTGGGTGAACAATGCT
Top2b-R	qRT-PCR	TGGCTCCACTGATCCAATGTAT
Trp53inp1-F	qRT-PCR	AAGTGGTCCCAGAATGGAAGC
Trp53inp1-R	qRT-PCR	GGCGAAAACTCTTGGGTTGT
Zfp618-F	qRT-PCR	CCAACCAGTCCCGATCTCC
Zfp618-R	qRT-PCR	GGATTACACTGTTAGGCGTCAAA
1700019G17Rik-F	qRT-PCR	TGCTGACACTACCTCAGACTC
1700019G17Rik-R	qRT-PCR	CAAGAAAGCCAGATAAGGAGCC
28S rRNA-F	qRT-PCR	CCCGACGTACGCAGTTTTAT
28S rRNA-R	qRT-PCR	CCTTTTCTGGGGTCTGATGA
45S rRNA-F	qRT-PCR	ACACGCTGTCCTTTCCCTATTAACACTAAA
45S rRNA-R	qRT-PCR	AGTAAAAAGAATAGGCTGGACAAGCAAAAC
Prm1-5'-F	ChIP-qPCR	CCACAGACGGCACAACT

Prm1-5'-R	ChIP-qPCR	AGTGAGTAGATATGTGCGGATG
Prm1-A-F	ChIP-qPCR	GAATTGGCTGAGGTGGAGTG
Prm1-A-R	ChIP-qPCR	TCACCCTTCTGCCTACCTGT
Prm1-B-F	ChIP-qPCR	GTGCCACACACCTGCTTCTA
Prm1-B-R	ChIP-qPCR	GCAACTCTGAGACCCTCTGG
Prm1-P-F	ChIP-qPCR	TCCTGGTCCTCTTTGACTTCATAAT
Prm1-P-R	ChIP-qPCR	ATCTGCTCCTGCTTTTGCTG
Prm1-C-F	ChIP-qPCR	CTTTTGAAGCCCTTCCCATT
Prm1-C-R	ChIP-qPCR	AGAGCATCTCGCCACATCTT
G-Actin-F	Genotype	GGTCAGAAGGACTCCTATGTGG
G-Actin-R	Genotype	TGTCGTCCCAGTTGGTAACA
Neo-F	Genotype	ATGGGATCGGCCATTGAA
Neo-R	Genotype	GAACTCGTCAAGAAGGCG
Tm1b-F	Genotype	GAGCTAGGCAGGGAAGCAGTGTGG
Tm1b-R	Genotype	CAACGGGTTCTTCTGTTAGTCC
Tm1b-WT-R	Genotype	GGGTGACCTTCAGTTTCTCTGAGC

References

1. Felsenfeld, G. and M. Groudine, *Controlling the double helix.* Nature, 2003. **421**(6921): p. 448-53.

2. Luger, K., *et al.*, *Crystal structure of the nucleosome core particle at 2.8 A resolution.* Nature, 1997. **389**(6648): p. 251-60.

3. Horn, P.J. and C.L. Peterson, *Molecular biology. Chromatin higher order folding--wrapping up transcription.* Science, 2002. **297**(5588): p. 1824-7.

4. Ordog, T., *et al.*, *Epigenetics and chromatin dynamics: a review and a paradigm for functional disorders.* Neurogastroenterol Motil, 2012. **24**(12): p. 1054-68.

5. Clapier, C.R. and B.R. Cairns, *The biology of chromatin remodeling complexes.* Annu Rev Biochem, 2009. **78**: p. 273-304.

6. Wang, G.G., C.D. Allis, and P. Chi, *Chromatin remodeling and cancer, Part II: ATP-dependent chromatin remodeling.* Trends Mol Med, 2007. **13**(9): p. 373-80.

7. Wu, J.I., *Diverse functions of ATP-dependent chromatin remodeling complexes in development and cancer.* Acta Biochim Biophys Sin (Shanghai), 2012. **44**(1): p. 54-69.

8. Tateno, H., Y. Kimura, and R. Yanagimachi, *Sonication per se is not as deleterious to sperm chromosomes as previously inferred.* Biol Reprod, 2000. **63**(1): p. 341-6.

9. Ward, W.S. and D.S. Coffey, *DNA packaging and organization in mammalian spermatozoa: comparison with somatic cells.* Biol Reprod, 1991. **44**(4): p. 569-74.

10. Carrell, D.T., *Epigenetics of the male gamete.* Fertil Steril, 2012. **97**(2): p. 267-74.

11. Kimmins, S. and P. Sassone-Corsi, *Chromatin remodelling and epigenetic features of germ cells.* Nature, 2005. **434**(7033): p. 583-9.

12. Rousseaux, S., *et al.*, *Epigenetic reprogramming of the male genome during gametogenesis and in the zygote.* Reprod Biomed Online, 2008. **16**(4): p. 492-503.

13. Hud, N.V., *et al.*, *Identification of the elemental packing unit of DNA in mammalian sperm cells by atomic force microscopy.* Biochem Biophys Res Commun, 1993. **193**(3): p. 1347-54.

14. Oakberg, E.F., *Duration of spermatogenesis in the mouse and timing of stages of the cycle of the seminiferous epithelium.* Am J Anat, 1956. **99**(3): p. 507-16.

15. Hess, R.A. and L. Renato de Franca, *Spermatogenesis and cycle of the seminiferous epithelium.* Adv Exp Med Biol, 2008. **636**: p. 1-15.

16. Oakberg, E.F., *A description of spermiogenesis in the mouse and its use in analysis of the cycle of the seminiferous epithelium and germ cell renewal.* Am J Anat, 1956. **99**(3): p. 391-413.

17. Ahmed, E.A. and D.G. de Rooij, *Staging of mouse seminiferous tubule cross-sections.* Methods Mol Biol, 2009. **558**: p. 263-77.

18. Meistrich, M.L. and R.A. Hess, *Assessment of spermatogenesis through staging of seminiferous tubules.* Methods Mol Biol, 2013. **927**: p. 299-307.

19. Churikov, D., I.A. Zalenskaya, and A.O. Zalensky, *Male germline-specific histones in mouse and man.* Cytogenet Genome Res, 2004. **105**(2-4): p. 203-14.

20. Grimes, S.R., Jr., *Nuclear proteins in spermatogenesis.* Comp Biochem Physiol B, 1986. **83**(3): p. 495-500.

21. Meistrich, M.L., *et al.*, *Highly acetylated H4 is associated with histone displacement in rat spermatids.* Mol Reprod Dev, 1992. **31**(3): p. 170-81.

22. Christensen, M.E., J.B. Rattner, and G.H. Dixon, *Hyperacetylation of histone H4 promotes chromatin decondensation prior to histone replacement by protamines during spermatogenesis in rainbow trout.* Nucleic Acids Res, 1984. **12**(11): p. 4575-92.

23. Sonnack, V., *et al.*, *Expression of hyperacetylated histone H4 during normal and impaired human spermatogenesis.* Andrologia, 2002. **34**(6): p. 384-90.

24. Awe, S. and R. Renkawitz-Pohl, *Histone H4 acetylation is essential to proceed from a histone- to a protamine-based chromatin structure in spermatid nuclei of Drosophila melanogaster.* Syst Biol Reprod Med, 2010. **56**(1): p. 44-61.

25. Gaucher, J., *et al.*, *From meiosis to postmeiotic events: the secrets of histone disappearance.* FEBS J, 2010. **277**(3): p. 599-604.

26. Bonisch, C., *et al.*, *H2A.Z.2.2 is an alternatively spliced histone H2A.Z variant that causes severe nucleosome destabilization.* Nucleic Acids Res, 2012. **40**(13): p. 5951-64.

27. Tachiwana, H., *et al.*, *Structural basis of instability of the nucleosome containing a testis-specific histone variant, human H3T.* Proc Natl Acad Sci U S A, 2010. **107**(23): p. 10454-9.

28. Meistrich, M.L., *et al.*, *Roles of transition nuclear proteins in spermiogenesis.* Chromosoma, 2003. **111**(8): p. 483-8.

29. Pivot-Pajot, C., *et al.*, *Acetylation-dependent chromatin reorganization by BRDT, a testis-specific bromodomain-containing protein.* Mol Cell Biol, 2003. **23**(15): p. 5354-65.

30. Moriniere, J., *et al.*, *Cooperative binding of two acetylation marks on a histone tail by a single bromodomain.* Nature, 2009. **461**(7264): p. 664-8.

31. Shang, E., *et al.*, *The first bromodomain of Brdt, a testis-specific member of the BET sub-family of double-bromodomain-containing proteins, is essential for male germ cell differentiation.* Development, 2007. **134**(19): p. 3507-15.

32. Kim, Y., A.M. Fedoriw, and T. Magnuson, *An essential role for a mammalian SWI/SNF chromatin-remodeling complex during male meiosis.* Development, 2012. **139**(6): p. 1133-40.

33. Caron, C., *et al.*, *Cdyl: a new transcriptional co-repressor.* EMBO Rep, 2003. **4**(9): p. 877-82.

34. McGraw, S., *et al.*, *Investigation of MYST4 histone acetyltransferase and its involvement in mammalian gametogenesis.* BMC Dev Biol, 2007. **7**: p. 123.

35. Lahn, B.T., *et al.*, *Previously uncharacterized histone acetyltransferases implicated in mammalian spermatogenesis.* Proc Natl Acad Sci U S A, 2002. **99**(13): p. 8707-12.

36. Hazzouri, M., *et al.*, *Regulated hyperacetylation of core histones during mouse spermatogenesis: involvement of histone deacetylases.* Eur J Cell Biol, 2000. **79**(12): p. 950-60.

37. Lu, L.Y., *et al.*, *RNF8-dependent histone modifications regulate nucleosome removal during spermatogenesis.* Dev Cell, 2010. **18**(3): p. 371-84.

38. Yu, Y.E., *et al.*, *Abnormal spermatogenesis and reduced fertility in transition nuclear protein 1-deficient mice.* Proc Natl Acad Sci U S A, 2000. **97**(9): p. 4683-8.

39. Shirley, C.R., *et al.*, *Abnormalities and reduced reproductive potential of sperm from Tnp1- and Tnp2-null double mutant mice.* Biol Reprod, 2004. **71**(4): p. 1220-9.

40. Prieto, M.C., A.H. Maki, and R. Balhorn, *Analysis of DNA-protamine interactions by optical detection of magnetic resonance.* Biochemistry, 1997. **36**(39): p. 11944-51.

41. Balhorn, R., *A model for the structure of chromatin in mammalian sperm.* J Cell Biol, 1982. **93**(2): p. 298-305.

42. Hud, N.V., F.P. Milanovich, and R. Balhorn, *Evidence of novel secondary structure in DNA-bound protamine is revealed by Raman spectroscopy.* Biochemistry, 1994. **33**(24): p. 7528-35.

43. Bedford, J.M. and H.I. Calvin, *The occurrence and possible functional significance of -S-S- crosslinks in sperm heads, with particular reference to eutherian mammals.* J Exp Zool, 1974. **188**(2): p. 137-55.

44. Wouters-Tyrou, D., *et al.*, *Nuclear basic proteins in spermiogenesis.* Biochimie, 1998. **80**(2): p. 117-28.

45. Lewis, J.D., *et al.*, *A walk though vertebrate and invertebrate protamines.* Chromosoma, 2003. **111**(8): p. 473-82.

46. Pogany, G.C., *et al.*, *DNA and protein content of mouse sperm. Implications regarding sperm chromatin structure.* Exp Cell Res, 1981. **136**(1): p. 127-36.

47. Oliva, R., *Protamines and male infertility.* Hum Reprod Update, 2006. **12**(4): p. 417-35.

48. Hammoud, S.S., *et al.*, *Distinctive chromatin in human sperm packages genes for embryo development.* Nature, 2009. **460**(7254): p. 473-8.

49. Lewis, J.D., *et al.*, *Histone H1 and the origin of protamines.* Proc Natl Acad Sci U S A, 2004. **101**(12): p. 4148-52.

50. Cho, C., *et al.*, *Haploinsufficiency of protamine-1 or -2 causes infertility in mice.* Nat Genet, 2001. **28**(1): p. 82-6.

51. Cho, C., *et al.*, *Protamine 2 deficiency leads to sperm DNA damage and embryo death in mice.* Biol Reprod, 2003. **69**(1): p. 211-7.

52. Carrell, D.T. and L. Liu, *Altered protamine 2 expression is uncommon in donors of known fertility, but common among men with poor fertilizing capacity, and may reflect other abnormalities of spermiogenesis.* J Androl, 2001. **22**(4): p. 604-10.

53. de Yebra, L., *et al.*, *Detection of P2 precursors in the sperm cells of infertile patients who have reduced protamine P2 levels.* Fertil Steril, 1998. **69**(4): p. 755-9.

54. Aoki, V.W., *et al.*, *Protamine levels vary between individual sperm cells of infertile human males and correlate with viability and DNA integrity.* J Androl, 2006. **27**(6): p. 890-8.

55. Steger, K., *Haploid spermatids exhibit translationally repressed mRNAs.* Anat Embryol (Berl), 2001. **203**(5): p. 323-34.

56. Steger, K., *et al.*, *Expression of mRNA and protein of nucleoproteins during human spermiogenesis.* Mol Hum Reprod, 1998. **4**(10): p. 939-45.

57. Morales, C.R., Y.K. Kwon, and N.B. Hecht, *Cytoplasmic localization during storage and translation of the mRNAs of transition protein 1 and protamine 1, two translationally regulated transcripts of the mammalian testis.* J Cell Sci, 1991. **100 (Pt 1)**: p. 119-31.

58. Kleene, K.C., *Patterns of translational regulation in the mammalian testis.* Mol Reprod Dev, 1996. **43**(2): p. 268-81.

59. Aoki, V.W. and D.T. Carrell, *Human protamines and the developing spermatid: their structure, function, expression and relationship with male infertility.* Asian J Androl, 2003. **5**(4): p. 315-24.

60. Kleene, K.C., *Poly(A) shortening accompanies the activation of translation of five mRNAs during spermiogenesis in the mouse.* Development, 1989. **106**(2): p. 367-73.

61. Lee, K., *et al.*, *Premature translation of protamine 1 mRNA causes precocious nuclear condensation and arrests spermatid differentiation in mice.* Proc Natl Acad Sci U S A, 1995. **92**(26): p. 12451-5.

62. Choudhary, S.K., *et al.*, *A haploid expressed gene cluster exists as a single chromatin domain in human sperm.* J Biol Chem, 1995. **270**(15): p. 8755-62.

63. Martins, R.P., G.C. Ostermeier, and S.A. Krawetz, *Nuclear matrix interactions at the human protamine domain: a working model of potentiation.* J Biol Chem, 2004. **279**(50): p. 51862-8.

64. McCarrey, J.R., C.B. Geyer, and H. Yoshioka, *Epigenetic regulation of testis-specific gene expression.* Ann N Y Acad Sci, 2005. **1061**: p. 226-42.

65. Zhang, J.F., *et al.*, *[Advance on research of gene expression during spermiogenesis at transcription level]*. Yi Chuan, 2013. **35**(5): p. 587-94.

66. DeJong, J., *Basic mechanisms for the control of germ cell gene expression.* Gene, 2006. **366**(1): p. 39-50.

67. Steger, K., *et al.*, *Expression of protamine-1 and -2 mRNA during human spermiogenesis.* Mol Hum Reprod, 2000. **6**(3): p. 219-25.

68. Tanaka, H. and T. Baba, *Gene expression in spermiogenesis.* Cell Mol Life Sci, 2005. **62**(3): p. 344-54.

69. Maclean, J.A., 2nd and M.F. Wilkinson, *Gene regulation in spermatogenesis.* Curr Top Dev Biol, 2005. **71**: p. 131-97.

70. Okada, Y., *et al.*, *Histone demethylase JHDM2A is critical for Tnp1 and Prm1 transcription and spermatogenesis.* Nature, 2007. **450**(7166): p. 119-23.

71. Nantel, F., *et al.*, *Spermiogenesis deficiency and germ-cell apoptosis in CREM-mutant mice.* Nature, 1996. **380**(6570): p. 159-62.

72. Kwon, Y.K. and N.B. Hecht, *Cytoplasmic protein binding to highly conserved sequences in the 3' untranslated region of mouse protamine 2 mRNA, a translationally regulated transcript of male germ cells.* Proc Natl Acad Sci U S A, 1991. **88**(9): p. 3584-8.

73. Iuchi, Y., *et al.*, *Expression of a Y-box protein, YB2/RYB-a, precedes protamine 2 expression during spermatogenesis in rodents.* Mol Hum Reprod, 2001. **7**(11): p. 1023-31.

74. Fajardo, M.A., *et al.*, *Germ cell-specific proteins interact with the 3' untranslated regions of Prm-1 and Prm-2 mRNA.* Dev Biol, 1994. **166**(2): p. 643-53.

75. Fajardo, M.A., *et al.*, *Separate elements in the 3' untranslated region of the mouse protamine 1 mRNA regulate translational repression and activation during murine spermatogenesis.* Dev Biol, 1997. **191**(1): p. 42-52.

76. Yang, J., *et al.*, *Deletion of the DNA/RNA-binding protein MSY2 leads to post-meiotic arrest.* Mol Cell Endocrinol, 2006. **250**(1-2): p. 20-4.

77. Chennathukuzhi, V., *et al.*, *Mice deficient for testis-brain RNA-binding protein exhibit a coordinate loss of TRAX, reduced fertility, altered gene expression in the brain, and behavioral changes.* Mol Cell Biol, 2003. **23**(18): p. 6419-34.

78. Lee, K., M.A. Fajardo, and R.E. Braun, *A testis cytoplasmic RNA-binding protein that has the properties of a translational repressor.* Mol Cell Biol, 1996. **16**(6): p. 3023-34.

79. Zhong, J., *et al.*, *A double-stranded RNA binding protein required for activation of repressed messages in mammalian germ cells.* Nat Genet, 1999. **22**(2): p. 171-4.

80. Calvin, H.I. and J.M. Bedford, *Formation of disulphide bonds in the nucleus and accessory structures of mammalian spermatozoa during maturation in the epididymis.* J Reprod Fertil Suppl, 1971. **13**: p. Suppl 13:65-75.

81. Yelick, P.C., *et al.*, *Mouse protamine 2 is synthesized as a precursor whereas mouse protamine 1 is not.* Mol Cell Biol, 1987. **7**(6): p. 2173-9.

82. Green, G.R., *et al.*, *Synthesis and processing of mammalian protamines and transition proteins.* Mol Reprod Dev, 1994. **37**(3): p. 255-63.

83. Marfella, C.G. and A.N. Imbalzano, *The Chd family of chromatin remodelers.* Mutat Res, 2007. **618**(1-2): p. 30-40.

84. Hall, J.A. and P.T. Georgel, *CHD proteins: a diverse family with strong ties.* Biochem Cell Biol, 2007. **85**(4): p. 463-76.

85. Woodage, T., *et al.*, *Characterization of the CHD family of proteins.* Proc Natl Acad Sci U S A, 1997. **94**(21): p. 11472-7.

86. Delmas, V., D.G. Stokes, and R.P. Perry, *A mammalian DNA-binding protein that contains a chromodomain and an SNF2/SWI2-like helicase domain.* Proc Natl Acad Sci U S A, 1993. **90**(6): p. 2414-8.

87. Watson, A.A., *et al.*, *The PHD and chromo domains regulate the ATPase activity of the human chromatin remodeler CHD4.* J Mol Biol, 2012. **422**(1): p. 3-17.

88. Bouazoune, K. and R.E. Kingston, *Chromatin remodeling by the CHD7 protein is impaired by mutations that cause human developmental disorders.* Proc Natl Acad Sci U S A, 2012. **109**(47): p. 19238-43.

89. Thompson, B.A., *et al.*, *CHD8 is an ATP-dependent chromatin remodeling factor that regulates beta-catenin target genes.* Mol Cell Biol, 2008. **28**(12): p. 3894-904.

90. Lutz, T., R. Stoger, and A. Nieto, *CHD6 is a DNA-dependent ATPase and localizes at nuclear sites of mRNA synthesis.* FEBS Lett, 2006. **580**(25): p. 5851-7.

91. Lusser, A., D.L. Urwin, and J.T. Kadonaga, *Distinct activities of CHD1 and ACF in ATP-dependent chromatin assembly.* Nat Struct Mol Biol, 2005. **12**(2): p. 160-6.

92. Pray-Grant, M.G., *et al.*, *Chd1 chromodomain links histone H3 methylation with SAGA- and SLIK-dependent acetylation.* Nature, 2005. **433**(7024): p. 434-438.

93. Akhtar, A., D. Zink, and P.B. Becker, *Chromodomains are protein-RNA interaction modules.* Nature, 2000. **407**(6802): p. 405-9.

94. Sims, R.J., *et al.*, *Human but not yeast CHD1 binds directly and selectively to histone H3 methylated at lysine 4 via its tandem chromodomains.* Journal of Biological Chemistry, 2005. **280**(51): p. 41789-41792.

95. Brehm, A., *et al.*, *The many colours of chromodomains.* Bioessays, 2004. **26**(2): p. 133-40.

96. Fischle, W., *et al.*, *Molecular basis for the discrimination of repressive methyl-lysine marks in histone H3 by Polycomb and HP1 chromodomains.* Genes Dev, 2003. **17**(15): p. 1870-81.

97. Min, J.R., Y. Zhang, and R.M. Xu, *Structural basis for specific binding of polycomb chromodomain to histone H3 methylated at Lys 27.* Genes & Development, 2003. **17**(15): p. 1823-1828.

98. Eissenberg, J.C., *Structural biology of the chromodomain: form and function.* Gene, 2012. **496**(2): p. 69-78.

99. Ooi, S.K.T., *et al.*, *DNMT3L connects unmethylated lysine 4 of histone H3 to de novo methylation of DNA.* Nature, 2007. **448**(7154): p. 714-U13.

100. Li, H.T., *et al.*, *Molecular basis for site-specific read-out of histone H3K4me3 by the BPTF PHD finger of NURF.* Nature, 2006. **442**(7098): p. 91-95.

101. Pena, P.V., *et al.*, *Molecular mechanism of histone H3K4me3 recognition by plant homeodomain of ING2.* Nature, 2006. **442**(7098): p. 100-103.

102. Wysocka, J., *et al.*, *A PHD finger of NURF couples histone H3 lysine 4 trimethylation with chromatin remodelling.* Nature, 2006. **442**(7098): p. 86-90.

103. Lan, F., *et al.*, *Recognition of unmethylated histone H3 lysine 4 links BHC80 to LSD1-mediated gene repression.* Nature, 2007. **448**(7154): p. 718-U14.

104. Paul, S., *et al.*, *Chd5 requires PHD-mediated histone 3 binding for tumor suppression.* Cell Rep, 2013. **3**(1): p. 92-102.

105. Boyer, L.A., R.R. Latek, and C.L. Peterson, *The SANT domain: a unique histone-tail-binding module?* Nat Rev Mol Cell Biol, 2004. **5**(2): p. 158-63.

106. Urquhart, A.J., *et al.*, *ATM mediated phosphorylation of CHD4 contributes to genome maintenance.* Genome Integr, 2011. **2**(1): p. 1.

107. O'Shaughnessy, A. and B. Hendrich, *CHD4 in the DNA-damage response and cell cycle progression: not so NuRDy now.* Biochem Soc Trans, 2013. **41**(3): p. 777-82.

108. Larsen, D.H., *et al.*, *The chromatin-remodeling factor CHD4 coordinates signaling and repair after DNA damage.* J Cell Biol, 2010. **190**(5): p. 731-40.

109. Pan, M.R., *et al.*, *Chromodomain helicase DNA-binding protein 4 (CHD4) regulates homologous recombination DNA repair, and its deficiency sensitizes cells to poly(ADP-ribose) polymerase (PARP) inhibitor treatment.* J Biol Chem, 2012. **287**(9): p. 6764-72.

110. Goodarzi, A.A., T. Kurka, and P.A. Jeggo, *KAP-1 phosphorylation regulates CHD3 nucleosome remodeling during the DNA double-strand break response.* Nat Struct Mol Biol, 2011. **18**(7): p. 831-9.

111. Rajagopalan, S., J. Nepa, and S. Venkatachalam, *Chromodomain helicase DNA-binding protein 2 affects the repair of X-ray and UV-induced DNA damage.* Environ Mol Mutagen, 2012. **53**(1): p. 44-50.

112. Nagarajan, P., *et al.*, *Role of chromodomain helicase DNA-binding protein 2 in DNA damage response signaling and tumorigenesis.* Oncogene, 2009. **28**(8): p. 1053-62.

113. Ling, T., *et al.*, *CHD4/NuRD maintains demethylation state of rDNA promoters through inhibiting the expression of the rDNA methyltransferase recruiter TIP5.* Biochem Biophys Res Commun, 2013.

114. Zentner, G.E., *et al.*, *CHD7 functions in the nucleolus as a positive regulator of ribosomal RNA biogenesis.* Hum Mol Genet, 2010. **19**(18): p. 3491-501.

115. Yuan, C.C., *et al.*, *CHD8 associates with human Staf and contributes to efficient U6 RNA polymerase III transcription.* Mol Cell Biol, 2007. **27**(24): p. 8729-38.

116. Burkhardt, L., *et al.*, *CHD1 is a 5q21 tumor suppressor required for ERG rearrangement in prostate cancer.* Cancer Res, 2013. **73**(9): p. 2795-805.

117. Bagchi, A., *et al.*, *CHD5 is a tumor suppressor at human 1p36.* Cell, 2007. **128**(3): p. 459-75.

118. Sawada, G., *et al.*, *CHD8 is an independent prognostic indicator that regulates Wnt/beta-catenin signaling and the cell cycle in gastric cancer.* Oncol Rep, 2013.

119. de Arriba Munoz, A., *et al.*, *CHARGE syndrome and CHD7 gene mutation.* Neurologia, 2011. **26**(4): p. 255.

120. Papantonis, A., *et al.*, *CHD1 assumes a central role during follicle development.* J Mol Biol, 2008. **383**(5): p. 957-69.

121. Chris M. Egan, U.N., Julie Skotte, Gundula Streubel, Siobhán Turner, David J. O'Connell, Vilma Rraklli, Michael J. Dolan, Naomi Chadderton, Klaus Hansen, Gwyneth Jane Farrar, Kristian Helin, Johan Holmbergsend email, Adrian P. Bracken, *CHD5 Is Required for Neurogenesis and Has a Dual Role in Facilitating Gene Expression and Polycomb Gene Repression.* Developmental Cell, 2013. **26**(3): p. 223-236.

122. Williams, C.J., *et al.*, *The chromatin remodeler Mi-2 beta is required for CD4 expression and T cell development.* Immunity, 2004. **20**(6): p. 719-733.

123. Kashiwagi, M., B.A. Morgan, and K. Georgopoulos, *The chromatin remodeler Mi-2beta is required for establishment of the basal epidermis and normal differentiation of its progeny.* Development, 2007. **134**(8): p. 1571-82.

124. Kulkarni, S., *et al.*, *Disruption of chromodomain helicase DNA binding protein 2 (CHD2) causes scoliosis.* Am J Med Genet A, 2008. **146A**(9): p. 1117-27.

125. Lathrop, M.J., *et al.*, *Deletion of the Chd6 exon 12 affects motor coordination.* Mamm Genome, 2010. **21**(3-4): p. 130-42.

126. Capelli, L.P., *et al.*, *Deletion of the RMGA and CHD2 genes in a child with epilepsy and mental deficiency.* Eur J Med Genet, 2012. **55**(2): p. 132-4.

127. Neale, B.M., *et al.*, *Patterns and rates of exonic de novo mutations in autism spectrum disorders.* Nature, 2012. **485**(7397): p. 242-5.

128. Talkowski, M.E., *et al.*, *Sequencing chromosomal abnormalities reveals neurodevelopmental loci that confer risk across diagnostic boundaries.* Cell, 2012. **149**(3): p. 525-37.

129. CHD2, C.a.C.i.n.d., *et al.*, *Targeted resequencing in epileptic encephalopathies identifies de novo mutations in CHD2 and SYNGAP1.* Nat Genet, 2013. **45**(7): p. 825-30.

130. Bergman, J.E., *et al.*, *CHD7 mutations and CHARGE syndrome: the clinical implications of an expanding phenotype.* J Med Genet, 2011. **48**(5): p. 334-42.

131. Jongmans, M.C., *et al.*, *CHARGE syndrome: the phenotypic spectrum of mutations in the CHD7 gene.* J Med Genet, 2006. **43**(4): p. 306-14.

132. Wincent, J., *et al.*, *CHD7 mutation spectrum in 28 Swedish patients diagnosed with CHARGE syndrome.* Clin Genet, 2008. **74**(1): p. 31-8.

133. Martin, D.M., *Chromatin remodeling in development and disease: focus on CHD7.* PLoS Genet, 2010. **6**(7): p. e1001010.

134. Layman, W.S., E.A. Hurd, and D.M. Martin, *Chromodomain proteins in development: lessons from CHARGE syndrome.* Clin Genet, 2010. **78**(1): p. 11-20.

135. McDaniel, I.E., *et al.*, *Investigations of CHD1 function in transcription and development of Drosophila melanogaster.* Genetics, 2008. **178**(1): p. 583-7.

136. Thompson, P.M., *et al.*, *CHD5, a new member of the chromodomain gene family, is preferentially expressed in the nervous system.* Oncogene, 2003. **22**(7): p. 1002-11.

137. Lai, A.Y. and P.A. Wade, *Cancer biology and NuRD: a multifaceted chromatin remodelling complex.* Nat Rev Cancer, 2011. **11**(8): p. 588-96.

138. Bagchi, A. and A.A. Mills, *The quest for the 1p36 tumor suppressor.* Cancer Res, 2008. **68**(8): p. 2551-6.

139. Fujita, T., *et al.*, *CHD5, a tumor suppressor gene deleted from 1p36.31 in neuroblastomas.* J Natl Cancer Inst, 2008. **100**(13): p. 940-9.

140. Garcia, I., *et al.*, *Expression of the neuron-specific protein CHD5 is an independent marker of outcome in neuroblastoma.* Mol Cancer, 2010. **9**: p. 277.

141. Li, H., *et al.*, *Genistein demethylates the promoter of CHD5 and inhibits neuroblastoma growth in vivo.* Int J Mol Med, 2012. **30**(5): p. 1081-6.

142. Koyama, H., *et al.*, *Mechanisms of CHD5 Inactivation in neuroblastomas.* Clin Cancer Res, 2012. **18**(6): p. 1588-97.

143. Mulero-Navarro, S. and M. Esteller, *Chromatin remodeling factor CHD5 is silenced by promoter CpG island hypermethylation in human cancer.* Epigenetics, 2008. **3**(4): p. 210-5.

144. Wang, L., *et al.*, *Downregulation of chromatin remodeling factor CHD5 is associated with a poor prognosis in human glioma.* J Clin Neurosci, 2013. **20**(7): p. 958-63.

145. Wu, X., *et al.*, *Chromodomain helicase DNA binding protein 5 plays a tumor suppressor role in human breast cancer.* Breast Cancer Res, 2012. **14**(3): p. R73.

146. Zhao, R., *et al.*, *CHD5, a tumor suppressor that is epigenetically silenced in lung cancer.* Lung Cancer, 2012. **76**(3): p. 324-31.

147. Wong, R.R., *et al.*, *CHD5 Downregulation Associated with Poor Prognosis in Epithelial Ovarian Cancer.* Gynecol Obstet Invest, 2011. **72**(3): p. 203-7.

148. Wang, X., *et al.*, *CHD5 is down-regulated through promoter hypermethylation in gastric cancer.* J Biomed Sci, 2009. **16**: p. 95.

149. Du, X., *et al.*, *Decreased expression of chromodomain helicase DNA-binding protein 5 is an unfavorable prognostic marker in patients with primary gallbladder carcinoma.* Clin Transl Oncol, 2013. **15**(3): p. 198-204.

150. Cai, C., *et al.*, *MicroRNA-211 expression promotes colorectal cancer cell growth in vitro and in vivo by targeting tumor suppressor CHD5.* PLoS One, 2012. **7**(1): p. e29750.

151. Lang, J., E.S. Tobias, and R. Mackie, *Preliminary evidence for involvement of the tumour suppressor gene CHD5 in a family with cutaneous melanoma.* Br J Dermatol, 2011. **164**(5): p. 1010-6.

152. Wang, J., *et al.*, *The involvement of CHD5 hypermethylation in laryngeal squamous cell carcinoma.* Oral Oncol, 2011. **47**(7): p. 601-8.

153. Hall, W.A., *et al.*, *Low CHD5 expression activates the DNA damage response and predicts poor outcome in patients undergoing adjuvant therapy for resected pancreatic cancer.* Oncogene, 2013.

154. Vestin, A. and A.A. Mills, *The tumor suppressor Chd5 is induced during neuronal differentiation in the developing mouse brain.* Gene Expr Patterns, 2013.

155. Vestin, A. and A.A. Mills, *The tumor suppressor Chd5 is induced during neuronal differentiation in the developing mouse brain.* Gene Expr Patterns, 2013. **13**(8): p. 482-9.

156. Potts, R.C., *et al.*, *CHD5, a brain-specific paralog of Mi2 chromatin remodeling enzymes, regulates expression of neuronal genes.* PLoS One, 2011. **6**(9): p. e24515.

157. Bungum, M., L. Bungum, and A. Giwercman, *Sperm chromatin structure assay (SCSA): a tool in diagnosis and treatment of infertility.* Asian J Androl, 2011. **13**(1): p. 69-75.

158. Carrell, D.T., B.R. Emery, and S. Hammoud, *Altered protamine expression and diminished spermatogenesis: what is the link?* Hum Reprod Update, 2007. **13**(3): p. 313-27.

159. Qian, M.X., *et al.*, *Acetylation-mediated proteasomal degradation of core histones during DNA repair and spermatogenesis.* Cell, 2013. **153**(5): p. 1012-24.

160. Kramers, K., *et al.*, *Specificity of monoclonal anti-nucleosome auto-antibodies derived from lupus mice.* J Autoimmun, 1996. **9**(6): p. 723-9.

161. Chodaparambil, J.V., *et al.*, *Nucleosome structure and function.* Ernst Schering Res Found Workshop, 2006(57): p. 29-46.

162. Leduc, F., *et al.*, *DNA damage response during chromatin remodeling in elongating spermatids of mice.* Biol Reprod, 2008. **78**(2): p. 324-32.

163. Marcon, L. and G. Boissonneault, *Transient DNA strand breaks during mouse and human spermiogenesis new insights in stage specificity and link to chromatin remodeling.* Biol Reprod, 2004. **70**(4): p. 910-8.

164. Sakkas, D., *et al.*, *Origin of DNA damage in ejaculated human spermatozoa.* Rev Reprod, 1999. **4**(1): p. 31-7.

165. Laberge, R.M. and G. Boissonneault, *On the nature and origin of DNA strand breaks in elongating spermatids.* Biol Reprod, 2005. **73**(2): p. 289-96.

166. Smeenk, G., *et al.*, *The NuRD chromatin-remodeling complex regulates signaling and repair of DNA damage.* J Cell Biol, 2010. **190**(5): p. 741-9.

167. Polo, S.E., *et al.*, *Regulation of DNA-damage responses and cell-cycle progression by the chromatin remodelling factor CHD4.* Embo Journal, 2010. **29**(18): p. 3130-9.

168. Brown, D.T., *Histone variants: are they functionally heterogeneous?* Genome Biol, 2001. **2**(7): p. REVIEWS0006.

169. Kamakaka, R.T. and S. Biggins, *Histone variants: deviants?* Genes Dev, 2005. **19**(3): p. 295-310.

170. Malik, H.S. and S. Henikoff, *Phylogenomics of the nucleosome.* Nat Struct Biol, 2003. **10**(11): p. 882-91.

171. Talbert, P.B., *et al.*, *A unified phylogeny-based nomenclature for histone variants.* Epigenetics Chromatin, 2012. **5**: p. 7.

172. Kempisty, B., P. Jedrzejczak, and P.P. Jagodzinski, *[Structure and role of protamines 1 and 2 in spermatogenesis and male infertility]*. Ginekol Pol, 2006. **77**(3): p. 238-45.

173. Wang, P.J., D.C. Page, and J.R. McCarrey, *Differential expression of sex-linked and autosomal germ-cell-specific genes during spermatogenesis in the mouse.* Hum Mol Genet, 2005. **14**(19): p. 2911-8.

174. Reddi, P.P., C.J. Flickinger, and J.C. Herr, *Round spermatid-specific transcription of the mouse SP-10 gene is mediated by a 294-base pair proximal promoter.* Biol Reprod, 1999. **61**(5): p. 1256-66.

175. Mali, P., *et al.*, *Stage-specific expression of nucleoprotein mRNAs during rat and mouse spermiogenesis.* Reprod Fertil Dev, 1989. **1**(4): p. 369-82.

176. Yeung, C.H., *et al.*, *Aquaporin isoforms involved in physiological volume regulation of murine spermatozoa.* Biol Reprod, 2009. **80**(2): p. 350-7.

177. Trapnell, C., *et al.*, *Transcript assembly and quantification by RNA-Seq reveals unannotated transcripts and isoform switching during cell differentiation.* Nat Biotechnol, 2010. **28**(5): p. 511-5.

178. Huang da, W., B.T. Sherman, and R.A. Lempicki, *Systematic and integrative analysis of large gene lists using DAVID bioinformatics resources.* Nat Protoc, 2009. **4**(1): p. 44-57.

179. Arnesen, T., *et al.*, *A novel human NatA Nalpha-terminal acetyltransferase complex: hNaa16p-hNaa10p (hNat2-hArd1).* BMC Biochem, 2009. **10**: p. 15.

180. Chi, Y.H., *et al.*, *Histone acetyltransferase hALP and nuclear membrane protein hsSUN1 function in de-condensation of mitotic chromosomes.* J Biol Chem, 2007. **282**(37): p. 27447-58.

181. Liu, H., *et al.*, *DNA damage induces N-acetyltransferase NAT10 gene expression through transcriptional activation.* Mol Cell Biochem, 2007. **300**(1-2): p. 249-58.

182. Sarkar, S., R. Kiely, and P.J. McHugh, *The Ino80 chromatin-remodeling complex restores chromatin structure during UV DNA damage repair.* J Cell Biol, 2010. **191**(6): p. 1061-8.

183. Dinant, C., A.B. Houtsmuller, and W. Vermeulen, *Chromatin structure and DNA damage repair.* Epigenetics Chromatin, 2008. **1**(1): p. 9.

184. Martinez, E., *et al.*, *Human STAGA complex is a chromatin-acetylating transcription coactivator that interacts with pre-mRNA splicing and DNA damage-binding factors in vivo.* Mol Cell Biol, 2001. **21**(20): p. 6782-95.

185. Teng, Y., *et al.*, *Saccharomyces cerevisiae Rad16 mediates ultraviolet-dependent histone H3 acetylation required for efficient global genome nucleotide-excision repair.* EMBO Rep, 2008. **9**(1): p. 97-102.

186. Wang, J.C., *Cellular roles of DNA topoisomerases: a molecular perspective.* Nat Rev Mol Cell Biol, 2002. **3**(6): p. 430-40.

187. Feng, L., *et al.*, *RIF1 counteracts BRCA1-mediated end resection during DNA repair.* J Biol Chem, 2013. **288**(16): p. 11135-43.

188. *RIF1 operates downstream of 53BP1 to block homologous recombination.* Cancer Discov, 2013. **3**(3): p. OF10.

189. Daley, J.M. and P. Sung, *RIF1 in DNA break repair pathway choice.* Mol Cell, 2013. **49**(5): p. 840-1.

190. Escribano-Diaz, C., *et al.*, *A cell cycle-dependent regulatory circuit composed of 53BP1-RIF1 and BRCA1-CtIP controls DNA repair pathway choice.* Mol Cell, 2013. **49**(5): p. 872-83.

191. Chapman, J.R., *et al.*, *RIF1 is essential for 53BP1-dependent nonhomologous end joining and suppression of DNA double-strand break resection.* Mol Cell, 2013. **49**(5): p. 858-71.

192. Di Virgilio, M., *et al.*, *Rif1 prevents resection of DNA breaks and promotes immunoglobulin class switching.* Science, 2013. **339**(6120): p. 711-5.

193. Zimmermann, M., *et al.*, *53BP1 regulates DSB repair using Rif1 to control 5' end resection.* Science, 2013. **339**(6120): p. 700-4.

194. Boissonneault, G., *Chromatin remodeling during spermiogenesis: a possible role for the transition proteins in DNA strand break repair.* FEBS Lett, 2002. **514**(2-3): p. 111-4.

195. Laberge, R.M. and G. Boissonneault, *Chromatin remodeling in spermatids: a sensitive step for the genetic integrity of the male gamete.* Arch Androl, 2005. **51**(2): p. 125-33.

196. Leduc, F., G.B. Nkoma, and G. Boissonneault, *Spermiogenesis and DNA repair: a possible etiology of human infertility and genetic disorders.* Syst Biol Reprod Med, 2008. **54**(1): p. 3-10.

197. Kierszenbaum, A.L., *Transition nuclear proteins during spermiogenesis: unrepaired DNA breaks not allowed.* Mol Reprod Dev, 2001. **58**(4): p. 357-8.

198. Idler, R.K. and W. Yan, *Control of messenger RNA fate by RNA-binding proteins: an emphasis on mammalian spermatogenesis.* J Androl, 2012. **33**(3): p. 309-37.

199. Kleene, K.C., *Multiple controls over the efficiency of translation of the mRNAs encoding transition proteins, protamines, and the mitochondrial capsule selenoprotein in late spermatids in mice.* Dev Biol, 1993. **159**(2): p. 720-31.

200. Schmidt, E.E., E.S. Hanson, and M.R. Capecchi, *Sequence-independent assembly of spermatid mRNAs into messenger ribonucleoprotein particles.* Mol Cell Biol, 1999. **19**(5): p. 3904-15.

201. Kotaja, N., *et al.*, *The chromatoid body of male germ cells: similarity with processing bodies and presence of Dicer and microRNA pathway components.* Proc Natl Acad Sci U S A, 2006. **103**(8): p. 2647-52.

202. Kotaja, N. and P. Sassone-Corsi, *The chromatoid body: a germ-cell-specific RNA-processing centre.* Nat Rev Mol Cell Biol, 2007. **8**(1): p. 85-90.

203. Ohno, M., *et al.*, *PHAX, a mediator of U snRNA nuclear export whose activity is regulated by phosphorylation.* Cell, 2000. **101**(2): p. 187-98.

204. Lyons, S.M., *et al.*, *The C-terminal extension of Lsm4 interacts directly with the 3' end of the histone mRNP and is required for efficient histone mRNA degradation.* RNA, 2013.

205. He, W. and R. Parker, *Functions of Lsm proteins in mRNA degradation and splicing.* Curr Opin Cell Biol, 2000. **12**(3): p. 346-50.

206. Dass, B., *et al.*, *Loss of polyadenylation protein tauCstF-64 causes spermatogenic defects and male infertility.* Proc Natl Acad Sci U S A, 2007. **104**(51): p. 20374-9.

207. Lee, Y., *et al.*, *Drosha in primary microRNA processing.* Cold Spring Harb Symp Quant Biol, 2006. **71**: p. 51-7.

208. Wu, Q., *et al.*, *The RNase III enzyme DROSHA is essential for microRNA production and spermatogenesis.* J Biol Chem, 2012. **287**(30): p. 25173-90.

209. Meister, G., *et al.*, *Identification of novel argonaute-associated proteins.* Curr Biol, 2005. **15**(23): p. 2149-55.

210. Daniels, S.M. and A. Gatignol, *The multiple functions of TRBP, at the hub of cell responses to viruses, stress, and cancer.* Microbiol Mol Biol Rev, 2012. **76**(3): p. 652-66.

211. Ma, X.M. and J. Blenis, *Molecular mechanisms of mTOR-mediated translational control.* Nat Rev Mol Cell Biol, 2009. **10**(5): p. 307-18.

212. Morimoto, A., *et al.*, *A conserved KASH domain protein associates with telomeres, SUN1, and dynactin during mammalian meiosis.* J Cell Biol, 2012. **198**(2): p. 165-72.

213. Gob, E., *et al.*, *Mammalian sperm head formation involves different polarization of two novel LINC complexes.* PLoS One, 2010. **5**(8): p. e12072.

214. Nery, F.C., *et al.*, *TorsinA binds the KASH domain of nesprins and participates in linkage between nuclear envelope and cytoskeleton.* J Cell Sci, 2008. **121**(Pt 20): p. 3476-86.

215. Ketema, M., *et al.*, *Requirements for the localization of nesprin-3 at the nuclear envelope and its interaction with plectin.* J Cell Sci, 2007. **120**(Pt 19): p. 3384-94.

216. Wilhelmsen, K., *et al.*, *Nesprin-3, a novel outer nuclear membrane protein, associates with the cytoskeletal linker protein plectin.* J Cell Biol, 2005. **171**(5): p. 799-810.

217. McMurray, C.T. and I.V. Kortun, *Repair in haploid male germ cells occurs late in differentiation as chromatin is condensing.* Chromosoma, 2003. **111**(8): p. 505-8.

218. Marchetti, F. and A.J. Wyrobek, *Mechanisms and consequences of paternally-transmitted chromosomal abnormalities.* Birth Defects Res C Embryo Today, 2005. **75**(2): p. 112-29.

219. Emery, B.R. and D.T. Carrell, *The effect of epigenetic sperm abnormalities on early embryogenesis.* Asian J Androl, 2006. **8**(2): p. 131-42.

220. Tesarik, J., E. Greco, and C. Mendoza, *Late, but not early, paternal effect on human embryo development is related to sperm DNA fragmentation.* Hum Reprod, 2004. **19**(3): p. 611-5.

221. Singh, N.P., C.H. Muller, and R.E. Berger, *Effects of age on DNA double-strand breaks and apoptosis in human sperm.* Fertil Steril, 2003. **80**(6): p. 1420-30.

222. Kong, A., *et al.*, *Rate of de novo mutations and the importance of father's age to disease risk.* Nature, 2012. **488**(7412): p. 471-5.

223. O'Roak, B.J., *et al.*, *Sporadic autism exomes reveal a highly interconnected protein network of de novo mutations.* Nature, 2012. **485**(7397): p. 246-50.

224. Hehir-Kwa, J.Y., *et al.*, *De novo copy number variants associated with intellectual disability have a paternal origin and age bias.* J Med Genet, 2011. **48**(11): p. 776-8.

225. Zhao, M., *et al.*, *Utp14b: a unique retrogene within a gene that has acquired multiple promoters and a specific function in spermatogenesis.* Dev Biol, 2007. **304**(2): p. 848-59.

226. Zhao, M., *et al.*, *Targeted disruption of the transition protein 2 gene affects sperm chromatin structure and reduces fertility in mice.* Molecular and Cellular Biology, 2001. **21**(21): p. 7243-55.

227. Wu, J., *et al.*, *OLego: fast and sensitive mapping of spliced mRNA-Seq reads using small seeds.* Nucleic Acids Res, 2013. **41**(10): p. 5149-5163.

228. Wu, J., *et al.*, *SpliceTrap: a method to quantify alternative splicing under single cellular conditions.* Bioinformatics, 2011. **27**(21): p. 3010-6.

229. Pruitt, K.D., T. Tatusova, and D.R. Maglott, *NCBI reference sequences (RefSeq): a curated non-redundant sequence database of genomes, transcripts and proteins.* Nucleic Acids Res, 2007. **35**(Database issue): p. D61-5.

230. Hsu, F., *et al.*, *The UCSC Known Genes.* Bioinformatics, 2006. **22**(9): p. 1036-46.

231. Zhang, C., *et al.*, *Dual-specificity splice sites function alternatively as 5′ and 3′ splice sites.* Proc Natl Acad Sci U S A, 2007. **104**(38): p. 15028-33.

232. Quinlan, A.R. and I.M. Hall, *BEDTools: a flexible suite of utilities for comparing genomic features.* Bioinformatics, 2010. **26**(6): p. 841-2.